TECHNISCHE UNIVERSITÄT MÜNCHEN

Fachgebiet für Experimentelle Radioonkologie / Strahlenbiologie

# Epigenetic regulation of stemness and malignancy in Ewing Tumors

Stephanie Julia Christin Plehm

Vollständiger Abdruck der von der Fakultät Wissenschaftszentrum Weihenstephan für Ernährung, Landnutzung und Umwelt der Technischen Universität München zur Erlangung des akademischen Grades eines

Doktors der Naturwissenschaften

genehmigten Dissertation.

Vorsitzender: Univ.-Prof. Dr. S. Scherer

Prüfer der Dissertation:

1. Univ.-Prof. Dr. G. Multhoff
2. Univ.-Prof. Dr. St. Burdach
3. Univ.-Prof. Dr. A. Skerra

Die Dissertation wurde am 20.10.2010 bei der Technischen Universität München eingereicht und durch die Fakultät Wissenschaftszentrum Weihenstephan für Ernährung, Landnutzung und Umwelt am 30.05.2011 angenommen.

*der kleinen Laura gewidmet*

# Table of contents

# 1. Introduction

## 1.1. Epigenetics and Cancer

Epigenetics is defined as heritable changes in gene expression not encoded by the DNA sequence itself. Epigenetic regulation includes alterations in chromatin structure and DNA methylation. DNA methylations occur almost exclusively in cytosins that precede guanines, called CpG dinucleotides. CpG-rich regions, known as CpG islands, are not randomly distributed in the genome, but span the 5`end of the regulatory region of many genes [1, 2]. DNA methylation is catalyzed by DNA methyltransferases (DNMTs), which mediate transcriptional gene silencing, since promoter DNA methylation is generally repressive for transcription [3]. CpG islands are usually not methylated in normal cells, however, methylation of particular subgroups of promoter CpG islands can be detected in normal tissue. These include genomic imprinted genes (DNA methylation at one of the two parental alleles of a gene to ensure monoallelic expression), X-chromosome encoded genes in females, germline-specific as well as certain tissue-specific genes [4-6]. DNA methylation appears in the context of chemical modifications of histone proteins, and a number of proteins involved in DNA methylation directly interact with histone-modifying enzymes [4, 7]. Alterations in chromatin structure are generated, primarily, by covalent post-translational modifications of histone tails through acetylation, methylation, phosphorylation and ubiquitination, but also via substitution of histone variants within the nucleosomes. The basic unit of chromatin is the nucleosome, an octamer containing two molecules each of core histone proteins H2A, H2B, H3 and H4. Histone H1, the linker histone, is located at the outer surface of the nucleosome and stabilizes the interaction of the DNA that is wrapped around the nucleosome (147 bp of DNA) [8]. Histone modifications occur in different histone proteins and histone residues such as lysine, arginine and serine. These modifications not merely comprise different chemical groups (acetyl, methyl and phosphate) but also different degrees of methylation (e.g. mono-, di- and trimethylation). In general, histone acetylation is associated with transcriptional activation, while histone methylation can lead to both, gene activation or inactivation, depending on the type of amino acid and its position in the histone tail [4]. For example, di- and trimethylation of histone H3 at lysine 4 (H3K4me2/me3) is associated with “active” chromatin, while di- and trimethylation of histone H3 at lysine 27 (H3K27me2/me3) as well as at lysine 9 (H3K9me3) are repressive marks. These modifications are mediated by histone lysine methyltransferases (HKMTs) that contain a SET (Su-(var)3-9;E(z);Trithorax) domain, possessing lysine methyltransferase activity

[9]. Post-translational histone modifications regulate gene expression by modulating chromatin conformation, mediating access of regulatory elements to the DNA sequence or its blockage [10]. Histone hyper-acetylation opens up chromatin structure, thereby designating transcriptionally competent euchromatin, i.e. histone acetyltransferases (HATs) tend to be transcriptional activators whereas histone deacetylases (HDACs) incline to be repressors. Heterochromatic regions, areas of compact chromatin that create physical barriers to productive transcription, are associated with hypo-acetylation, and carry the epigenetic modifications H3K9me3 and H3K27me2/me3 [11, 12]. However, the active mark H3K4me3 as well as the silent mark H3K27me3 have been found to coexist at gene promoters in embryonic stem cells (ES cells), lineage-committed (differentiated) cells as well as in cancer cells [13-17]. Bernstein et al. proposed that the presence of concurrent histone marks, termed bivalent chromatin, silence developmental genes in ES cells while keeping them poised for activation during differentiation [14]. Thus, the heritable (from mother to daughter cell) modification of chromatin and DNA is the basis for both activation and silencing of gene expression. While polycomb group proteins (PcGs) mediate epigenetic gene silencing through e.g. H3K27me3, the Trithorax group proteins (trxG) mediate epigenetic gene activation, e.g. via H3K4me3. TrxGs functionally counter the activity of PcGs and it is presumed, that the epigenetic state of target genes can be switched by the PcG/trxG regulatory system e.g. upon differentiation, when the “balanced” state (bivalent state) frequently transits into fully repressed or fully active states. This transition can be reversed and is governed not only by PcGs and trxGs but also by specific activators and repressors of the individual genes [18]. The bivalent epigenetic modification is linked to pluripotency in ES cells [14] and this pattern is aberrantly altered in different stem cell-like aggressive cancers [19, 20]. Aberrant epigenetic modifications occur due to deregulation of DNMTs and histone-modifying enzymes, whose over-expression or suppression is linked to cancer progression in humans [21-23]. The epigenetic aberrations observed in cancer cells result in abnormal i) transcriptional silencing of genes (e.g. tumor suppressors, differentiation genes); ii) transcriptional activation of genes (e.g. oncogenic genes); iii) global genomic hypo-methylation that leads to a loss of imprinting (LOI) events, reactivation of transposable elements and chromosomal instability [8, 24]. Both, environmental factors as well as genetic factors can cause a deregulation of DNMTs and histone-modifying enzymes. Cadmium ions, e.g. present in water and food, increase the level of genomic DNA methylation and the enzyme activity of DNMTs in human embryo fibroblast cells [25]. Chromosomal translocations involving the *MLL1* gene, most prominently result in a loss of trxG/H3K4 lysine methyltransferase domain and occur in ~80% of infant leukemia’s

of different subtypes, and somatic mutations of the histone acetyltransferase *p300* were reported to be present in a number of malignancies [26, 27]. However, in a variety of human tumors the over-expression or suppression of histone-modifying enzymes is associated with cancer progression and the regulatory mechanisms leading to their deregulation are matter of intensive investigations [26, 28]. One example is the histone lysine methyltransferase EZH2 (enhancer of zeste, *Drosophila,* homolog 2), which belongs to the polycomb group proteins (PcGs). EZH2 is frequently over-expressed in many cancers [29], but the mechanisms involving EZH2 abundance are only beginning to be identified.

### 1.1.1. PcG protein EZH2

EZH2, a protein that is expressed only in proliferating cells [30, 31], harbors histone lysine methyltransferase activity within its SET domain and is the catalytic subunit of the polycomb repressive complex (PRC2). Two additional PcG proteins, embryonic ectoderm development (EED) and suppressor of zeste 12 homolog *Drosophila* (SUZ12), are required for PRC2-mediated transcriptional repression. EED functions as a scaffold protein by physically linking EZH2 and histone H3 substrates, and acts as a mediator of histone deacetylation by specifically interacting with histone deacetylase 2 (HDAC2) [32, 33]. SUZ12 is required for nucleosome recognition and stability of EZH2, and the fourth core component of human PRC2, RbAp46/48 (Retinoblastoma protein associated protein 46/48) is a histone-binding protein [34, 35]. These four components form the PRC2/EED-EZH2 complex, predominantly mediating di- and trimethylation at lysine 27 of histone H3 (H3K27me2/me3) but also methylation at lysine 9 and lysine 26 of histone H3 and H1, respectively. Several studies showed that the EZH2 homolog EZH1 (enhancer of zeste, *Drosophila*, homolog 1) could replace EZH2 in non-canonical PRC2/EED-EZH1. EZH1 similarly has histone lysine methyltransferase activity and complements EZH2 in mediating H3K27me3 and gene repression in ES cells [36]. However, it was shown that PRC2/EED-EZH1 is less abundant in embryonic stem cells and has weaker H3K27me3 activity than PRC2/EED-EZH2. Additionally, Margueron et al. observed, that EZH2 but not EZH1 expression is associated with proliferative tissue, and that EZH1 gene targeting is independent of EZH2 [31]. The mechanism by which both methyl transferases, and human PcGs in general are recruited to their targets is still unknown. In *Drosophila*, PcGs are recruited to the chromatin by specific PREs (PcG-response elements), regulatory sequences whose activity depends on the binding of many different sequence-specific binding factors [37, 38]. *Drosophila* PREs are relatively large and complex DNA regions and they can be located as far as 10

kilobases apart from the gene they regulate [39]. Recently, the first putative mammalian PREs were identified [39-41], indicating that there is conservation of the mechanisms that target PcG function, since several human homologues of *Drosophila* PREs are involved. These include YIN-YANG-1 (YY1), the human homolog of *Drosophila* Pho and the YY1-interacting protein RYBP (RING1 and YY1 binding protein) [39, 42]. However, also OCT4 (Octamer binding transcription factor 4, also known as POU5F1) has been implicated as a recruiter. OCT4 and the associated pluripotency transcription factors SOX2 (SRY-related HMG-box gene 2) and NANOG (Homeobox transcription factor Nanog) bind together with PcGs to many repressed target genes in human ES cells [43], and PRC2 chromatin binding is reduced upon OCT4 knock down [44, 45].

The H3K27me3 histone mark generated by PRC2 is recognized by the second human PcG multimeric complex PRC1, which is thought to further maintain the silent state of the target gene [8]. The PRC1 complex contains at least 10 components, including the BMI1 polycomb ring finger oncogene and other PcG proteins. The observed partnership between PRC1 and 2 is supported by several studies, that demonstrated i) a co-occupancy by both PRCs at many polycomb target gene promoters [46] and ii) a requirement of PRC2 for PRC1 recruitment to these genes [47]. However, PRC1 can be recruited independently of PRC2 [48] and further studies are required to answer the question, whether abnormal PRC2 function in cancer cells depends on or is independent of PRC1.

The great majority of studies reported EZH2 to be a transcriptional repressor that silences target genes in human cancer cells. *E-cadherin* and the *cyclin-dependent kinase inhibitor CDKN1C (p57$^{KIP2}$)* are examples of tumor suppressor genes that are direct targets of EZH2 in tumor cells and silenced through H3K27me3 [49, 50]. Interestingly, several studies provided evidence for the activation of target genes by EZH2: (i) Knock down of EZH2 resulted in a suppression of several direct PRC2 target genes in colon cancer [51]. (ii) In human fibroblasts as well as in breast cancer cells, PRC2 rather activates than silences proliferation and cell cycle control genes [30, 52, 53]. (iii) A dual role for the *Drosophila* homolog E(z) in gene silencing and activation has long been considered [29]. However, further investigations are required to elucidate the underlying mechanism.

EZH2-mediated gene regulation via H3K27me3 was shown to be independent of promoter DNA methylation [54], but it was similarly reported that H3K27me3 pre-marks genes for *de novo* promoter DNA methylation in cancer [55]. EZH2 may act as a recruiting platform to target DNA methyltransferases (DNMTs) to PcG-silenced genes,

resulting in *de novo* methylation, mediated by the cytosine methyltransferases DNMT3A and 3B [56]. DNMT1 is required to maintain the promoter methylation pattern throughout cell division [57]. A growing number of PcG target genes have been found to be hyper-methylated (and thus silenced) in tumors, and many of them are tumor suppressors or are involved in cell differentiation [8]. The tumor suppressor locus *INK4a/4b/ARF* is deactivated by CpG island hyper-methylation in numerous cancers [58]. In ES cells this locus is silenced by PcGs to enable rapid self-renewal [59]. The proteins encoded by this locus activate the retinoblastoma (Rb) pathway that regulates the transition through G1 of the cell cycle via repression of E2F transcription factor activity [30, 60]. These E2F transcription factors were shown to induce the expression of *EZH2* [30, 61], thus mediating induction of PRC2 upon silencing of the *INK4a/4b/ARF* locus and subsequent inactivation of the Rb pathway in cancer cells. With regard to possible post-translational mechanisms that regulate EZH2 activity, several studies have shown that Akt-mediated phosphorylation of EZH2 indirectly inhibits the repressive activity of EZH2 [62], and that EZH2 contains multiple sumoylation sites, which are sumoylated *in vivo* (in human embryonic kidney 293T cells) [63]. Additionally, a growing number of microRNAs (miRNA) were reported recently to regulate EZH2 mRNA levels, including miRNA-26a, miRNA-101, miRNA-241 and miRNA-137 [64-67]. MiRNA-26a and miRNA-101 are repressed or lost in different cancer types, leading to an over-expression of EZH2 [64, 67]. However, several findings strongly suggest that PcG complexes themselves are involved in aberrant silencing of non-coding miRNAs in cancer [8].

### 1.1.2. Non-coding RNAs

The Nobel Prize in Physiology or Medicine 2006 was jointly awarded to Andrew Z. Fire and Craig C. Mello, who discovered that double stranded RNA, which is not translated into a protein, mediates gene silencing (called RNA interference; RNAi) [68]. Today, RNAi has become a standard laboratory technique to investigate gene function by knock down of the corresponding mRNAs. Also in this study, exogenous small interfering RNAs (siRNAs) were introduced into human cells to analyze changes in gene expression and phenotype upon knock down of the corresponding mRNAs and proteins, respectively.

In humans, the group of endogenous non-coding RNAs (ncRNA) include small nucleolar RNAs (snoRNAs), small nuclear RNAs (snRNAs) microRNAs (miRNAs), small interfering RNAs (siRNAs), piwi-interacting RNAs (piRNAs) as well as antisense RNAs (asRNAs) and long non-coding RNAs (long ncRNAs), which differ not only in

their size but also in their specific function [69, 70]. MiRNAs, siRNAs, piRNAs, asRNAs and long ncRNAs are regulatory RNAs that influences gene expression on transcriptional as well as on translational levels [69]. They are critical regulators of cellular processes such as cell differentiation, growth/proliferation, migration, apoptosis/death, metabolism and defense and are involved in the pathogenesis of diverse diseases including cancer [71]. Regulatory ncRNAs were shown to be involved in the formation of a repressive chromatin state, inter alia by the recruitment of PcGs [42, 72], and to regulate the expression of different histone-modifying enzymes [8]. Numerous miRNAs, ncRNAs that bind complementary mRNAs leading to post-transcriptional modulation of target gene expression, were reported to be aberrantly activated or epigenetically silenced in a variety of human tumors [73].

MiRNAs are transcribed by RNA polymerase II into primary miRNAs and are subsequently processed in the nucleus by RNase III-like enzymes (such as Drosha) into ~70 bp precursor miRNAs (pre-miRNAs). These stem loop precursors are transported into the cytoplasm by Exportin-5/Ran-GTP and are further processed by another RNase complex, including DICER, cleaving the precursors into small 21-25 bp double stranded (ds) RNA fragments (miRNA duplexes). The miRNA duplexes are composed of a guiding and a passenger strand. Typically, the guiding strand is incorporated into RISC (RNA-induced silencing complex), while the passenger strand is cleaved and discarded [74]. The core components of RISC are the TAR (HIV-1) RNA binding protein (TARBP) as well as members of the Argonaute (AGO) family, which exhibit strand-dissociating activity of miRNA duplexes. The RISC associates miRNA-dependent with target mRNAs, primarily in the 3`UTR of mRNAs. If the complementarity between miRNA and target mRNA is perfect, the target mRNA is cleaved by the AGO protein (only AGO2 exhibits target mRNA cleavage activity). Is the complementarity incomplete, translational repression (block of mRNA protein translation) and destabilization of target mRNA occurs, similarly leading to post-transcriptional gene silencing (PTGS) of target genes [75-78].

Thus, a single miRNA can modulate protein output from hundreds of target genes. Cells of a particular type exhibit defined miRNA expression patterns, that are linked to corresponding phenotypic characteristics and to the maintenance of cell identity [8]. In ES cells several miRNA promoters are epigenetically silenced by the repressive H3K27me3 mark and these promoters are occupied by PcGs. The same miRNAs promoters lost their H3K27me3 mark and are expressed in differentiated cells in a tissue-specific manner [79], indicating that PcGs may regulate stem cell properties via epigenetic control of miRNA expression. Alterations of cellular miRNA levels are

associated with the progression of a variety of cancer types, since miRNAs may act as either tumor suppressors or oncogenes, depending upon the particular gene they regulate [73]. MiRNAs can be hosted within introns or exons of a specific gene as well as in intergenic regions [80]. Aberrant expression of tumor suppressor miRNAs or oncogenic miRNAs in cancer cells may be caused by i) mutations, ii) amplifications iii) deregulation by oncogenic transcription factors, e.g. by the Proto-oncogene c-Myc [81] or by cancer-specific fusion proteins [82, 83], iiii) deletions and by epigenetic modifications [73]. The best known epigenetic abnormality in cancer is the hyper-methylation of CpG islands in the promoter regions of tumor suppressor miRNAs that mediate their transcriptional repression. Although the complexity of the networks leading to epigenetic silencing of miRNAs is yet to be elucidated, several factors such as cancer-specific fusion proteins or cytokines have been implicated. One example is the AML-ETO fusion protein, product of a frequently observed chromosomal translocation in acute myeloid leukemia (AML), that was found to bind to the miRNA-223 promoter and recruits an epigenetic silencing complex consisting of DNMTs and HDACs. The silencing of miRNA-223 expression via CpG methylation sustains the block in myeloid differentiation, maintaining the characteristic AML phenotype [84]. Interleukin-6 (IL-6) belongs to the cytokines that have been implicated in aberrant miRNA silencing, since IL-6 may indirectly up-regulate DNMT1 gene expression by activation of the transcription factor Friend leukemia virus integration 1 (FLI1) [85]. It has been proposed, that IL-6, which is over-expressed in cholangiocarcinoma, activates expression of DNMT1, thus leading to promoter hyper-methylation and decreased expression of the tumor suppressor miRNA-370 [80].

As mentioned before, miRNAs themselves can regulate the expression of components of the epigenetic machinery. MiRNAs of the miRNA-29 family regulate the expression of the *de novo* methyltransferases DNMT3A and DNMT3B as well as DNMT1, and are inactivated in several tumor entities. Re-activation of miRNA-29 family members resulted in the loss of tumorigenicity of lung cancer and AML cancer cells [86, 87]. MiRNA-449a was reported to target HDAC1 in prostate cancer [88], miRNA-128 targets BMI1 in malignant gliomas and the MYC-mediated inhibition of miRNA-26a results in an over-expression of its target EZH2 in lymphomas [8, 64]. Taken together, the alteration in cellular miRNA levels by different mechanisms may contribute to cancer progression, and therapies based on synthetic miRNAs or anti-miRNAs (antagomirs) are promising strategies to reverse the transformed phenotype of cancer cells.

### 1.1.3. Argonaute Proteins

Argonaute (AGO) proteins are key players of RNAi- and miRNA-mediated gene regulation. AGO proteins bind to siRNAs or miRNAs to guide post-transcriptional gene silencing (PTGS) either by cleavage of the complementary mRNA or by translational repression. In humans there are eight Argonaute genes, which can be divided into the AGO and the PIWI (P-element-induced wimpy testis) subfamily. While the AGO (AGO1-4) proteins are ubiquitously expressed, PIWI proteins are restricted to the germ line. All Argonaute proteins contain a PAZ, MID and PIWI domain. The PAZ domain binds the two-nucleotide 3` overhang (that results from cleavage into small dsRNA fragments by DICER) of the siRNA and miRNA duplexes, respectively. The middle (MID) domain provides a binding pocket for the phosphate at the 5` end of the RNAs. The PIWI domain shows extensive homology to RNase H and contains endonuclease activity. While AGO1 and AGO2 were shown to possess endonuclease activity in humans, AGO3 and AGO4 proteins are endonucleolytically inactive [74, 89-91]. AGO2 has the most well established role in RNAi, referred as the ´catalytic engine` that is responsible for recognition of mRNA and subsequent cleavage [90]. AGO1 is 80% identical to AGO2, but lacks endonuclease activity that enables target mRNA cleavage [92]. Within RISC both, AGO1 and AGO2 showed passenger strand cleavage activity of siRNA duplexes, indicating that passenger strand and mRNA endonuclease activities are mechanistically distinct. Furthermore, AGO1 and AGO2 possess strand-dissociating activity of miRNA duplexes, thus exhibiting RISC-loading activity [74]. In addition to their key role in PTGS, AGO proteins were also shown to be involved in ncRNA-mediated transcriptional gene silencing (TGS). Several studies reported, that nuclear AGO proteins are required for the initiation of siRNA-, miRNA- and asRNA-mediated TGS [72, 90, 93]. Additionally, AGO-ncRNA nucleoprotein complexes were shown to interact with histone modifying enzymes, such as EZH2, and to direct epigenetic complexes to target gene promoters [93-95]. Kim et al. demonstrated, that AGO1 co-localizes with EZH2 and H3K27me3 onto several human gene promoters, e.g. the *myelin transcription factor 1* (*MYT1*) promoter [94]. Since *MYT1* is a known PcG target [51] it is suggested, that endogenous ncRNAs as well as AGO proteins might be involved in the epigenetic mechanism of Polycomb silencing. In contrast with the well-documented role of AGO proteins in translational repression, the exact mechanism of AGO-ncRNA complex-mediated TGS is not yet known.

Even less understood is the role of AGO proteins in gene activation. However, several studies reported recently that AGO2 is involved in non-coding RNA-mediated translational and transcriptional activation [90, 96-98]. Indeed, AGO2 was first reported

to stimulate translational initiation (Roy et al. 1988 [99]), explaining why AGO proteins are also known as eukaryotic translation initiation factor 2C (EIF2C). Argonaute proteins are comprised of a highly conserved gene family, whose members have been implicated not only in RNAi mechanisms, but also in cell fate determination. They assume functions in the development of varied tissues in diverse organisms, and alterations in AGO protein expression have been shown to affect stem cell fate (loss of stem cell character and induction of differentiation). AGO proteins are interconnected with the Wingless (WNT) and Hedgehog signal transduction pathways, that control cell fate and developmental patterning [100]. WNT pathway deregulation and cancer progression in Wilms tumors, often associates with a loss of *AGO1* gene expression, accompanied by mutations of *CTNNB1* (encoding ß-catenin), an integral component in the WNT signaling pathway [100, 101].

In addition, several studies reported, that genes involved in miRNA maturation, including AGO2 [77], are deregulated in various types of cancer, including breast [102], colon [103], prostate and esophageal cancer [104] as well as in multiple myeloma [105]. Increased AGO2 expression was accompanied by increased amounts of miRNA and correlated with a transformed as well as aggressive phenotype [102, 103, 105]. In breast cancer cells, ectopic expression of AGO2 resulted in elevated levels of miRNA-206 as well as in a higher degree of migratory/invasive capabilities compared to parental MCF-1 breast cancer cells (due to AGO2-mediated reduction of cell-cell adhesion and reduced levels of E-cadherin and β-catenin expression). Thus, the authors concluded that AGO2 might promote transformation via a miRNA-dependent as well as a miRNA-independent mechanism. Furthermore, they demonstrated, that the epidermal growth factor (EGF) induces *AGO2* gene expression and enhances AGO2 protein stability via the Mitogen-activated protein kinase (MAPK) pathway in breast cancer cells [102].

The human *AGO2* gene is located on chromosome 8, while *AGO1*, *AGO3* and *AGO4* genes are clustered on chromosome 1 [89]. *AGO1* is located in the region 1p34-p35, a genomic region that is frequently lost in human cancers such as neuroblastoma, breast, liver and colon cancer [101]. On the other hand, *AGO1* expression was shown to be increased in tumors that lacked functional copies of the Wilms tumor suppressor gene *WT1*, and *AGO1* over-expression was significantly associated with transformed colon cancer tissue [103]. However, the exact mechanisms how AGO proteins contribute to cancerogenesis still need to be further elucidated.

## 1.2. Ewing family of Tumors

The Ewing Family of Tumors (ET) is the second most common malignancy of bone and soft tissue in children and young adults next to osteosarcoma. 10% of primary malignant bone tumors in children are identified as ET and slightly more male than female patients are diagnosed with ET (3:2). The tumors commonly develop in the second decade of life, and approximately 80% of patients with ET are younger than twenty years [106]. The overall 5-year disease-free survival rate for localized ET patients treated with surgery, radiation and multiagent chemotherapy is 65-76% [107, 108]. Important prognostic factors are the presence of metastases and their location, the tumor size as well as the site of the primary tumor. 25% of patients already exhibit metastases at the time of initial diagnosis, and the disease-free survival rate drops down to less than 27% in patients with metastatic ET, despite multimodal treatment regimens [109-111].

ET features are an aggressive osteolytic behavior and a strong tendency for dissemination, predominantly into the lungs, bone and bone marrow [112]. ET cells are poorly differentiated, uniformly small round cells of uncertain histogenesis. Since its initial description by James Ewing in 1921, who referred to it as *diffuse endothelioma of bone* [113], classification of ET was difficult due to the lack of ET-specific markers. ET cells display mesenchymal, neuroectodermal as well as endothelial features, suggesting being either of mesenchymal or neuroectodermal origin [113-115]. The marker CD99 [116], a membrane protein that is expressed in most ET, may advert to ET disease but is not specific enough for an exact classification. But only the discovery of a specific chromosomal translocation, that fuses the *Ewing sarcoma breakpoint region 1* (*EWSR1*) located on chromosome 22 to an *ETS* (E-twenty six) family gene on chromosome 11, enabled a precise classification of ET [117-119]. Today, this group of tumors comprises highly malignant classical Ewing Tumors, malignant peripheral neuroectodermal tumors (MPNT) as well as the Askin tumor of the thoracic wall, all of them expressing oncogenic EWS/ETS fusion proteins [120]. These fusion proteins act as aberrant transcription factors, targeting genes involved in cell proliferation, survival and cell differentiation [121]. The most common translocation (85% of cases) fuses the *EWSR1* with the *Friend leukemia virus integration 1* (*FLI1*) gene, resulting in the generation of the EWS/FLI1 fusion protein. The EWS/FLI1 transcript encodes a 68 kDa protein with two primary domains. The EWS domain is a potent transcriptional activator, while the FLI1 domain contains a highly conserved ets DNA binding domain [122]. In another 10% of tumors, a gene fusion between *EWSR1* and *ets-related gene* (*ERG*) is found [123]. Rare cases carry one of three alternative rearrangements of the

*EWSR1* gene with either *ETV1* (*ets variant 1*), *ETV4* (*ets variant 4)* or *FEV (ETS oncogene family)* gene [124].

EWS/FLI1 has a great potential as a molecular target for therapy, and strategies to eliminate or inactivate the EWS/FLI1 fusion protein are the subject of intense investigations [125-127]. However, no therapeutic applications targeting EWS/FLI1 reached clinical trial status so far. The facts that patients with metastases in bone or bone marrow have a very poor prognosis and that current treatment strategies (surgery, radiation and multiagent chemotherapy) are associated with intense short- and long-term adverse effects [109], emphasize the urgent need for new therapeutic treatment modalities. The elucidation of ET-specific gene expression profiles and the identification of EWS/ETS down-stream targets are first steps towards alternative targeted therapies. A pool of new potential targets was provided by the work of Staege et al. in 2004 [128]. This DNA microarray analysis revealed 37 genes that are highly up-regulated or even specifically expressed in primary ET tissues. Among them, *enhancer of zeste (Drosophila) homolog 2* (*EZH2*) was highly expressed in primary ET samples compared to 133 normal tissues of diverse origin.

## 1.3. Aim of this study and overview of the experimental approach

The goal of this work was to illuminate the role of EZH2 in the pathology of ET, and to identify the regulatory mechanisms upstream and downstream of EZH2. To assess whether EWS/ETS fusion proteins bind to the *EZH2* promoter, *in vitro* and *in vivo* binding assays in different established ET cell lines, carrying either the EWS/FLI1 type 1 or type 2 fusion transcript were performed. In order to analyze an EWS/FLI1-dependent *EZH2* expression, EZH2 mRNA levels were quantified upon ectopic EWS/FLI1 expression in mesenchymal stem cells (MSC) as well as after RNAi-mediated knock down of EWS/FLI1 in different ET cell lines. To investigate the potential contribution of EZH2 to ET pathogenesis, EZH2 was transiently and constitutively knocked down in different ET cell lines by RNAi. The influence of EZH2 knock down on ET phenotype and tumorigenicity was analyzed in a xenograft mouse model as well as by the use of different *in vitro* assays. Microarray and ChIP-on-chip analyses were performed to identify EZH2 downstream targets, and to elucidate the mechanism of their regulation. Several *in vitro* assays as well as Western blot and quantitative RT-PCR analyses were used to verify these results. Furthermore, the involvement of Argonaute (AGO) proteins and miRNAs in ET pathogenesis was analyzed, due to their potential interconnection with EZH2. Here again, RNAi-experiments as well as different *in vitro* and *in vivo* assays were established to analyze

the effect of AGO knock down on ET phenotype and tumorigenicity. Microarray analyses have been used as well to identify possible AGO downstream targets.
This study may contribute to the long-term aim to disclose new ET-specific targets for alternative target-orientated therapeutic strategies.

# 2. Materials

## 2.1. List of manufacturers

| Manufacturers | Locations |
|---|---|
| Abcam | Cambridge, UK |
| Abgent | San Diego, USA |
| AEG | Nürnberg, Germany |
| Ambion | Austin, Texas, USA |
| Amersham Biosciences | Piscataway, New Jersey, USA |
| Applied Biosystems | Darmstadt, Germany |
| ATCC | Rockyville, Maryland, USA |
| B. Braun Biotech Int. | Melsungen, Germany |
| Bayer HealthCare Pharmaceuticals | Leverkusen, Germany |
| BD Biosciences Europe | Heidelberg, Germany |
| Beckman Coulter | Palo Alto, California, USA |
| Becton Dickinson (BD) | New Jersey, USA |
| Berthold detection systems | Pforzheim, Germany |
| Biochrom | Berlin, Germany |
| Biometra | Göttingen, Germany |
| BioRad | Richmond, California, USA |
| Biowhittaker | East Rutherford, New Jersey, USA |
| Biozym | Hess. Olendorf, Germany |
| Branson | Dietzenbach, Germany |
| Carestream Health, Inc. | Stuttgart, Germany |
| Cayman Chemical Company | Ann Arbor, Michigan, USA |
| Cell Signaling Technology | Frankfurt a. M., Germany |
| Covance | New Jersey, USA |
| DSMZ | Braunschweig, Germany |
| Eppendorf | Hamburg, Germany |
| Falcon | Oxnard, California, USA |
| Fermentas | St. Leon-Rot, Germany |
| GE Healthcare | Uppsala, Sweden |
| Genomed | St. Louis, Missouri, USA |

| | |
|---|---|
| Genzyme | Neu-Isenburg, Germany |
| GLW | Würzburg, Germany |
| Greiner | Nürtingen, Germany |
| Heidolph Instruments | Schwabach, Germany |
| Heraeus | Hanau, Germany |
| ImaGenes GmbH | Berlin, Germany |
| Invitrogen | Karlsruhe, Germany |
| Jackson ImmunoResearch Laboratories | Baltimore, USA |
| Leica | Wetzlar, Germany |
| Lonza | Basel, Switzerland |
| Macherey-Nagel | Düren, Germany |
| Merck | Darmstadt, Germany |
| Millipore | Billerica, Massachusetts, USA |
| Miltenyi Biotec GmbH | Bergisch Gladbach, Germany |
| Molecular BioProducts, MbP | San Diego, California, USA |
| Nalgene | Rochester, New York, USA |
| New England BioLabs | Frankfurt am Main, Germany |
| Nunc | Naperville, USA |
| PAA | Cölbe, Germany |
| Pan Biotech GmbH | Aidingen, Germany |
| Pechiney Plastic Packaging | Menasha, Wisconsin, USA |
| Peske OHG | München, Germany |
| Promega | Madison, Wisconsin, USA |
| Qiagen | Chatsworth, California, USA |
| R&D Systems | Minneapolis, Minnesota, USA |
| Roche | Mannheim, Germany |
| (Carl) Roth | Karlsruhe, Germany |
| Santa Cruz Biotechnology | Heidelberg, Germany |
| Sartorius | Göttingen, Germany |
| Schleicher und Schüll | Dassel, Germany |
| Scientific Industries | Bohemia, New York, USA |
| Sempermed | Wien, Austria |
| Sigma | St. Louis, Missouri, USA |
| Stratagene | Cedar Creek, Texas, USA |

| | |
|---|---|
| Syngene | Cambridge, UK |
| Thermo Scientific | Braunschweig, Germany |
| TPP | Trasadingen, Switzerland |
| Thermo Fisher Scientific | Ulm, Germany |
| Whatman | Dassel, Germany |
| Zeiss | Jena, Germany |

## 2.2. General material

| **Materials** | **Manufacturers** |
|---|---|
| Cryovials | Nunc |
| Culture plates (100 mm ∅) | Nunc |
| Cuvettes | Roth |
| Filters for cells, Cell Strainer | Falcon |
| Filters for solutions (0.2 µm and 0.45 µm) | Sartorius |
| Flasks for cell culture (75 $cm^2$ and 175 $cm^2$) | TPP |
| Flasks for cell culture (75 $cm^2$ and 175 $cm^2$) | Falcon |
| Gloves (nitrile, latex) | Sempermed |
| Hybond-P PVDF membrane | GE Healthcare |
| Hypodermic needle (23 G) | BBraun |
| Parafilm | Pechiney Plastic Packaging |
| Pasteur pipettes | Peske OHG |
| Petri dishes | Falcon |
| Pipettes (2, 5, 10 and 25 ml) | Falcon |
| Pipette tips (10, 200 and 1000 µl) | MbP |
| Pipette tips (10, 200 and 1000 µl with a filter) | Biozym |
| Plates for cell culture (6-well, 24-well and 96-well) | TPP |
| Scalpels (Nr. 12, 15, 20) | Feather |
| Tubes for cell culture (polystyrene, 15 ml) | Falcon |
| Tubes for cell culture (polypropylene, 15 ml and 50 ml) | Falcon |
| Tubes for molecular biology, Safelock (1.5 ml and 2 ml) | Eppendorf |
| Tubes for FACS™ (5 ml) | Falcon |
| Whatman paper | Whatman |

## 2.3. Instruments and Equipment

| Type of device | | Manufacturer |
|---|---|---|
| Bacteria shaker | Certomat BS-T | Sartorius |
| Ice machine | AF 100 | Scotsman |
| Cell counting chamber | Neubauer | Brand |
| Centrifuge | Multifuge 3 S-R | Heraeus |
| Centrifuge | Biofuge fresco | Heraeus |
| Controlled-freezing box | | Nalgene |
| Electroporator | Gene Pulser Xcell™ | BioRad |
| Electrophoresis chamber | | BioRAD |
| ELISA Reader | Multiskan Ascent | Thermo Scientific |
| Flow cytometer | FACSCalibur™ | Becton Dickinson |
| Freezer (-80 °C) | Hera freeze | Heraeus |
| Freezer (-20 °C) | cool vario | Siemens |
| Fridge (+4 °C) | cool vario | Siemens |
| Gel documentation | Gene Genius | Syngene |
| Incubator | Hera cell 150 | Heraeus |
| Liquid Nitrogen Tank | L-240 K series | Taylor-Wharton |
| Luminometer | Sirius Luminometer | Berthold detection systems |
| Multichannel pipette | (10-100 µl) | Eppendorf |
| Heating block | Thermomixer Comfort | Eppendorf |
| Micropipettes | (0.5-10 µl, 10-100 µl, 20-200 µl, 100-1000 µl) | Eppendorf |
| Microscope (fluorescence) | AxioVert 100 | Zeiss |
| Microscope | | Leica |
| Microwave oven | | Siemens, AEG |
| PCR cycler | iCycler | BioRAD |
| Pipetting assistant | Easypet | Eppendorf |
| Power supplier | Standard Power Pack P25 | Biometra |
| Rotator | | GLW |
| Semi-Dry Transfer Apparatus | Fastblot | Biometra |
| SDS-PAGE chamber | Minigel-Twin | Biometra |
| Shaker | Polymax 2040 | Heidolph Instruments |

| | | |
|---|---|---|
| Spectrophotometer | GeneQuant II | Amersham Biosciences |
| Sterile Bench | | Heraeus |
| Sonifier | Digital Sonifier® | BRANSON |
| Water bath | | GFL |
| Western blot documentation | Gel Logic 1500 imaging sytem | Carestream Health, Inc. |
| Real Time PCR | 7300 Real-Time PCR | Applied Biosystems |
| Vortexer | Vortex-Genie 2 | Scientific Industries |
| Water purification system | TKA GenPure | TKA GmbH |

## 2.4. Chemical and biological reagents

| Reagents | Manufacturer |
|---|---|
| Agar | Sigma |
| Agarose | Invitrogen |
| Ampicillin | Merck |
| AmpliTaq DNA Polymerase | Invitrogen |
| Ammonium persulfate (APS) | Sigma |
| β-Mercaptoethanol | Sigma |
| BCP (1-bromo-3-chloropropane) | Sigma |
| BenchMark™ Prestained Protein Ladder | Invitrogen |
| BHA (butylated hydroxyanisole) | Sigma |
| Blue Juice Gel Loading Buffer | Invitrogen |
| Bradford reagent | BioRAD |
| Calcein AM | Merck |
| DEPC (diethyl pyrocarbonate) | Sigma |
| Deoxycholic acid | Roth |
| Dimethylformamide | Roth |
| dNTPs | Roche |
| DMEM medium | Invitrogen |
| DMSO (dimethyl sulfoxide) | Merck |
| DTT (DL-Dithiothreitol) | Sigma |
| EDTA (ethylenediaminetetraacetate) | Merck |
| EtBr (Ethidium bromide) | BioRAD |
| Ethanol | Merck |

| | |
|---|---|
| FBS (fetal bovine serum) | Biochrom |
| 37% Formaldehyde | Merck |
| Gentamycin | Biochrom |
| Glycerol | Merck |
| Glycine | Merck |
| G418 | PAA |
| HBSS (Hank's buffered salt solution) | Invitrogen |
| HCl (hydrochloric acid) | Merck |
| HEPES | Sigma |
| Herring sperm DNA, denaturated | Sigma |
| HiPerFect Transfection Reagent | Qiagen |
| Human IgG | Genzyme |
| Isopropanol | Sigma |
| KCl (potassium chloride) | Merck |
| L-glutamine | Invitrogen |
| Matrigel Matrix | BD Biocoat |
| Maxima™ Probe / ROX qPCR Master Mix (2 x) | Fermentas |
| Methanol | Roth |
| Methylcellulose | R&D Systems |
| $MgCl_2$ (magnesium chloride) | Invitrogen |
| MS-275 | Sigma |
| $NaHCO_3$ (sodium hydrogen carbonate) | Merck |
| $NaN_3$ (sodium azide) | Merck |
| NaOH (sodium hydroxide) | Merck |
| Nonidet-P40 (NP40) | Sigma |
| PBS 10 x (phosphate buffered saline) | Invitrogen |
| PCR Buffer (10 x) | Invitrogen |
| Peptone | Invitrogen |
| Penicillin / streptomycin | Invitrogen |
| PFA (paraformaldehyde) | Merck |
| PMSF (phenylmethanesulfonylfluoride) | Sigma |
| Polyacrylamide (30% Acrylamide / Bis) | Merck |
| Polybrene (hexadimethrine bromide) | Sigma |
| Propidium iodide | Sigma |

| | |
|---|---|
| Protease Inhibitor cocktail tablets | Roche |
| Proteinase K | Sigma |
| Protein A/G Plus agarose beads | Santa Cruz |
| Puromycin | PAA |
| Ready-Load 1 Kb DNA Ladder | Invitrogen |
| RNase A (Ribonuclease A) | Roche |
| RPMI 1640 medium | Invitrogen |
| SDS | Sigma |
| Skim milk powder | Merck |
| Sodium chloride | Merck |
| Streptavidin-agarose beads | Merck |
| SYBR Green Master Mix | Applied Biosystems |
| TEMED (N,N,N′,N′-Tetramethylethan-1,2-diamin) | Sigma |
| Trichostatin A | Sigma |
| Tris | Merck |
| Triton X-100 | Sigma |
| Trypan blue | Sigma |
| Trypsin / EDTA | Invitrogen |
| Tween 20 | Sigma |

## 2.5. Commercial Reagent Kits

| **Name** | **Manufacturer** |
|---|---|
| Annexin V-PE Apoptose Detection Kit I | BD Biosciences |
| Cell Invasion Assay | BD Biosciences |
| Cell proliferation ELISA BrdU Kit | Roche |
| DNeasy® Blood & Tissue Kit | Qiagen |
| ECL-Plus Western Blot Detection System | GE Healthcare |
| High-Capacity cDNA Reverse Transcription Kit | Applied Biosystems |
| RNeasy® Mini Kit | Qiagen |
| NucleoSpin® Plasmid Kit | Macherey-Nagel |
| QIAEX II Gel Extraction Kit | Qiagen |
| QIAquick PCR Pufification Kit | Qiagen |
| TRI Reagent RNA Isolation Kit | Ambion |

| | |
|---|---|
| TaqMan® Gene Expression Assays | Applied Biosystems |
| TaqMan® MicroRNA Assays | Applied Biosystems |
| TaqMan® MicroRNA Reverse Transcription Kit | Applied Biosystems |
| MycoAlert Mycoplasma Detection Kit | Lonza |

## 2.6. Media, Buffers and Solutions

**Table 1: Cell culture media and universal solutions**

| Name | Ingredients |
|---|---|
| **Standard tumor medium** | 500 ml RPMI 1640 or DMEM<br>10% FBS, 2 mM L-glutamine, 1 mg Gentamycin |
| **RIPA Buffer** | 150 mM NaCl, 1% NP40 (igepal), 0.5% Deoxycholic acid (10%), 0.1% SDS (10%), 50 mM TrisHCl pH 8 |
| **4% paraformaldehyde** | 4% PFA in 1 x PBS, adjusted to pH 7.4 with NaOH |
| **4% formaldehyde** | 4% Formalin, 55 mM $Na_2HPO_4$, 12 mM $NaH_2PO_4 \cdot 2\ H_2O$ |
| **Staining Buffer** | 2% FBS, 0.05% $NaN_3$ dissolved in 1 x PBS |

**Table 2: Buffers and Gels for Western blot analysis**

| Name | Ingredients |
|---|---|
| **Laemmli buffer (3 x)** | 188 mM Tris/HCl pH 6.8, 3% SDS, 45% Glycerol, 0.05% Bromphenol blue, 7.5% ß-Mercaptoethanol |
| **SDS running buffer (1 x)** | 25 mM Tris, 200 mM Glycine, 0.1% (w/v) SDS |
| **Separating buffer (4 x)** | 1.5 M Tris, 0.4% SDS, adjusted to pH 8.8 with HCl |
| **Separating Gel (8-12.5%)** | (10%): 3.33 ml 30% Acrylamide / Bis, 2.5 ml Separating Buffer (4 x), 4.17 ml water, 50 µl APS (10%), 20 µl TEMED |
| **Stacking buffer (4 x)** | 0.5 M Tris, 0.4% SDS, adjusted to pH 6.8 with HCl |
| **Stacking Gel (4.5%)** | 750 µl 30% Acrylamide / Bis, 1.25 ml Stacking Buffer (4 x), 3 ml water, 50 µl APS (10%), 20 µl TEMED |
| **Transfer buffer (5 x)** | 25 mM Tris pH 8.3, 192 mM Gylcine |

| | |
|---|---|
| **TBS (10 x)** | 0.5 M Tris-HCl pH 7.4, 1.5 M NaCl |
| **TBST** | 1 x TBS including 0.05% (v/v) Tween 20 |

**Table 3: Buffer and Gel for DNA / RNA electrophoresis**

| Name | Ingredients |
|---|---|
| **TAE Rrunning buffer** | 50 x TAE: 2 M Tris, 10% EDTA (0.5 M), 5.71% HCl |
| **Electrophoresis gel** | 200 ml TAE buffer (1 x), 0.7-3% agarose, 3 µl EtBr |

**Table 4: Buffers for ABCD Assay**

| Name | Ingredients |
|---|---|
| **Annealing Buffer** | 0.5 M NaCl, 0.2 M Tris pH 7.4 |
| **NETN Buffer** | 10 mM Tris pH 8, 100 mM NaCl, 1 mM EDTA, 10% Glycerol, 0.5% NP-40, 1 mM DTT, 0.5 mM PMSF |
| **Buffer H** | 20 mM HEPES pH 7.8, 50 mM KCl, 20% Glycerol, 0.1% NP-40, 1 mM DTT |

**Table 5: Buffers for ChIP Assay**

| Name | Ingredients |
|---|---|
| **Low Salt Buffer** | 0.1% SDS, 1% Triton-X 100, 2 mM EDTA, 20 mM Tris pH 8.1, 150 mM NaCl |
| **High Salt Buffer** | 0.1% SDS, 1% Triton-X 100, 2 mM EDTA, 20 mM Tris pH 8.1, 500 mM NaCl |
| **Elution Buffer** | 1% SDS, 0.1 M $NaHCO_3$ |

**Table 6: Buffers and solutions for Cell Cycle Analysis**

| Name | Ingredients |
|---|---|
| **Probe Buffer** | 0.1% Glucose (w/v) in 1 x PBS, 0.22 µm filtration, stored at 4°C |
| **PI Staining solution** | 50 µg / ml Propidium iodide and 100 U / ml RNase A in probe buffer |

## 2.7. Antibodies

**Table 7: Antibodies for Western Blot**

| Antibody | Source | Dilution | Product No. | Manufacturer |
|---|---|---|---|---|
| anti-AGO1 | rabbit | 1:1000 | 07-599 | Millipore/Upstate |
| anti-AGO2 | rabbit | 1:1000 | 07-590 | Millipore/Upstate |
| anti-EZH2 | rabbit | 1:1000 | 4905 | Cell Signaling |
| anti-Fli-1 (C-19) | rabbit | 1:500 | sc-356 | Santa Cruz |
| anti-GAP43 | rabbit | 1:10000 | ab7462 | Abcam |
| anti-HPRT (FL-218) | rabbit | 1:500 | sc-20975 | Santa Cruz |
| anti-H3K9/14 acetyl | rabbit | 1:5000 | 06-599 | Millipore/Upstate |
| anti-H3K9me2 | rabbit | 1:500 | 17-648 | Millipore |
| anti-H3K9me3 | rabbit | 1:500 | 07-442 | Millipore |
| anti-H3K4me2/3 | rabbit | 1:500 | 04-745 | Millipore |
| anti-H3K27me3 | rabbit | 1:1000 | 07-449 | Millipore |
| anti-H3 | rabbit | 1:5000 | ab1791 | Abcam |
| anti-rabbit IgG HRP | bovine | 1:1000 | sc-2370 | Santa Cruz |
| anti-mouse IgG HRP | goat | 1:1000 | sc-2031 | Santa Cruz |
| Streptavidin-HRP | | 1:100 | 554066 | BD Pharmingen |

**Table 8: Antibodies for Immuncytology and ChIP**

| Antibody | Source | Dilution / Amount | Product No. | Manufacturer |
|---|---|---|---|---|
| anti-GFAP | mouse | 1:100 | 556330 | BD Pharmingen |
| anti-mouse IgG+IgM $F(ab`)_2$-FITC | goat | 1:100 | 115-096-068 | Jackson ImmunoResearch |
| anti-FLI1 (C-19) | rabbit | 3 µg | sc-356 | Santa Cruz |
| anti-H3K27me3 | rabbit | 3 µg | ab6002 | Abcam |
| anti-H3 | rabbit | 3 µg | ab1791 | Abcam |
| Control IgG | rabbit | 3 µg | ab46540 | Abcam |

**Table 9: Antibodies for Flow cytometry**

| Antibody | Conjugation | Dilution | Product No. | Manufacturer |
|---|---|---|---|---|
| CD271 (LNGFR) | FITC | 1:20 | 130-091-917 | Miltenyi Biotec |
| Isotype mouse IgG | FITC | 1:20 | 345815 | Becton Dickinson |

| | | | | |
|---|---|---|---|---|
| CD133/2 (PROM1) | APC | 1:20 | 130-090-854 | Miltenyi Biotec |
| Isotype mouse IgG | APC | 1:20 | 345818 | Becton Dickinson |

**Table 10: Antibodies for Immunohistology**

| Antibody | Source | Dilution | Product No. | Manufacturer |
|---|---|---|---|---|
| anti-CD99 (O13) | mouse | 1:40 | SIG-3620 | Covance |
| anti-EZH2 | rabbit | 1:30 | AP2512c | Abgent |

## 2.8. Small interfering RNAs

Small interfering RNAs (siRNAs) were obtained from Qiagen, except EWS/FLI1 I and II siRNAs, that were synthesized by Eurofins MWG GmbH (Ebersberg, Germany).

**Table 11: Small interfering RNA used for transient transfection**

| siRNA Name | Target Sequence (5'-3') |
|---|---|
| Control (non-silencing) siRNA | 5´-AAT TCT CCG AAC GTG TCA CGT-3` |
| EED_6 siRNA | 5´-AAT CCG GTT GTT GCA ATC TTA-3´ |
| AGO1_2 siRNA | 5´-CTC CAA GAA TTG TGC AAG TAA-3´ |
| AGO1_3 siRNA | 5´-CAG CTA CAA CTT AGA TCC CTA-3´ |
| AGO2_5 siRNA | 5´-CAG CAC CGG CAG GAG ATC ATA-3´ |
| AGO2_6 siRNA | 5´-CAG GCG TTA CAC GAT GCA CTT-3´ |
| EWS/FLI1 I siRNA | 5´-GCU ACG GGC AGC AGA ACC CUU-3´ |
| EWS/FLI1 II siRNA | 5´-GCA GAA CCC UUC UUA UGA CUU-3´ |
| EZH2_2 siRNA | 5´-AAG CAA ATT CTC GGT GTC AAA-3´ |
| EZH2_7 validated siRNA | 5´-AAC CAT GTT TAC AAC TAT CAA-3´ |
| HDAC1_6 siRNA | 5´-CAC CCG GAG GAA AGT CTG TTA-3´ |
| HDAC2_3 siRNA | 5´-TCC CAA TGA GTT GCC ATA TAA-3´ |
| HDAC3_4 siRNA | 5´-GAC CAT GAC AAT TGA CAA GGA A-3´ |
| HDAC9_5 siRNA | 5´-TTG GCT CAG CTG GTC ATT CAA-3´ |
| SUZ12_6 validated siRNA | 5´-TAG CAT AAT GTC AAT AGA TAA-3´ |

## 2.9. Oligonucleotides for Retroviral Gene Transfer and ABCD Assay

All oligonucleotides were obtained from Metabion International AG (Martinsried, Germany).

**Table 12: Oligonucleotides used for retroviral gene transfer**

| Name | Sequence (5'-3') |
|---|---|
| AGO1-for | 5´-GAT CCG GCT ACA ACT TAG ATC CCT ATT CAA GAG ATA GGG ATC TAA GTT GTA GCC TTT TTT CTA GAG-3´ |
| AGO1-rev | 5`-AAT TCT CTA GAA AAA AGG CTA CAA CTT AGA TCC CTA TCT CTT GAA TAG GGA TCT AAG TTG TAG CCG-3´ |
| AGO2-for | 5´-GAT CCG GCA CCG GCA GGA GAT CAT ATT CAA GAG ATA TGA TCT CCT GCC GGT GCC TTT TTT CTA GAG-3´ |
| AGO2-rev | 5`-AAT TCT CTA GAA AAA AGG CAC CGG CAG GAG ATC ATA TCT CTT GAA TAT GAT CTC CTG CCG GTG CCG-3´ |
| control-for | 5`-GAT CCG TTC TCC GAA CGT GTC ACG TTT CAA GAG AAC GTG ACA CGT TCG GAG AAC TTT TTT CTA GAG-3´ |
| control-rev | 5`-AAT TCT CTA GAA AAA AGT TCT CCG AAC GTG TCA CGT TCT CTT GAA ACG TGA CAC GTT CGG AGA ACG-3 |
| EWS/FLI1-for | 5`-GAT CCG AGC AGA ACC CTT CTT ATG ACT T CAA GAG AGT CAT AA GA AGG GTT CTG GTC TTT TTT CTA GAG-3´ |
| EWS/FLI1-rev | 5`-AAT TCT CTA GAA AAA AGA GCA GAA CCC TTC TTA TGA C TCT CTT GAA GTC ATA AGA AGG GTT CTG CT CG-3 |
| EZH2-for | 5´-GAT CCG GAG GTT CAG ACG AGC TGA TTT CAA GAG AAT CAG CTC GTC TGA ACC TCC TTT TTT CTA GAG-3´ |
| EZH2-rev | 5´- AAT TCT CTA GAA AAA AGG AGG TTC AGA CGA GCT GAT TCT CTT GAA ATC AGC TCG TCT GAA CCT CCG-3´ |

**Table 13: Oligonucleotides for ABCD Assay**

| Name | Sequence (5'-3') |
|---|---|
| EZH2361f | 5`-BIOTIN-ATGTGAGGAATGGGATGGTGATTTAGGAAAGGCGGGAAAATTATG-3` |
| EZH2361r | 5`-CATAATTTTCCCGCCTTTCCTAAATCACCATCCCATTCCTCACAT-3` |
| EZH2upcf | 5`-BIOTIN-GTTCTGAGAAGTGAAGGGATGGAAAGGGAAGTTTGCTGGCTGACA-3` |
| EZH2upcr | 5`-TGTCAGCCAGCAAACTTCCCTTTCCATCCCTTCACTTCTCAGAAC-3` |
| EZH2docf | 5`-BIOTIN-CGCGCCATTGCACTCCAGCCTGGACAACCAGAGCGAAACTCCGTC-3` |
| EZH2docr | 5`-GACGGAGTTTCGCTCTGGTTGTCCAGGCTGGAGTGCAATGGCGCG-3` |

## 2.10. Primers for PCR and qRT-PCR

**Table 14: Primers for qRT-PCR (SYBR Green-based detection) and PCR**

| Name | Sequence (5'-3') |
|---|---|
| EWS/FLI1 for | 5'-TAG TTA CCC ACC CAA ACT GGA T-3' |
| EWS/FLI1 rev | 5'-GGG CCG TTG CTC TGT ATT CTT AC-3' |
| ACTB for | 5`-GGC ATC GTG ATG GAC TCC G-3` |
| ACTB rev | 5`-GCT GGA AGG TGG ACA GCG A-3` |
| pMSCVneo / pSIREN for | 5`-GGG CAG GAA GAG GGC CTA T-3` |
| pMSCVneo / pSIREN rev | 5`-GAG ACG TGC TAC TTC CAT TTG TC-3` |
| TRIM36 for | 5`-GCC CGC TTC TTG CTT TCC-3` |
| TRIM36 rev | 5`-CCG CCC ATA AGC TGT TAA CC-3` |

**Table 15: Primers for ChIP-qRT-PCR**

| Name | Sequence (5'-3') |
|---|---|
| -4400bp for | 5`-GCA CAT CAG CCA CGC TTC T-3` |
| -4400bp rev | 5´-GGA GCT GAG GGA GCA TTT ACT G-3` |
| -3778bp for | 5`-ATC CAG CCC CAA GCT GTT T-3` |
| -3778bp rev | 5`-GAA CAT GAG GTG GTG ATA AAA ATA AGG-3` |
| -2120bp for | 5`-CCA ACA TTG GAG TGA TTC AG-3` |
| -2120bp rev | 5´-TCA TCA GAT GAT TTA GCC CA-3´ |
| -1081bp for | 5´-GACACGTGCTTAGAACTA ACG AAC AG-3´ |
| -1081bp rev | 5´-TTT GGC TGG CCG AGC TT-3´ |

## 2.11. TaqMan Gene Expression Assays

All TaqMan Gene Expression Assays were obtained from Applied Biosystems.

**Table 16: TaqMan Gene Expression Assays**

| Gene | Assay ID |
|---|---|
| *ABCG2* | Hs00184979_m1 |
| *ALCAM* | Hs00233455_m1 |
| *EED* | Hs00537777_m1 |
| *AGO1 (EIF2C1)* | Hs00201864_m1 |

| | |
|---|---|
| *AGO2 (EIF2C2)* | Hs00293044_m1 |
| *EMP1* | Hs00923125_g1 |
| *EPHB2* | Hs00362096_m1 |
| *EZH2* | Hs00544830_m1 |
| *GAPDH* | Hs99999905_m1 |
| *GAP43* | Hs00176645_m1 |
| *G1P2 (ISG15)* | Hs00192713_m1 |
| *GFAP* | Hs00157674_m1 |
| *HDAC1* | Hs00606262_g1 |
| *HDAC2* | Hs00231032_m1 |
| *HDAC3* | Hs00187320_m1 |
| *HDAC9* | Hs00206843_m1 |
| *IFITM1* | Hs01652522_g1 |
| *NANOG* | Hs02387400_g1 |
| *NGFR* | Hs00182120_m1 |
| *PROM1* | Hs01009250_m1 |
| *OCT4 (POU5F1)* | Hs03005111_g1 |
| *SUZ12* | Hs00248742_m1 |

## 2.12. Expression Vectors

Expression vectors were obtained from Clontech-Takara Bio Europe (Saint-Germain-en-Laye, France).

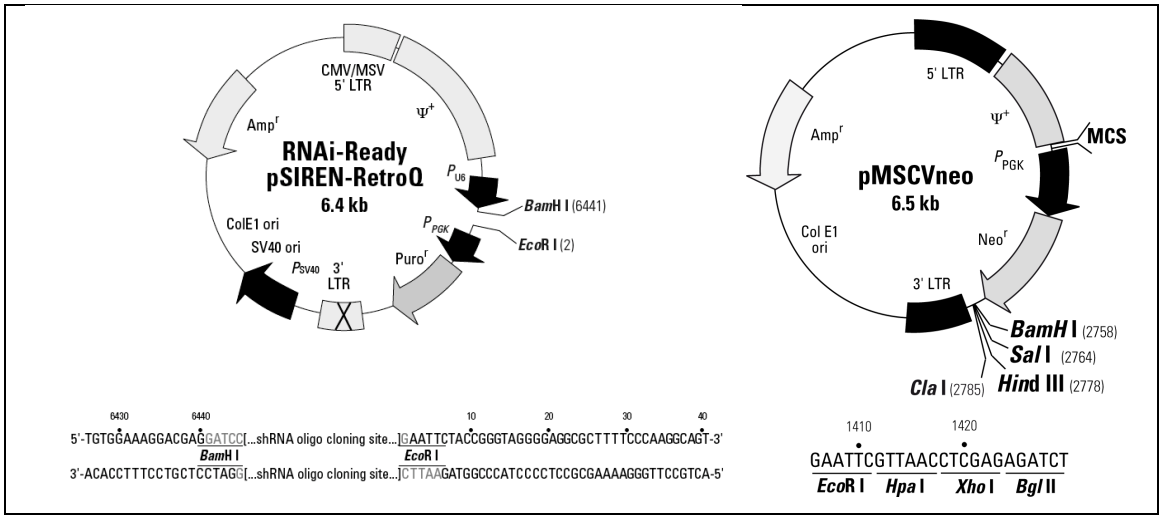

## 2.13. Human Cell Lines, Mouse Strain and Bacterial Strain

Human cell lines were purchased from the German Collection of Microorganisms and Cell Cultures (DSMZ), except A673 ET cell line, which was purchased from ATCC. SB-KMS-KS1 ET cell line was generated in the laboratory and EW7 ET cell line was kindly provided by Prof. Olivier Delattre (Institut National de la Santè et de la Recherche Medicale U830, Paris, France).

**Table 17: Description of utilized human cell lines**

| Cell Line | Description |
|---|---|
| A673 | ET cell line (type 1 translocation), established from the primary tumor of a 15-year-old woman with Ewing Tumor [129] |
| (MHH)-cALL2 | human B cell precursor leukemia, established from the peripheral blood of a 15-year-old Caucasian girl with acute lymphoblastic leukemia (cALL) [130] |
| CHP126 | Neuroblastoma cell line, established from a large retroperitoneal mass excised from a 14-month-old girl with neuroblastoma (stage III) [131] |
| EW7 | ET cell line (type 1 translocation), established from the primary tumor localized on scapula of a Ewing Tumor patient |
| MHH-ES1 | ET cell line (type 2 translocation), established from the ascites of a 12-year-old Turkish boy with Ewing Tumor of the left pelvis (with peritoneal metastasis) |
| MHH-NB11 | Neuroblastoma cell line, established from a neuroblastoma metastasis at an adrenal site of a 4-year-old white boy |
| Nalm6 | human B cell precursor leukemia, established from the peripheral blood of a 19-year-old man with acute lymphoblastic leukemia (ALL) in relapse |
| RD-ES | ET cell line (type 2 translocation), established from the primary tumor of a 19-year-old Caucasian man with Ewing Tumor of the humerus |
| SB-KMS-KS1 | ET cell line (type 1 translocation), established from an extraosseous inguinal metastasis of a 17-year old female Ewing Tumor patient (new nomenclature, originally designated as SBSR-AKS) |

| | |
|---|---|
| SH-SY5Y | Neuroblastoma cell line, established from the bone marrow biopsy of a 4-year-old girl with metastatic neuroblastoma |
| SK-ES1 | ET cell line (type 2 translocation), established from the Ewing Tumor of an 18-year-old man |
| SK-N-MC | ET cell line (type 1 translocation), established from the supraorbital metastasis of a 14-year-old girl; SK-N-MC was first classified as neuroblastom but is now widely regarded as having originated from the morphologically similar Askin's tumor related to Ewing Tumors |
| TC-71 | ET cell line (type 1 translocation), established from the tumor of a 22-year-old man with metastatic Ewing Tumor that arose in the humerus; cell line was derived in 1981 from a biopsy of recurrent tumor at the primary site |
| VH64 | ET cell line (type 2 translocation), established from an extraosseous lung metastasis of a Ewing Tumor patient [132] |
| 697 | human B cell precursor leukemia, established from the bone marrow of a 12-year-old boy with acute lymphoblastic leukemia (cALL) at relapse |

**Table 18: Description of utilized Mouse strain**

| Mouse strain | Characteristics | Origin |
|---|---|---|
| BALB/c $Rag2^{-/-}\gamma c^{-/-}$ | Absence of all T-lymphocyte, B-lymphocyte and NK cell function | Central Institute for Experimental Animals (Kawasaki, Japan). |

The *Recombination activating gene 2* (*Rag2*)-*gamma(c)* knock out (KO) mouse is a severely immunodeficient model that can be used in studies addressing vaccine development, cancer biology, or transplantation paradigms. This mutated mouse strain was generated by back-crossing of two immunocompromised mouse models, the *Rag2* KO and *gamma(c)* KO mice. Homozygous *gamma(c)* KO mice lack the *gamma(c)* receptor gene and thus, lymphocyte development is severely compromised. As a result, natural killer (NK) cell population is severely depleted in these mice, but they do have a small number of T and B cells. In order to completely eliminate the T and B lymphocyte population in that animal model, the *gamma(c)* KO mouse was back-crossed onto the *Rag2* KO mouse. Homozygous $Rag2^{-/-}$ mice lack several exons of the

*Rag2* gene, and exhibit the inability to initiate V(D)J rearrangement. These mice are therefore incapable of generating any T- and B-lymphocytes [133].

**Table 19: Description of utilized Bacterial strain**

| ***E. coli* strain** | **Genotype Description** | **Origin** |
|---|---|---|
| One Shot® TOP10 Chemically Competent | F- *mcr*A ∆(*mrr-hsd*RMS-*mcr*BC) φ80*lac*Z∆M15 ∆*lac*X74 *rec*A1 *ara*D139 ∆(*ara-leu*)7697 *gal*U *gal*K *rps*L (StrR) *end*A1 *nup*G | Invitrogen |

# 3. Methods

## 3.1. Cell culture

ET and adherent neuroblastoma cell lines were cultured in RPMI standard tumor medium (see Table 1) at 37°C (5% $CO_2$) in a humidified atmosphere. The volume of medium in a middle-sized culture flask (75 $cm^2$ adherence surface) was 20 ml and 30 ml in a large-sized flask (175 $cm^2$ adherence surface). When cells grew to confluence (every 3-4 days) the medium was removed and cells were split 1:2 to 1:10. To detach the tumor cells they were washed once with 1 x PBS and incubated 5 min with 3 ml and 5 ml 1 x trypsin at 37°C (5% $CO_2$), respectively. Detached cells were resuspended in fresh RPMI medium, centrifuged at 1300 rpm for 7 min and spread in new culture flasks.
The cALL tumor cell lines and neuroblastoma cell line CHP126 growing in suspension culture were cultured in a humidified atmosphere at 37°C (5% $CO_2$) with 30 ml RPMI standard tumor medium in a middle-sized culture flasks. Approximately every 4 days, cells were split 1:1 and cultured in 30 ml fresh medium.

Dependent on tumor cell line concentrations between 1 x $10^6$ and 1 x $10^7$ cells per 1 ml FBS / 10% DMSO were frozen in liquid nitrogen (- 192°C). After resuspension of cell pellets in an appropriate volume of pre-cooled FBS / 10% DMSO, 1 ml aliquots of the cell suspension were transferred into pre-cooled cryovials. The cryovials were placed into controlled freezing boxes, stored 12-18 h at – 80°C and were then transferred into the liquid nitrogen freezer for long-term storage.

To re-culture the cryopreserved cells, cryovials were thawed at room temperature until only small ice crystals were seen floating inside the cryovial. The content of a vial was rapidly transferred into a 50 ml Falcon tube containing 10 ml of fresh RPMI standard tumor medium. Cells were pelletized by centrifugation at 1300 rpm for 7 min, resuspended in pre-warmed culture medium and transferred into a middle-sized culture flask.

Cell amounts were determined by use of a Neubauer hemocytometer. Cell viability was assessed by trypan blue exclusion.

Cultured cells were routinely tested for mycoplasma using MycoAlert™ Mycoplasma Detection Kit according to manufacturer's instructions (Lonza Insert 2007).

## 3.2. Transient RNA interference

For transient protein knock down, transfections with short interfering RNA (siRNA) were done using HiPerFect Transfection Reagent according to standard procedures for large-scale transfection in 100 mm dishes (Qiagen Handbook 05/2008). Briefly, 1-3 x $10^6$ cells were plated into 100 mm culture dishes at a final volume of 12 ml medium containing 5 nM siRNA (see Table 11) and 36 µl transfection reagent and incubated 48-70 hours at 37 °C (5% $CO_2$) in a humidified atmosphere. To analyze transient gene knock down compared to siRNA control, RNA was isolated and gene expression was examined by quantitative RT-PCR (see 3.6. and 3.9.). To exclude an unspecific down-regulation and induction of an interferon (IFN) response, mRNA levels of IFN responsive genes were monitored by the use of specific *G1P2* and *IFITM1* gene expression assays. When expression of one of the genes was induced more than twofold after siRNA treatment, the respective siRNA was not used for further experiments.

## 3.3. Retrovirus-mediated stable RNA interference

To induce stable protein knock down, synthetic oligonucleotides corresponding to siRNA sequences (with best knock down efficiency) were cloned into the pSIREN-RetroQ retroviral vector according to manufacturer's instructions (Clontech Manual Version No. PR631543). To generate small hairpin RNAs (shRNAs) the synthetic oligonucleotides (see Table 12) were annealed to generate double strand (ds) oligonucleotides and ligated into pSIREN-RetroQ retroviral vector. The constructs were transformed into chemically competent TOP10 *E. coli* bacteria and plasmid DNA was purified using NucleoSpin® Plasmid Kit according to manufacturer's instructions (Macherey-Nagel Manual 03/2005/ Rev 02). After sequencing, the correct constructs were transfected by electroporation (capacitance of 960 µF and 270 V / 0.4 cm) into RetroPack PT67 packaging cells and viral supernatant were isolated 48 h after transfection (performed by Colette Zobywalski). To infect ET cell lines 1 x $10^5$ target cells/well were seeded into six well culture plates and incubated 12-18 h at 37°C (5% $CO_2$) in a humidified atmosphere. Subsequently, cells were incubated 24-48 h with 1 ml viral supernatant in the presence of 4 µg/ml polybrene. Selection of stable infectants occurred using 2 µg puromycin per ml RPMI medium. To analyze stable gene knock down compared to shRNA control, RNA was isolated and gene expression was examined by quantitative RT-PCR (see 3.6. and 3.9.). The mRNA levels of the IFN responsive genes *G1P2* and *IFITM1* were monitored to exclude an unspecific down-regulation and induction of genes due to an IFN response (see 3.2.).

## 3.4. Retrovirus-mediated recombinant protein expression

cDNA encoding EZH2 was purchased from ImaGenes GmbH within a pCMV-Sport6 vector (clone ID IRATp970F1210D). The sequences encoding EZH2 and the EWS/FLI1 fusion protein (described in [128]) were subcloned into the retroviral expression vector pMSCVneo according to manufacturer's instructions (Clontech Manual Version No. PR58897; performed by Colette Zobywalski). Briefly, the cDNA was ligated within pMSCVneo retroviral vector and constructs were transformed into chemically competent TOP10 *E. coli* bacteria cells. Plasmid DNA was purified using NucleoSpin® Plasmid Kit according to manufacturer's instructions, sequenced and transfected by electroporation (capacitance of 960 µF and 270 V / 0.4 cm) into RetroPack PT67 packaging cells. Viral supernatant were isolated 48 h after transfection and 1 ml were used to infect ET cell lines and MSC, respectively (see 3.3). Stable infectants were selected using 600 µg G418 per 1 ml medium. To analyze recombinant gene expression compared to vector control, RNA was isolated and gene expression was examined by quantitative RT-PCR (see 3.6. and 3.9.).

## 3.5. Isolation of genomic DNA (gDNA)

To examine genomic integration of retroviral vector constructs, total DNA from cultured cells was isolated using the DNeasy® Blood & Tissue Kit according to manufacturer's instructions (Qiagen Handbook 07/2006). In brief, 1-5 x $10^6$ cells were lysed (in 200 µl PBS containing 20 µl proteinase K) and transferred onto a DNA-binding membrane within the DNeasy® column. Specialized buffers allowed direct cell lysis and selective binding of DNA. Membranes were washed and DNA was eluted in 100 µl sterile water. DNA concentration was determined photometrically at 260 nm.

Following primers and cycler conditions were used to amplify integrated pSIREN-RetroQ and pMSCVneo vector-derived DNA sequence by PCR analysis. PCR was performed using AmpliTaq DNA Polymerase and 2 µl gDNA in a final volume of 50 µl per reaction. Amplification of ß-actin was used as template control, purified plasmid DNA as a positive and $H_2O$ as a negative control. Separation of DNA fragments occurred in 1% agarose gel by electrophoresis.

**Table 20: Primer sequences and cycler conditions to detect genomic integration of retroviral vector constructs.**

| | |
|---|---|
| primer for | 5`-GGG CAG GAA GAG GGC CTA T-3` |
| primer rev | 5`-GAG ACG TGC TAC TTC CAT TTG TC-3` |
| cycler conditions | 5 min 94°C; [30 s 94°C; 30 s 58°C; 15 s 72°C] 40 x; 7 min 72°C; ∞ 4°C |

| | |
|---|---|
| ß-actin primer for | 5`-GGC ATC GTG ATG GAC TCC G-3` |
| ß-actin primer rev | 5`-GCT GGA AGG TGG ACA GCG A-3` |
| cycler conditions | 2 min 94°C; 1 min 60°C; 1 min 72°C [30 s 94°C; 30 s 60°C; 1 min 72°C] 30 x; 30 s 94°C; 30 s 60°C; 7 min 72°C; ∞ 4°C |

### 3.6. RNA isolation using RNeasy Mini Kit

To examine gene expression by quantitative RT-PCR, RNA from cultured cells was isolated using the RNeasy® Mini Kit according to manufacturer's instructions (Qiagen Handbook 04/2006). This procedure provides an enrichment of mRNA since RNA molecules smaller than 200 bases are selectively excluded under given high-salt conditions. Briefly, up to 1 x $10^7$ cells were lysed in an appropriate volume of RLT buffer (containing 10 µl ß-mercaptoethanol per 1 ml RLT), mixed with an equal amount of 70% ethanol and vortexed. The lysate was transferred onto RNeasy® column and centrifuged 1 min at 10000 rpm. This step enabled binding of the RNA to the silica-gel membrane within the RNeasy® column. The membrane was washed three times with wash buffers with a final centrifugation at 12000 rpm for 2 min to dry the membrane. Elution of RNA was carried out with 20-30 µl RNase-free water. RNA concentration was determined photometrically at 260 nm and RNA was stored at – 80°C.

### 3.7. Isolation of total RNA using TRI Reagent RNA Isolation Kit

Isolation of RNA from frozen tissue was done using TRI Reagent RNA Isolation Kit according to manufacturer's instructions (Ambion Manual Version 0610). Briefly, frozen tissue was mechanically crushed and homogenized in 1-2 ml TRI Reagent. After addition of 100 µl BCP (1-bromo-3-chloropropane) per 1 ml TRI Reagent, probes were vigorously vortexed for 20 s and centrifuged at 4000 rpm for 60 min at 4°C. The aqueous RNA phase was transferred into a new reaction tube and RNA was precipitated by adding 500 µl isopropanol per 1 ml TRI Reagent. Sample was vortexed and centrifuged at 4000 rpm for 30 min at 4°C. The RNA pellet was washed with 1 ml 75% ethanol and again centrifuged at 4000 rpm for 10 min at 4°C. After removal of ethanol the pellet was air-dried for 2-5 min and dissolved in 50-100 µl RNase-free water. RNA concentration was determined photometrically at 260 nm and RNA was stored at – 80°C.

This RNA isolation procedure was also used to isolate total RNA from cultured cells, since RNA isolation by RNeasy Mini Kit is not sufficient for the isolation of RNA molecules smaller than 200 bases (see 3.6.).

## 3.8. cDNA synthesis

To examine gene expression by quantitative RT-PCR, isolated RNA was reverse transcribed into complementary DNA (cDNA) using the High-Capacity cDNA Reverse Transcription Kit. According to manufacturer's instructions (Applied Biosystems Insert P/N 4375222 REV A) 10 µl of 2 x RT master mix containing dNTPs, MultiScribe™ Reverse Transcriptase (RT), RT Random Primers and RT Buffer were mixed with 10 µl RNA solution (containing ~ 1 µg purified RNA). The cDNA was synthesized under the following thermal cycling conditions: 10 min 25°C; 120 min 37°C; 5 s 85°C; ∞ 4°C.

## 3.9. Quantitative Real Time PCR (qRT-PCR)

Quantification of synthesized cDNA by qRT-PCR allows examination of differential gene expression, as the amount of cDNA correspond to the amount of cellular mRNA. qRT-PCR was performed by use of Maxima™ Probe/ROX qPCR Master Mix (2x) containing Hot Start *Taq* Polymerase, PCR buffer and dNTPs. Gene-specific expression assays (see Table 16) were obtained from Applied Biosystems which consisted of a FAM™ dye-labeled TaqMan® MGB probe and two unlabeled PCR primers (TaqMan®-based detection). According to manufacturer's instructions (Fermentas PureExtreme™ Insert) analysis were carried out in 96-well format whereupon 1.25 µl of these primer assays and 0.5 µl of cDNA template were added to 12.5 µl of Maxima™ Probe/ROX qPCR Master Mix (2 x) and adjusted to a final volume of 25 µl with RNase-free water. The final concentration of primers and probe were 0.9 and 0.25 µM respectively. Gene expression profiles were normalized to the mRNA levels of the housekeeping gene *GAPDH* and calculated using the $2^{-ddCt}$ method. The mean value and standard deviation of duplicates are displayed graphically using Microsoft Excel. Fluorescence was measured with an AB 7300 Real-Time PCR System.

DNA intercalating dyes allow quantification of gene expression without requiring specific dye-labeled probes (SYBR Green-based detection). SYBR Green is a highly specific dsDNA binding fluorescent dye that enables detection of all amplified PCR products. SYBR Green-based qRT-PCR was performed by use of POWER SYBR™ GREEN PCR Master Mix (Applied Biosystems) containing SYBR Green I dye, AmpliTaq Gold® DNA Polymerase, PCR buffer and dNTPs. Gene specific primers (0.4 µM each) and 0.5 µl cDNA template were added to 12.5 µl master mix and adjusted to a final volume of 25 µl with RNase-free water. Gene expression profiles were normalized to the mRNA levels of β-actin (ACTB) and calculated using the $2^{-ddCt}$ method. The mean value and standard deviation of duplicates are displayed graphically

using Microsoft Excel. Fluorescence was measured with an AB 7300 Real-Time PCR System (Applied Biosystems).

## 3.10. Detection of EWS/FLI1

For detection of EWS/FLI1 type 1 mRNA levels no inventoried TaqMan® Gene Expression Assays was available. Thus, primers detecting EWS (sense) and FLI1 (antisense) of the fusion transcript and a probe detecting type 1 translocation were designed (see Table 21). The master mix was prepared by adding 10 µl of Maxima™ Probe/ROX qPCR Master Mix (2 x), 0.3 µM of each primer and 0.2 µM of FAM probe to 7.6 µl RNase-free water. To a final volume of 19.5 µl Master Mix per 96-well 0.5 µl of cDNA template was added. Gene expression profiles were normalized to GAPDH mRNA levels and calculated using the $2^{-ddCt}$ method. Fluorescence was measured with an AB 7300 Real-Time PCR System (Applied Biosystems).

**Table 21: Gene Expression Assay to detect EWS/FLI1 type 1 mRNA by qRT-PCR**.

| | |
|---|---|
| sense primer | 5'-TAG TTA CCC ACC CAA ACT GGA T-3' |
| antisense primer | 5'-GGG CCG TTG CTC TGT ATT CTT AC-3' |
| FAM probe | 5'-FAM-CAG CTA CGG GCA GCA GAA CCC TTC TT-TAMRA -3' |

*EWS/FLI1* type 2 translocation was detect by either SYBR Green based qRT-PCR (see 3.9.) or PCR using above-mentioned primers (see Table 21). PCR was performed using AmpliTaq DNA Polymerase and 1 µl cDNA in a final volume of 25 µl per reaction. Following cycler conditions were used: 2 min 94°C; [30 s 94°C; 30 s 59°C; 45 s 72°C] 35 x; 7 min 72°C; ∞ 4°C. Separation of PCR products occurred in 1% agarose gel by electrophoresis.

## 3.11. MicroRNA analysis

Total RNA was extracted from cells using TRI Reagent RNA Isolation Kit (see 3.7.). MicroRNA quantification was performed using the TaqMan™ MicroRNA Reverse Transcription Kit and specific TaqMan™ MicroRNA Assays as recommended by the manufacturer's instructions (Applied Biosystems Insert P/N 4367038 REV A). In brief, 1-10 ng total RNA were added to 3 µl microRNA specific RT primers and 7 µl master mix (containing MultiScribe™ Reverse Transcriptase (RT), RT Buffer, dNTPs and RNase inhibitor) to generate specific cDNA. The cDNA was synthesized under the following thermal cycling conditions: 30 min 16°C; 30 min 42°C; 5 min 85°C; ∞ 4°C.

For qRT-PCR analysis 1,33 µl of this cDNA were added to 10 µl Maxima™ Probe/ROX qPCR Master Mix (2 x) and 1 µl of specific FAM-labeled TaqMan™ MicroRNA Expression Assay at a final volume of 20 µl. Gene expression profiles were normalized to the small nucleolar RNA RNU19 and calculated using the $2^{-ddCt}$ method. The mean value and standard deviation of duplicates are displayed graphically using Microsoft Excel. Fluorescence was measured with an AB 7300 Real-Time PCR System.

### 3.12. Western Blot analysis

To examine protein expression by western blot whole protein lysates from cultured cells were generated. Cells were trypsinized, counted and washed twice with 1 x PBS. 2 – 4 x $10^6$ cells were resuspended in 200 µl 3 x Laemmli-buffer (containing 20 µl ß-mercaptoethanol per 1 ml 3 x Laemmli) and incubated at 70°C for 10 min to denature proteins. Lysates were then homogenized through a 23 gauge needle and centrifuged for 5 min at 14000 rpm. Aliquots of the supernatants were stored at - 80°C or immediately processed for SDS-polyacrylamide gel electrophoresis (SDS-PAGE).

Dependent on the molecular weight of separating protein 8-12.5% polyacrylamide gels were used for SDS-PAGE. 10 – 30 µl of protein sample were transferred to the gel and electrophoresis was carried out at 100-120 V for 1.5-2.5 h. Molecular weight of the separated proteins was determined by comparison with a prestained molecular weight standard.

For immunoblot analysis proteins were transferred onto Hybond-P PVDF membranes for 2 h at 0.8 mA / $cm^2$ using a "Semidry"-Blot device in presence of Transblot-SD buffer. After electroblotting the transferred proteins are bound to the surface of the PVDF membrane, providing access for reaction with immunodetection reagents. Unspecific binding sites were blocked by immersing the membrane in 5% skim milk / 0.05% Tween 20 for 1 h at RT or overnight at 4°C. The membrane was then probed with primary antibody (see Table 7) for appropriate time. Antibodies were diluted according to the manufacturers instructions in 5% skim milk / 0.05% Tween 20. The membrane was washed 3 x in 1 x TBST, incubated for 1 h with horseradish peroxidase (HRP) coupled secondary antibody and washed again as before plus once in 1 x TBS.

Antibody-antigen complexes were detected using the ECL-Plus Western Blotting Detection System according to manufacturer's instructions (GE Healthcare Booklet RPN2132PL Rev D 2006). This detection system is based on the oxidation of a Luminogen by HRP and peroxide, resulting in a chemoluminescent signal detectable

by a CCD camera. Signals were detected with the Gel Logic 1500 imaging system and analyzed with Kodak Molecular Imaging Software (Version 5.0).

To reactivate dried PVDF membrane, membrane was incubated in methanol (~1 min), washed once with 1 x TBST and blocked for 1 h in 5% skim milk / 0.05% Tween 20.

### 3.13. Flow cytometry

Flow cytometry was performed to analyze expression of cell surface antigens / proteins. Cells were trypsinized, counted and washed twice with 1 x PBS. Per sample 5 x $10^5$ cells were resuspended in 40 µl staining buffer with 100 µg / ml human IgG (10 µl) and incubated for 20 min on ice to block unspecific binding sites. After centrifugation (1500 rpm, 5 min, 4°C) the cells were washed once with 200 µl pre-cooled staining buffer and than incubated with 5 µl Fluorophore-labeled specific antibody (see Table 9), adjusted to a final volume of 100 µl with staining buffer. One unstained sample was used for setting up the correct forward scatter (FSC) and sideward scatter (SSC) for the cell population. One sample was stained with the isotype controls for every used fluorophore. This sample was used for setting up the correct parameters for detecting fluorescence. The samples were incubated on ice (shielded from light) for 30 minutes, washed twice with staining buffer, resuspended in 200 µl 1 x PBS and than measured with a FACSCalibur™ Flow cytometer. When the samples were to be stored for longer than two hours before measurement, the samples were fixated by resuspending in 200 µl 1 x PBS / 1% paraformaldehyde.

### 3.14. Apoptosis Assay

Apoptotic cells were analyzed using Annexin V-PE Apoptosis Detection Kit I according to manufacturer`s protocol (BD Biosciences Pharmingen™ Insert rev. 006). Briefly, 1 x $10^5$ cells were stained with 5 µl Annexin V-PE and 5 µl 7-AAD, vortexed and incubated for 15 min at RT shielded from light. Annexin-V binds to membrane phospholipid phosphatidylserine (PS). Only in apoptotic cells PS is accessible for binding through Annexin-V. 7-Amino-actinomycin (7-AAD) was used to distinguish viable from nonviable cells, since viable cells with intact cell membranes exclude 7-AAD. To set up the correct FSC, SSC and the correct parameters for detecting fluorescence an unstained sample as well as samples with Annexin V-PE and 7-AAD alone were included. Samples were measured within 1 h with a FACSCalibur™ Flow cytometer.

### 3.15. Cell cycle analysis

Cell cycle analysis was performed by flow cytometry using propidium iodide (PI), a DNA intercalating agent. Since PI fluoresces red when bound to DNA, fluorescence intensity of the stained cells correlate with the amount of DNA they contain. This allow differentiation between phases of cell cyle, as the fluorescence of cells in the $G_2$/M phase is twice as high as that of cells in the $G_0/G_1$ phase through DNA duplication during intermediate S phase. 2 x $10^6$ cells per sample were washed twice with pre-cooled probe buffer. After centrifugation at 1200 rpm for 10 min (4°C), cells were fixated by drop-wise addition of 1 ml ice-cold 70% ethanol while vortexing. Following incubation for 18-24 h at 4°C cells were centrifuged and resuspended in 1 ml staining buffer containing RNase A. Samples were incubated 30-60 min at RT (under agitation) to remove any RNA and subsequently measured with a FACSCalibur™ Flow cytometer.

### 3.16. ABCD Assay

The ABCD (avidin, biotin, complex, DNA) assay was performed to analyze binding of EWS/FLI1 fusion protein to ds oligonucleotides encoding different regions of *EZH2* promoter sequences and control sequence, respectively. The assay is based on precipitation of protein-DNA complexes via binding of biotin-labeled oligonucleotides to streptavidin-coated agarose beads followed by detection of bound protein through western blot analysis.

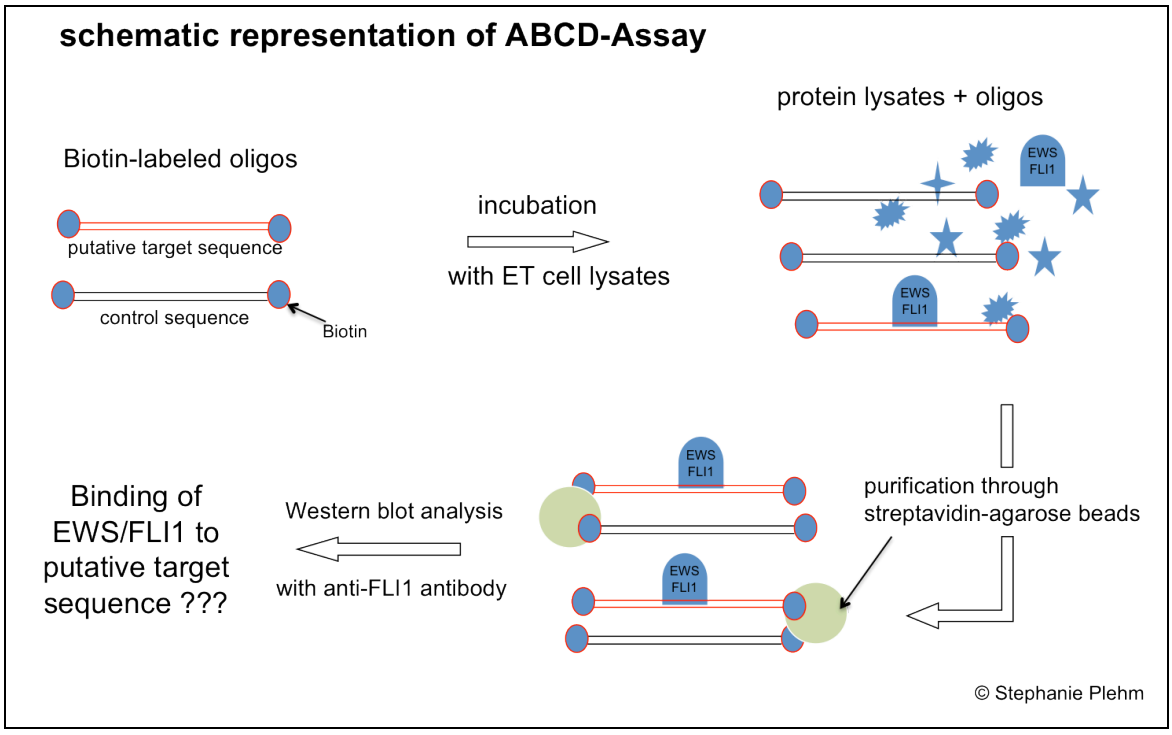


**Figure 1: Schematic representation of ABCD-Assay.**

For generation of whole cell extracts, 1 x $10^7$ cells were lysed in 1 ml NETN buffer followed by sonication (10 cycles a` 1 sec on / 1 sec off with 40% amplitude) with a Brandson Digital Sonifier. 50 µg of single stranded sense and corresponding 5`-biotinylated antisense oligonucleotides (see Table 13) were mixed 1:1 and resuspended in 10 µl 10 x Annealing Buffer at a final volume of 100 µl. Oligonucleotides were annealed under following cycling conditions (95°C 30 s, 50°C 2 min, 30°C 2 min). 200 µl of whole cell extract was mixed 1:1 with Buffer H and incubated with 2 µg of biotinylated ds oligonucleotids in the presence of 20 µg denaturated herring sperm DNA to block unspecific hybridization. Incubation occurred 5 min at 37°C followed by incubation on ice for 1 h. Per sample 50 µl streptavidin-agarose beads were added to precipitate protein-DNA complexes. After incubation at 4°C for 1 h with constant rotation, samples were washed five times with 1 ml of Buffer H and re-precipitated by centrifugation at 2200 rpm for 5 min at 4°C. Pellets were resuspended in 30 µl 3 x Laemmli Buffer and boiled for 5 min at 95°C to elute protein-DNA complexes from agarose beads. Western blot analysis (see 3.12.) with 10% SDS-gel and specific anti-FLI1 antibody was performed to detect EWS/FLI1 fusion protein. Streptavidin-HRP was used to detect biotin-labeled oligonucleotides on PVDF membranes, thereby serving as a loading control.

### 3.17. ChIP assay

Chromatin immunoprecipitation (ChIP) was performed (i) to analyze binding of EWS/FLI1 to *EZH2* promoter DNA and (ii) to analyze changes in histone modifications upon EZH2 knock down. The ChIP assay is based on precipitation of protein-gDNA-complexes through binding of specific antibodies to agarose beads followed by microarray analysis (ChIP-on-chip) or qRT-PCR analysis (ChIP-qRT-PCR) of purified genomic DNA fragments.

Crosslinking was performed with 3-5 x $10^7$ ET cells in RPMI medium with 1% formaldehyde for 10 min. After neutralization with 0.125 M glycine, cells were washed twice in ice-cooled 1 x PBS and then lysed in 1 ml RIPA-Buffer containing protease inhibitors. The genomic DNA was cut by sonication to an average DNA length of 500-1000 bp. Sample was precleared by incubation with 100 µl Protein A/G Plus agarose beads at 4°C for 1 h with constant rotation. Agarose was precipitated by centrifugation and protein concentrations of the supernatant was determined using Bio-Rad Protein Assay according to manufacturer's instructions (Bio-Rad Manual LIT33 Rev C). Immunoprecipitation was carried out by addition of 3 µg specific antibody or unspecific control IgG to 0.5 mg of precleared cell lysate at a final volume of 200 µl. Input control

of 0.1 mg precleared cell lysate was separated (no incubation with antibody) and then treated like other samples to reverse crosslink and remove proteins. After antibody incubation for 12-18 h at 4°C with constant rotation, 50 µl Protein A/G Plus agarose beads was added to the sample to precipitate protein-gDNA-complexes. Sample was incubated for 2 h at 4°C (rotation), centrifuged for 2 min at 4000 rpm and subsequently washed 3 x with 400 µl Low-Salt Buffer and two times with High-Salt Buffer. To elute DNA from agarose beads, sample was incubated with 100 µl Elution Buffer at 30°C for 30 min. Reverse crosslinking was performed by addition of 8 µl 5 M NaCl and 65 µg ribonuclease A and incubation at 65°C for 12-18 h. Proteins were removed through incubation of samples with 40 µg proteinase K for 1 h at 42°C. DNA fragments were purified using QIAquick PCR Purification Kit according to manufacturer's instructions (Qiagen Handbook 03/08). Purified genomic DNA fragments were resuspended in 30 µl $H_2O$ and 2.5 µl were used as template for control PCR. Control PCR was performed using AmpliTaq DNA Polymerase and specific *TRIM36* primers in a final volume of 25 µl per reaction (see Table 22 for primer sequences and cycling conditions). Separation of DNA fragments occurred in 3% agarose gel by electrophoresis. Purified gDNA fragments were used for analysis by qRT-PCR (SYBR Green-based detection, see 3.9. and Table 15: Primers for ChIP-qRT-PCR) or microarray technology (see 3.26.).

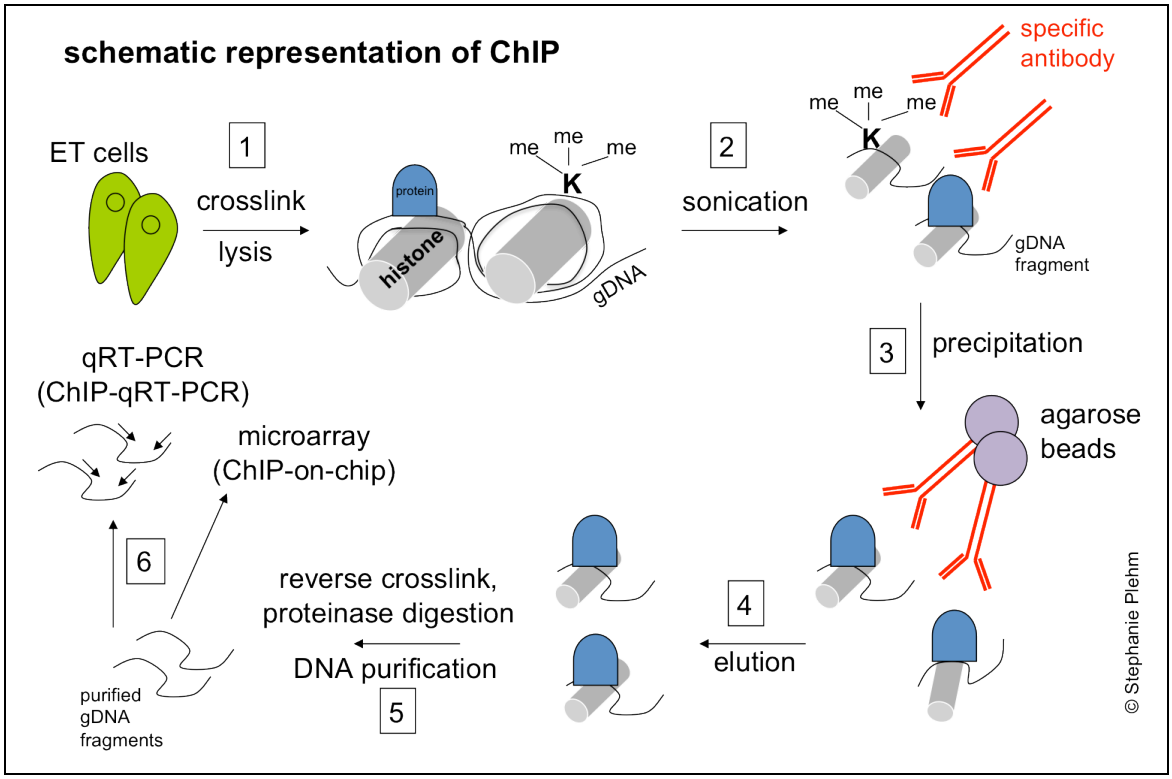


**Figure 2: Schematic representation of Chromatin Immunoprecipitation (ChIP)**

**Table 22: ChIP. Primer sequences and cycler conditions for Trim36 control PCR.**

| | |
|---|---|
| primer for | 5`- GCC CGC TTC TTG CTT TCC-3` |
| primer rev | 5`- CCG CCC ATA AGC TGT TAA CC-3` |
| cycler conditions | 1 min 95°C; [15 s 95°C; 30 s 60°C; 30 s 72°C] 33 x; 5 min 72°C; ∞ 4°C |

## 3.18. HDAC inhibitor treatment of cells

5 x $10^5$ cells per well were seeded at a final volume of 3 ml medium into six-well plates. After incubation for 24 h at 37°C (5% $CO_2$) in a humidified atmosphere, cells were treated for 24 h with 100 nM TSA and MS-275, respectively. RNA was isolated using the RNeasy® Mini Kit to analyze gene expression by qRT-PCR (see 3.6. and 3.9.).

## 3.19. BrdU incorporation assay

Cell proliferation was quantified using Cell Proliferation ELISA, BrdU (Colorimetric) Kit according to manufacturer`s protocol (Roche Instruction Manual 08/2007). Briefly, 2 x $10^3$ cells per 96-well were seeded in triplicates or octaplicates at a final volume of 100 µl and incubated at 37°C (5% $CO_2$) in a humidified atmosphere. BrdU labeling solution was added at defined times (0 h, 24 h, 48 h, 72 h). After appropriate incubation time cells were lysed and incubated with a specific peroxidase conjugated anti-BrdU-antibody to detect incorporated BrdU. Reaction product was quantified by measuring the absorbance (450 nm) using a Multiskan Ascent ELISA reader. The mean value and standard deviation are displayed graphically using Microsoft Excel. Determination of the statistical significance was carried out by using the conventional t-test. The absorbance values directly correlate to the amount of DNA synthesis and hereby to the proliferation rate of cells.

## 3.20. Endothelial tube formation assay

Cellular tube formation was tested using Matrigel Matrix assay according to the manufacturer's instruction (BD Biosciences Manual SPC-356234 Rev 5.0). Briefly, 4 - 7 x $10^4$ cells per well were seeded onto 75 µl Matrigel at a final volume of 100 µl in a 96-well plate. After 24-48 h incubation at 37°C (5% $CO_2$) in a humidified atmosphere, cells were washed and stained with 1 µg / ml Calcein AM Fluorescent Dye for 30 min. Tube formation was examined by fluorescence microscopy using a Nikon Eclipse TS 100 with an attached Nikon Coolpix 5400 camera.

## 3.21. Neuronal differentiation assay

To analyze neuron-like or astrocyte-like cell differentiation capacity of EZH2 shRNA treated A673 cells, 7 x $10^4$ cells were seeded at a final volume of 3 ml DMEM medium into six-well plates. After incubation for 24 h at 37°C (8% $CO_2$) in a humidified atmosphere, cells were treated for 5 days with 0.1 mM BHA (butylated hydroxyanisole) in the presence of 2% DMSO to induce neuronal differentiation [134]. Cells were fixated in 4% paraformaldehyde, washed two times with 1 x PBS and incubated for 30 min with 0.1% Triton X-100 to perforate membranes. To block unspecific binding sites cells were incubated for 30 min with 100 µg human IgG and then stained with an antibody directed against glial fibrillary acid protein (GFAP, see Table 8). After incubation for 12-18 h at 4°C with constant rotation cells were washed 3 x in 1 x PBS and then incubated with 10 µl FITC-labeled goat anti-mouse F(ab')2 fragment for 2 h at RT (shielded from light). Cells were washed 3 x in 1 x PBS, dried and analyzed by fluorescence microscopy using a Nikon Eclipse TS 100 with an attached Nikon Coolpix 5400 camera.

## 3.22. Colony forming assay

To analyze contact-independent growth capacity 5 x $10^3$ cells per 1.1 ml methylcellulose-based media were seeded in duplicate into a 35 mm plate according to the manufacturer's instruction (R&D Systems Manual 8/2004) and cultured for 14 days at 37°C (5% $CO_2$) in a humidified atmosphere.

## 3.23. Invasion assay

Cell invasion was studied by use of the BioCoat™ Angiogenesis System: Endothelial Cell Invasion Assay according to the manufacturer's instructions (BD Bioscience Manual SPC-354141-G rev 3.0). Briefly, for rehydration the plate was removed from − 20°C storage and allowed to adjust to room temperature. Pre-warmed RPMI medium was added to the interior of the insert wells and allowed to rehydrate for 2 h at 37°C (5% $CO_2$). Subsequently, 5 x $10^4$ cells (in 250 µl RPMI medium without FBS) were added to each insert well. As a chemoattractant, diluted bone marrow-derived serum from an ET patient was added to each of the bottom wells. The plate was incubated for 48 h at 37°C (5% $CO_2$) in a humidified atmosphere. Cell invasion was measured by staining and counting the invasive cells at the bottom side of the membranes using calcein AM solution at a concentration of 4 µg / ml. For each plate 12.5 ml of pre-warmed HBSS (Hank's buffered salt solution) was added to 50 µg calcein AM in 20 µl DMSO. The insert plate was transferred into a second BD Falcon 24-well plate

containing 0.5 ml / well of 4 µg / ml calcein AM in HBSS and incubated for 90 min at 37°C (5% $CO_2$). Cells were imaged by fluorescence microscopy using a Zeiss AxioVert 100 with AxioVision 4.7.1 software.

### 3.24. *In vivo* experiments

For the analysis of *in vivo* tumor growth 2-4 x $10^6$ ET cells and derivatives were harvested by trypsinization, washed twice with 1 x PBS and injected in a volume of 0.2 ml into immunodeficient Rag2$^{-/-}$γc$^{-/-}$ mice (see Table 18 for description of used mouse strain). To monitor local tumor growth cells were injected s.c. into the inguinal region and tumor size was determined. Mice bearing a tumor > 10 mm in diameter were considered as positive and sacrificed. Tumors were excised for immunohistology (see 3.25.) and RNA was prepared for gene expression analysis (see 3.7. and 3.9.).

For the analysis of *in vivo* invasive growth 2-4 x $10^6$ ET cells and derivatives were harvested by trypsinization and washed twice with 1 x PBS. Cells were injected in a volume of 0.2 ml intravenously into the tail vein of immunodeficient Rag2$^{-/-}$γc$^{-/-}$ mice. Four weeks later mice were sacrificed and metastatic spread was monitored in individual organs. Affected organs were excised and fixated with 4% formaldehyde for immunohistochemistry (see 3.25.).

### 3.25. Immunohistochemistry

Tumor samples and affected organs were fixated in 4% formaldehyde and paraffin embedded. Three to five micrometer thick sections from all tissues were cut and stained with antibodies and Hematoxylin and Eosin (H&E) respectively. PD Dr. med. Leticia Quintanilla-Martinez, Dr. Ilona Mossbrugger and PD Dr. Irene Esposito from the Institute of Pathology of the Helmholtz Zentrum München reviewed all sections.

### 3.26. Microarray analysis

Changes in gene expression profiles upon protein knock down by RNA interference (see 3.2. and 3.3.) were analyzed by microarray technology. Total RNA was extracted from cells using TRI Reagent RNA Isolation Kit (see 3.7.) and quantified spectrophotometrically. RNA quality was analyzed by 0.7% agarose gel electrophoresis. cRNA target synthesis and microarray hybridization were performed according to standard protocols (detailed procedure is available at www.affymetrix.com) by Ines Volkmer and Dr. Martin S. Staege (Department of Pediatrics, Martin-Luther-University Halle-Wittenberg). Data analyses occurred using Affymetrix software “Microarray Suite 5.0”. Samples were scaled to the same target intensity of 500. Subsequent analysis was

carried out with signal intensities that were log2 transformed for equal representation of over-expressed and suppressed genes and then median centered to remove biases based on single expression values. Hierarchical clustering [135] was accomplished by use of the “Genesis” software package [136]. For the identification of differentially expressed genes significance analysis of microarrays (SAM) were used [137].

ChIP-on-chip assay using promoter microarrays were performed to analyze changes in promoter DNA binding capacity and histone modifications upon protein knock down by RNA interference. The immunoprecipitated DNA (see 3.17.) was amplified using whole genome amplification (WGA) (Sigma). The products were purified and labeled with amino-allyl-conjugated dUTP using the BioPrime labeling kit (Invitrogen). Products were purified and coupled with monofunctional NHS-ester (cyanine dye) Cy3 or Cy5. Hybridization was performed for 24 h and slides were scanned using an Axon 4000B scanner. Scanned images were analyzed with Spotreader (Niles Scientific Inc.; Portola Valley, CA) software. The data analysis was performed with BRB Array Tool software (National Cancer Institute, http://linus.nci.nih.gov/BRB-ArrayTools.html). An oligonucleotide promoter microarray with 50mer oligonucleotides was utilized that represented more than 33000 genomic loci centered around the transcriptional start sites of ~ 10000 promoters of well characterized human genes and 500 miRNAs. On average three oligonucleotides represented each promoter and surrounded the transcriptional start site usually between - 1500 and + 500. Experiments were performed in duplicate (GSE15890). Rebecca Unland and Prof. Dr. Carsten Müller-Tidow (Department of Pediatric Hematology and Oncology, University Children’s Hospital, Münster) performed amplification, labeling and hybridization of DNA as well as data and statistical significance analyses.

# 4. Results

## 4.1. Role of PcG protein EZH2 in Ewing Tumor (ET) pathogenesis

### 4.1.1. EZH2 is over-expressed in primary ET tissue and ET cell lines

To identify an ET-specific gene expression profile customized high-density DNA microarrays (EOS-Hu01) containing 35356 oligonucleotide probe sets were carried out to query a total of 25194 gene clusters. 11 ET samples were analyzed in a previous study in comparison to 133 normal tissues of diverse origin. This analysis revealed 37 genes that are highly up-regulated or even specifically expressed in ET [128]. *EZH2* is one of those genes that are highly up-regulated, but not exclusively expressed in ET (see Figure 3).

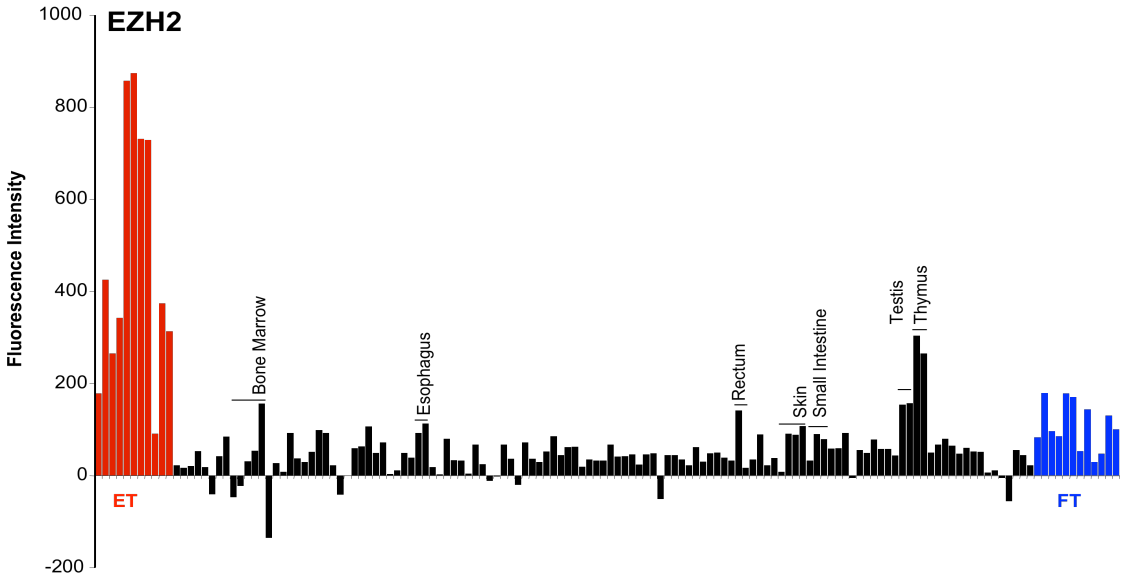


**Figure 3: EZH2 expression in ET compared to healthy tissue.** Microarray data that show expression of EZH2 on mRNA level in primary ET tissue samples (red bars) compared to normal body tissue (black bars) and fetal tissue (blue bars).

To verify the observed expression profile, EZH2 mRNA levels of established ET cell lines and of other pediatric tumor cell lines, which display a cytological appearance similar to ET (small-round-blue), were quantified. qRT-PCR analysis using a specific *EZH2* gene expression assay revealed considerably higher EZH2 mRNA levels in all analyzed ET cell lines compared to diverse neuroblastoma and common acute lymphoblastic leukemia (cALL) cell lines (Figure 4). In detail A673, TC71 and MHHES1 showed an almost 3-fold higher level of EZH2 mRNAs, while SK-ES1, SK-N-MC and SB-KMS-KS1 ET cell lines revealed EZH2 mRNA levels that were up to 12-20-fold higher as compared to neuroblastoma and cALL cell lines. Furthermore, EZH2

expression was similar in all tested ET cell lines, independent of the translocation type (*EWS/FLI1* type 1 [exon 7 of *EWSR1* is fused to exon 6 of *FLI1*]: SK-N-MC, TC71, SB-KMS-KS1 and A673; *EWS/FLI1* type 2 [includes *FLI1* exon 5]: MHHES1 and SK-ES1).

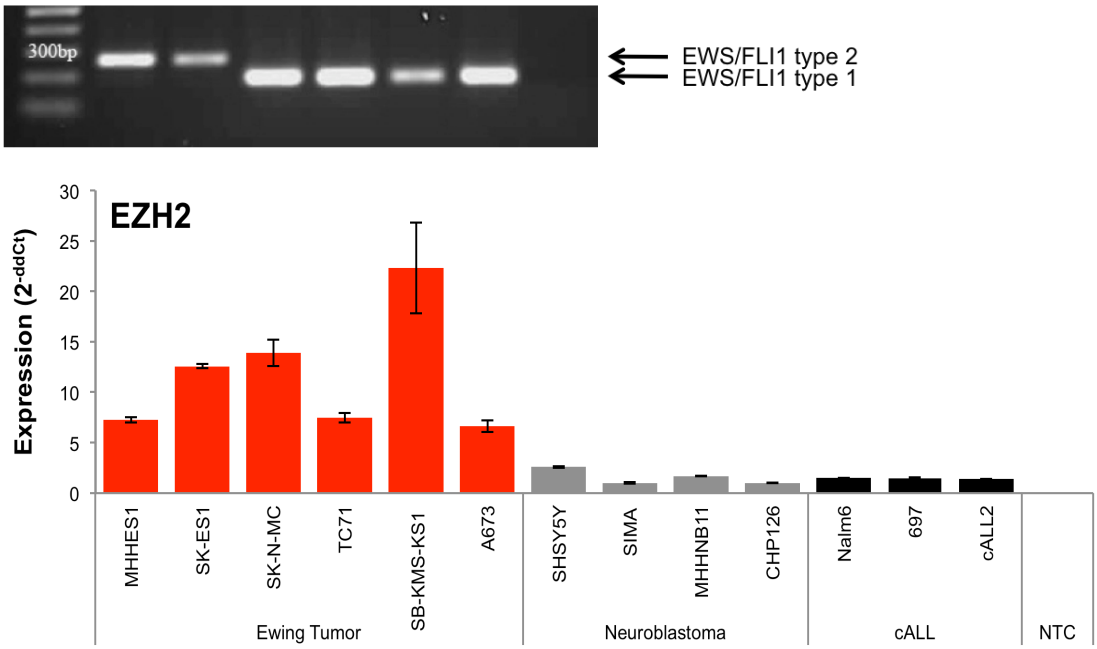


**Figure 4: EZH2 expression in different ET cell lines compared to other pediatric tumor cell lines.** Expression of EZH2 on mRNA level in different ET cell lines (red bars), neuroblastoma (gray bars) as well as common acute lymphoblastic leukemia (cALL) cell lines (black bars) quantified by qRT-PCR is shown. NTC, non-template control ($H_2O$). Error bars represent standard deviation (SD). Image of *EWS/FLI1* type 1 and type 2 PCR products separated in 1% agarose gel. *EWS/FLI1* type 2 translocations contain one additional exon of the *FLI1* fusion gene resulting in larger PCR products. *EWS/FLI1* PCR products correlate lower panel ET cell lines.

### 4.1.2. EWS/FLI1 fusion protein induces EZH2 expression

To assess whether *EZH2* expression is induced by the EWS/FLI1 fusion protein, cDNA of the EWS/FLI1 fusion gene was cloned into the pMSCVneo expression vector. Under the control of a stem cell virus LTR, EWS/FLI1 cDNA was over-expressed in the human mesenchymal stem cell (MSC) lines V54.2 and L87 [138]. The induction of ectopic EWS/FLI1 expression was detected by qRT-PCR with specific EWS/FLI1 primers (see 3.10.) and by Western blot analysis using an anti-FLI1 antibody, which detects the ~68 kDa EWS/FLI1 fusion protein.

Expression of the EWS/FLI1 fusion protein was verified on mRNA as well as on protein levels in several MSC cell clones (see Figure 5, upper and middle panel; Western blot analysis was performed by Diana Löwel, medical doctoral candidate).

MSC cell clones with highest ectopic EWS/FLI1 expression were analyzed for EZH2 induction by qRT-PCR. Expression of the EWS/FLI1 fusion protein in MSC led to an up to 3.5-fold increase of EZH2 mRNA level as compared to the corresponding vector control (Figure 5, lower panel). This up-regulation of EZH2 seems to be dose-dependent since MSC cell clones with strongest EWS/FLI1 induction showed the highest up-regulation of EZH2 expression (more than threefold) compared to vector control (VC).

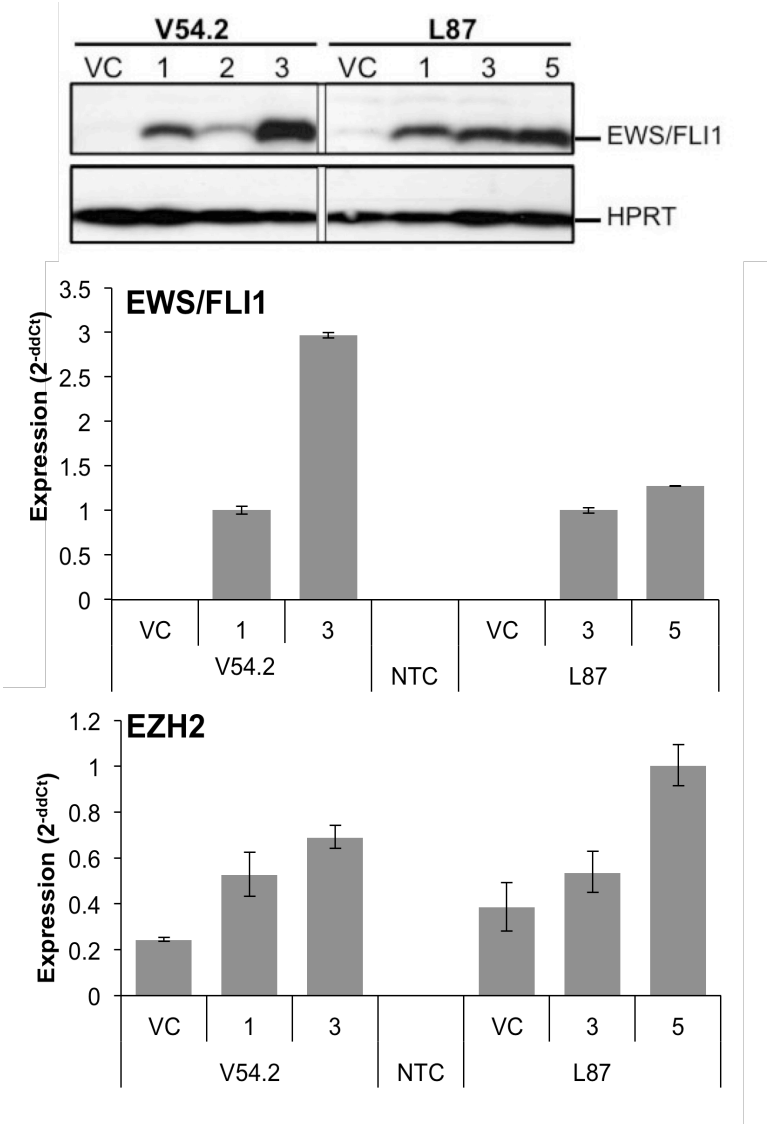


**Figure 5: Quantification of EZH2 mRNA levels of human MSC cell lines V54.2 and L87, which ectopically express the EWS/FLI1 fusion protein.**

**Upper panel:** Western blot analysis protein lysates of different MSC cell clones (numbered) after retroviral gene transfer of EWS/FLI1 cDNA. EWS/FLI1 fusion protein (~ 68kDa) was detected with an anti-FLI1 antibody (1:500). HPRT was used as loading control.
**Middle panel:** Quantification of EWS/FLI1 mRNA levels by qRT-PCR. Different MSC cell clones after retroviral gene transfer of EWS/FLI1 cDNA or empty pMSCVneo vector (VC) are shown.
**Lower panel:** Quantification of EZH2 mRNA levels of EWS/FLI1-expressing MSC cell clones and corresponding controls by qRT-PCR using a specific *EZH2* gene expression assay.
VC, vector control; NTC, non-template control ($H_2O$).

To further investigate, whether *EZH2* expression is influenced by the EWS/FLI1 fusion protein, EWS/FLI1 was knocked down in ET cell lines and subsequently analyzed for EZH2 mRNA expression. Two different specifically designed EWS/FLI1 siRNAs [139] were used for transient transfection of SK-N-MC and SB-KMS-KS1 ET cell lines (see Table 11 containing specific siRNA sequences and 3.2. for transient transfection). 85 h after transient transfection, RNA was isolated and qRT-PCR analyses were performed

to measure EWS/FLI1 and EZH2 mRNA expression, respectively. As shown in Figure 6, EWS/FLI1#II siRNA treatment reduced EWS/FLI1 mRNA levels down to 10-15% of normal values in both ET cell lines compared to control siRNA (non-silencing siRNA) transfected cells. Furthermore, knock down of EWS/FLI1 reduced EZH2 mRNA levels down to 25-50% compared to control cells.

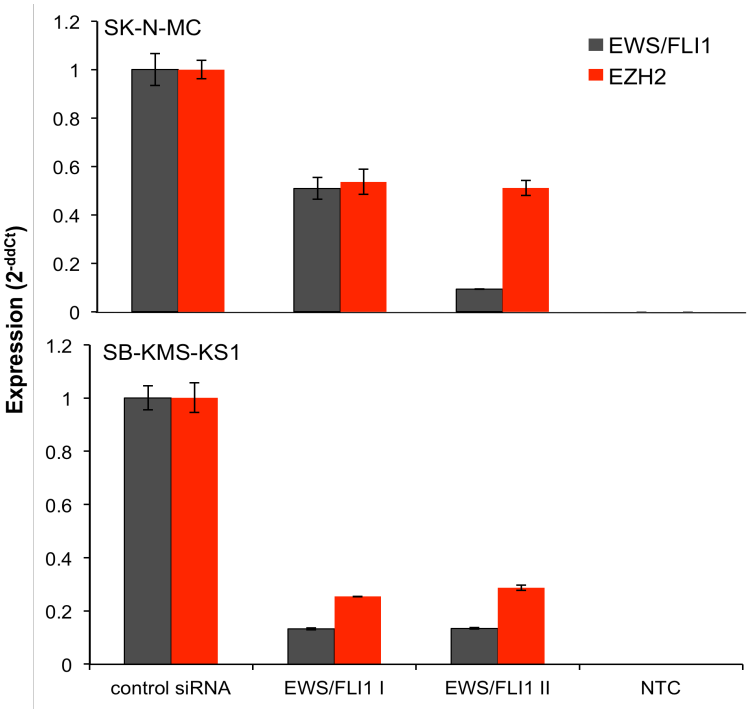


**Figure 6: Quantification of EZH2 mRNA levels (red bars) in EWS/FLI1 suppressed (grey bars) SK-N-MC and SB-KMS-KS1 ET cell lines as analyzed by qRT-PCR.** Two different EWS/FLI1 siRNAs were used to knock down EWS/FLI1 expression described as EWS/FLI1 I and EWS/FLI1 II, respectively. Control siRNA: non-silencing siRNA, NTC, non-template control ($H_2O$).

### 4.1.3. EWS/FLI1 fusion protein binds to *EZH2* promoter sequence *in vitro* and *in vivo*

To examine whether *EZH2* is a direct target of the EWS/FLI1 fusion protein in ET, the *EZH2* promoter region was analyzed for potential ETS transcription factor binding sites. ETS transcription factors contain an evolutionarily conserved domain of about 85 amino acid residues that mediate binding to purine-rich DNA sequences with a GGAA/T core consensus motif [140]. Analysis of the *EZH2* promoter sequence revealed several potential ETS recognition sites between - 1081 and - 3800 bp upstream of the transcriptional start site (TSS). Since the untranslocated allele of the *FLI1* gene is not expressed in ET [141], an anti-FLI1 antibody could be used to specifically detect the EWS/FLI1 fusion protein.

An ABCD (avidin, biotin, complex, DNA) assay was performed to evaluate binding of the EWS/FLI1 fusion protein to these ETS recognition sites *in vitro*. Biotin-labeled oligonucleotides encoding different ETS recognition sites (see Figure 7 upper panel A, B) and a control sequence (C, without any GGAA/T motif) were synthesized and incubated with whole cell lysates of A673 and MHHES1 ET cell lines (see 3.16. ABCD

assay and Table 13 with sequences of synthetic oligonucleotides). Precipitation of the biotin-labeled oligonucleotides with the help of streptavidin-coated agarose beads and subsequent Western blot analysis using an anti-FLI1 antibody showed binding of EWS/FLI1 fusion proteins to both synthetic oligonucleotides encoding identified ETS recognition sites (see Figure 7 lower panel). Endogenous EWS/FLI1 was detectable after incubation with oligonucleotides containing the GGAA/T motif 3 times (B) as well as 4 times (A), while no EWS/FLI1 was detectable after incubation with the control oligonucleotides (C).

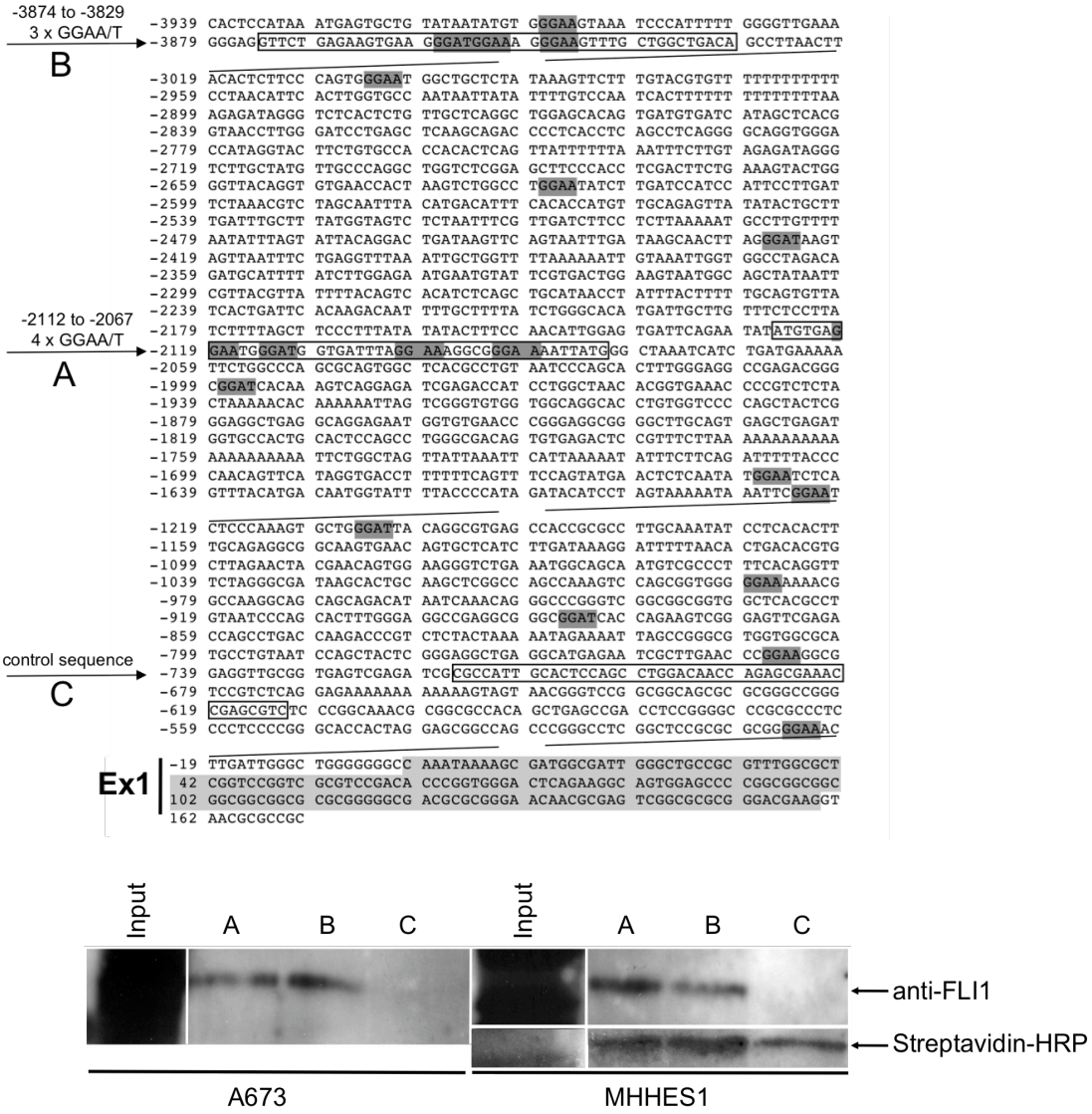


**Figure 7: ABCD Assay to analyze binding of EWS/FLI1 fusion protein to ETS transcription factor binding sites within *EZH2* promoter region *in vitro*. Upper panel:** Promoter sequence (- 1 to - 3939 bp upstream of the TSS) and first exon (Ex1) of *EZH2* gene. Sequences and positions (boxes) of used synthetic oligonucleotides encoding ETS binding motifs GGAA/T (A,B) and control sequence (C). **Lower panel:** Detection of endogenous, co-precipitated EWS/FLI1 fusion protein by Western blot analysis using an anti-FLI1 antibody. 10 µl of A673 and MHHES1 whole cell lysates served as input control. Streptavidin-HRP was used as loading control exemplarily shown for MHHES1 Western blot.

To validate native binding of the EWS/FLI1 fusion protein to ETS recognition sites within the *EZH2* promoter *in vivo*, chromatin immunoprecipitations (ChIP) with subsequent qRT-PCR analysis were performed (see 3.17. ChIP-qRT-PCR and Table 15 containing utilized primer pairs). These analyses included a third potential ETS recognition site at – 1081 bp upstream of the TSS and a control region at - 4400 bp, which is devoid of ETS recognition sequences. ChIPs were performed in A673 ET cells using the anti-FLI1 antibody and an unspecific rabbit control IgG to control for non-specific antibody binding. The precipitated and purified genomic DNA fragments were analyzed by PCR and qRT-PCR. Results were compared to and normalized for IgG and non-specific binding to an unrelated genomic region to exclude experimental artifacts, respectively.

PCR analysis of the eluted genomic fragments showed a precipitation of genomic fragments encoding the region - 1081 bp upstream of the *EZH2* transcriptional start site (see Figure 8 upper panel). No PCR products were detectable within the eluate of control IgG and $H_2O$ negative control. Comparison of the enrichment of all three potential ETS recognition sites by qRT-PCR (Figure 8 lower panel) showed a considerably lower enrichment of genomic fragments encoding ETS recognition sites at - 2120 bp and -3778 bp compared to region - 1081 bp identified in initial experiments. However, these analyses clearly revealed the binding of endogenous EWS/FLI1 to the *EZH2* promoter *in vivo*, especially to the conserved ETS recognition sequence at - 1081 bp upstream of the *EZH2* transcriptional start site.

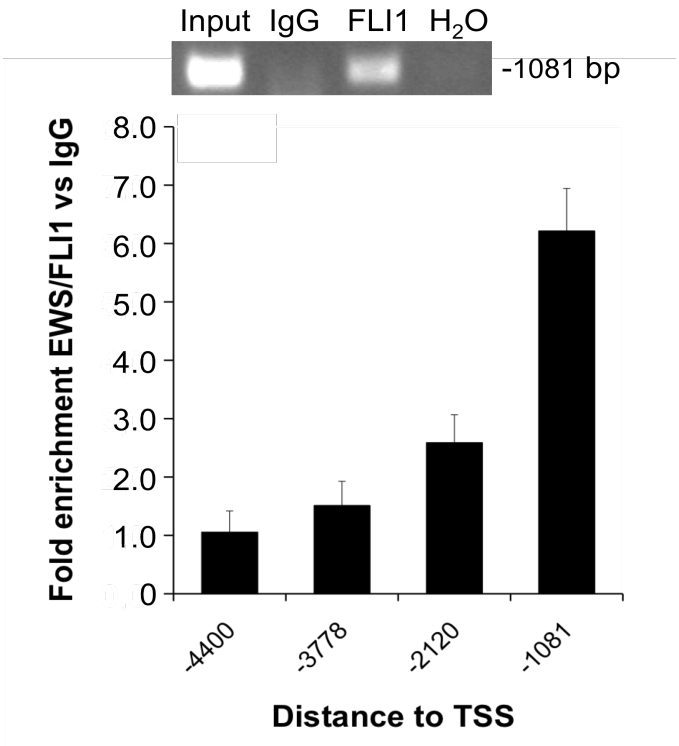


**Figure 8: ChIP experiments to analyze binding of EWS/FLI1 to *EZH2* promoter region *in vivo*.** PCR and qRT-PCR analyses of genomic fragments precipitated by anti-FLI1 antibody and control IgG antibody, respectively.
**Upper panel:** Analyses of eluates precipitated with anti-FLI1 or anti-IgG control antibodies by PCR using a specific primer pair that amplify the – 1081 region upstream of the *EZH2* transcriptional start site (TSS). Input control served as positive and $H_2O$ as negative control. PCR products were separated in 3% agarose gel. **Lower panel**: qRT-PCR analysis to compare enrichment of different potential ETS recognition sites within the *EZH2* promoter region after precipitation with anti-FLI1 antibody. The - 4400 region served as control. The bars indicate the mean of 4 independent ChIPs.

### 4.1.4. siRNA and shRNA treatment lead to reduced EZH2 mRNA level in different ET cell lines

To assess the role of EZH2 in ET pathogenesis, several *in vitro* and *in vivo* assays were performed using ET cell lines with siRNA- and shRNA-mediated suppression of EZH2 expression, respectively. To identify appropriate siRNAs for efficient EZH2 knock down, two different siRNAs were tested in several ET cell lines by transient RNA interference (see Table 11 for specific siRNA target sequences and 3.2. for transient transfection). 48-90 h after transient transfection, RNA was isolated and expression knock down efficiency was tested by qRT-PCR using a specific *EZH2* gene expression assay. Figure 9 shows, that transfection with siRNA EZH2_2 resulted in a down-regulation of EZH2 expression to 27-37% of the value measured in control siRNA treated cells. EZH2_7 siRNA treatment enabled a reduction of EZH2 mRNA levels down to ~12-29% as compared to corresponding controls in all tested ET cell lines. Thus, siRNA EZH2_7 was applied in further transient transfection experiments.

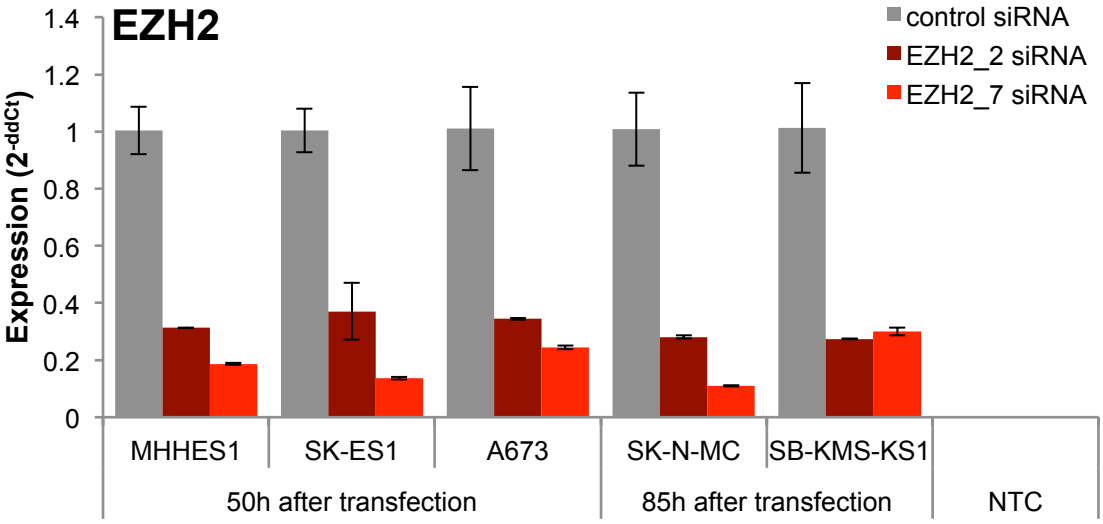


**Figure 9: Quantification of EZH2 mRNA levels after transient transfection assays with two different EZH2 targeting siRNAs (EZH2_2 and EZH2_7) by qRT-PCR analysis**. Several ET cell lines were tested for transient EZH2 knock down compared to corresponding controls, transfected with non-silencing control siRNA. Analyses were performed 50 h and 80 h after transient transfection, respectively. NTC, non-template control ($H_2O$).

To generate ET cell lines with constitutive EZH2 knock down, oligonucleotides encoding the target sequence of EZH2_7 siRNA were cloned into the pSIREN RetroQ vector (see Table 12 containing respective oligonucleotide sequences and 3.3. for retroviral gene transfer). This method enabled a constitutive knock down of EZH2, mediated by permanent expression of small hairpin RNAs (shRNA), which induce

Dicer-dependent cleavage of endogenous EZH2 mRNA. Retroviral gene transfer of this pSIREN$^{EZH2}$ construct into A673 ET cell line and subsequent analysis of stable infected A673 cells by qRT-PCR, showed a suppression of EZH2 mRNA levels down to 20-40% (two different pSIREN$^{EZH2}$-infected A673 clones are shown in Figure 10 lower panel) compared to control cells (pSIREN$^{neg.shRNA}$-infected and untreated A673 cells). Western blot analysis with whole cell extracts, separated in a 10% SDS-PAGE, revealed also a reduction of EZH2 on protein level. EZH2 mRNA amounts correlated with protein amounts (compare pSIREN$^{EZH2\#1}$ and pSIREN$^{EZH2\#2}$ mRNA and protein levels, Figure 10 upper panel). EZH2 protein expression was determined using an antibody, which specifically recognizes human EZH2 protein.

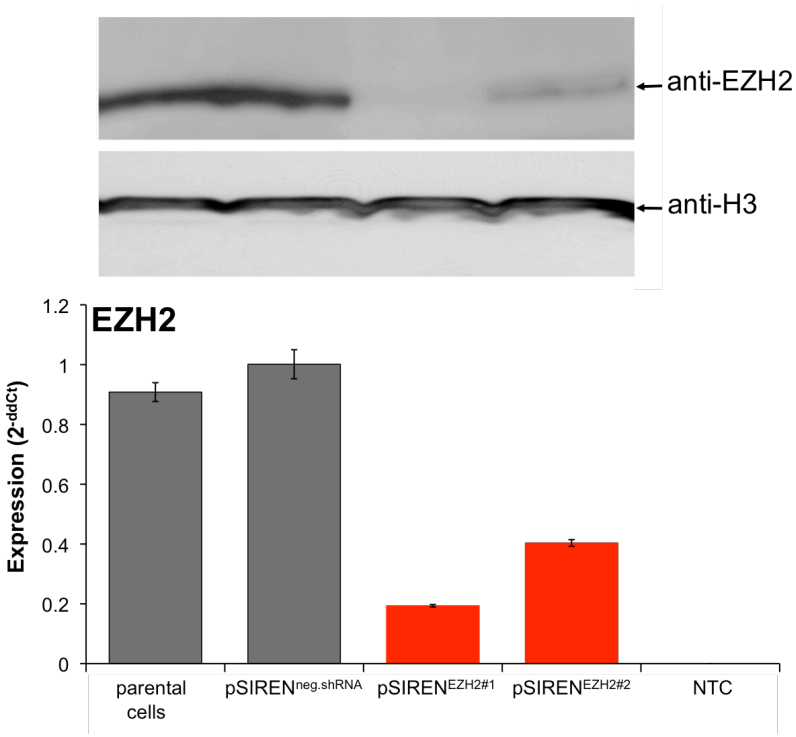


**Figure 10: Quantification of EZH2 expression on mRNA and protein level after constitutive EZH2 knock down in A673 ET cells.**
**Upper panel:** Detection of EZH2 protein amounts using a specific antibody that recognizes EZH2 protein (~ 100 kDA) by Western blot analysis. Detection of histone H3 by a specific anti-H3 antibody served as loading control**. Lower panel:** Quantification of EZH2 mRNA levels by qRT-PCR analysis. pSIREN$^{EZH2\#1}$ and pSIREN$^{EZH2\#2}$ represent two different A673 clones. neg.shRNA, non-silencing shRNA, NTC, non-template control.

### 4.1.5. EZH2 suppression influences neither apoptosis nor cell proliferation in ET cell lines

Proliferation and apoptosis assays were performed to address the question, whether EZH2 knock down alters the proliferative or apoptotic behavior of ET cells. Both transiently transfected and stably infected A673 cells with reduced EZH2 expression were analyzed using BrdU incorporation assay (see 3.19.) and Annexin V-PE Apoptosis Detection Kit I (see 3.14.). As exemplified for transient EZH2 suppressed A673 cells, neither proliferation (Figure 11) nor apoptosis (Table 23) was influenced by

EZH2 suppression. EZH2_7 siRNA and control siRNA treated cells showed similar absorption values and percentages of 7-AAD$^+$ and Annexin$^+$ apoptotic cells as analyzed by ELISA reader and FACS analysis, respectively.

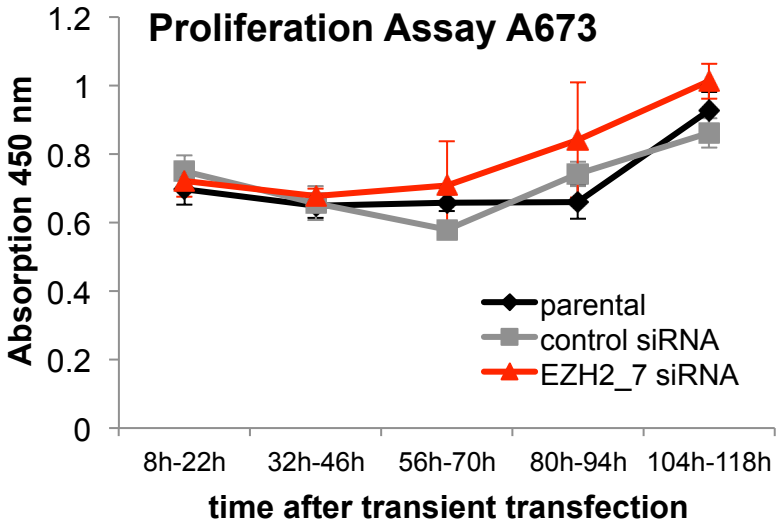


**Figure 11: Proliferation assay of EZH2 siRNA treated A673 cells and control cells.** Within each time period, cells were incubated with BrdU for 14 h before measurement. Simultaneously, RNA was isolated to monitor EZH2 suppression, which was down to 30% of normal values measured in control cells at each reading point. The error bars indicate standard deviation of triplicates.

**Table 23: Apoptosis assay of A673 cells and derivates.**
Results of a representative FACS analysis are shown.

| treatment | gated events / cell counts | 7-AAD$^+$/Annexin$^+$ |
|---|---|---|
| untreated | 4147 | 4.30% |
| control siRNA | 3728 | 5.10% |
| EZH2_7 siRNA | 4025 | 5.78% |

Additionally, cell cycle analyses of synchronized and EZH2 siRNA treated ET cells were performed to examine a possible correlation between EZH2 expression and cell cycle progression. This analysis identified neither cell cycle-dependent EZH2 expression nor a cell cycle arrest after EZH2 suppression (data not shown).

### 4.1.6. Knock down of EZH2 inhibits contact-independent growth *in vitro*

To test whether EZH2 influences contact-independent growth capacity of ET cells *in vitro*, colony formation assays using methylcellulose-based media were performed (see 3.22.). Stably pSIREN$^{EZH2}$-infected A673 cells (#1 and #2) and corresponding control A673 cells were tested in duplicates (5 x $10^3$ each) and incubated for 14 days at 37°C (5% $CO_2$) in a humidified atmosphere. As can be seen in Figure 12, both A673 pSIREN$^{EZH2}$ clones lost their ability for contact-independent growth in colony forming assay compared to parental (untreated) and pSIREN$^{neg.shRNA}$-infected A673 cells.

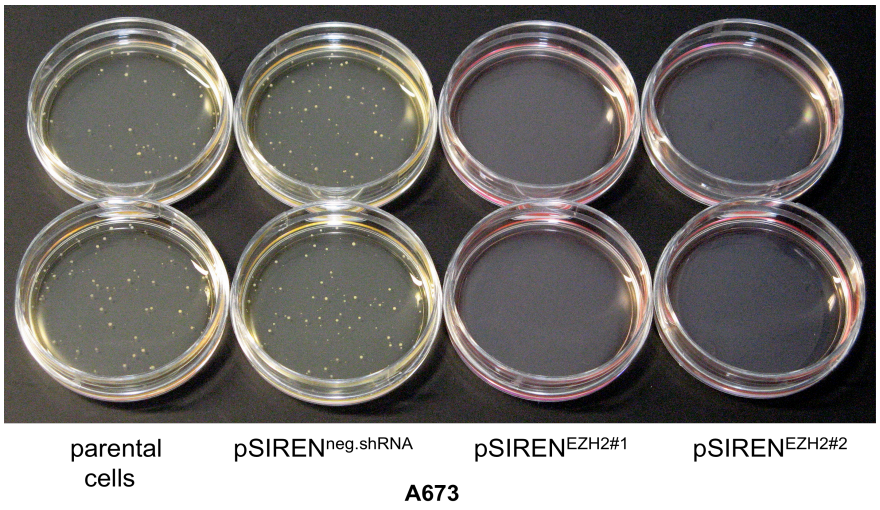


**Figure 12: Colony forming assay of A673 pSIREN$^{EZH2}$ – infected and control cells to analyze contact-independent growth *in vitro*.** EZH2#1 and #2 represent two different A673 pSIREN infectants. neg.shRNA, non-silencing shRNA.

### 4.1.7. Knock down of EZH2 inhibits tumor growth *in vivo*

To analyze whether down-regulation of EZH2 has an effect on the tumorigenic growth potential of ET cells *in vivo*, stably pSIREN$^{EZH2}$-infected A673 cells and the respective controls were injected subcutaneously into the inguinal region of immunodeficient Rag2$^{-/-}\gamma_C^{-/-}$ mice (see Table 18 for description of mouse model). As shown in Figure 13, reduction of EZH2 expression resulted in a considerable delay of tumor growth as compared to the controls. This inhibition seemed to be dose-dependent, since the clone with the stronger EZH2 suppression (EZH2#1) revealed the most prominent delay in tumor growth.

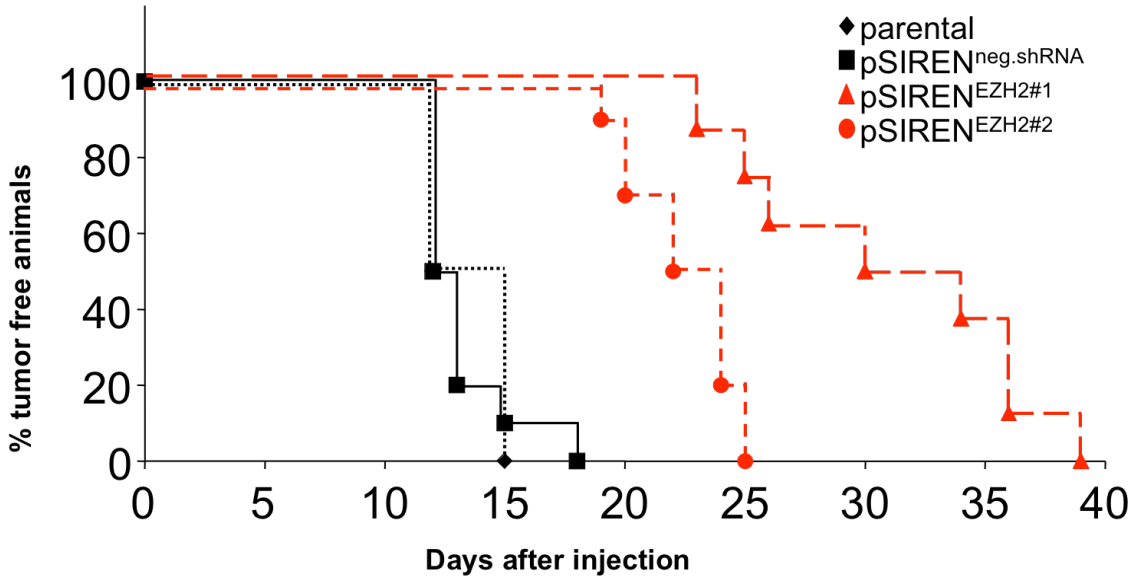


**Figure 13: Kaplan-Meier plot of local tumor growth.** The combined results of two individual experiments with altogether 9-10 mice per group are shown. Immunodeficient Rag2$^{-/-}\gamma_C^{-/-}$ mice with an average tumor size > 10 mm in diameter were considered positive and were sacrificed (dots).

Furthermore, to investigate the influence of EZH2 on metastatic behavior of ET cells, the same stably pSIREN$^{EZH2}$-infected A673 cells and corresponding controls were injected intravenously into the tail vein of Rag2$^{-/-}\gamma_C^{-/-}$ mice. As shown in Figure 14 metastasis into the lungs and liver was strongly inhibited by suppression of EZH2 (the mean number of apparent liver metastases is shown in Appendix 10.2.). While A673 control infectants (pSIREN$^{neg.shRNA}$) colonized the lungs and liver (metastases replaced almost the entire parenchyma of the lung), pSIREN$^{EZH2\#1}$ infectants lost their ability to metastasize in lung and liver tissue. Similarly, the inhibition of the metastatic behavior seems to be dose-dependent, since A673 pSIREN$^{EZH2\#2}$ cells with a lower reduction of EZH2 expression still metastasized into the lungs and liver but resulted in clearly decreased amounts of metastases within the lungs. Additionally, control infectants metastasized into the kidney (2/4) and into the subclavicular connective tissue (1/4).

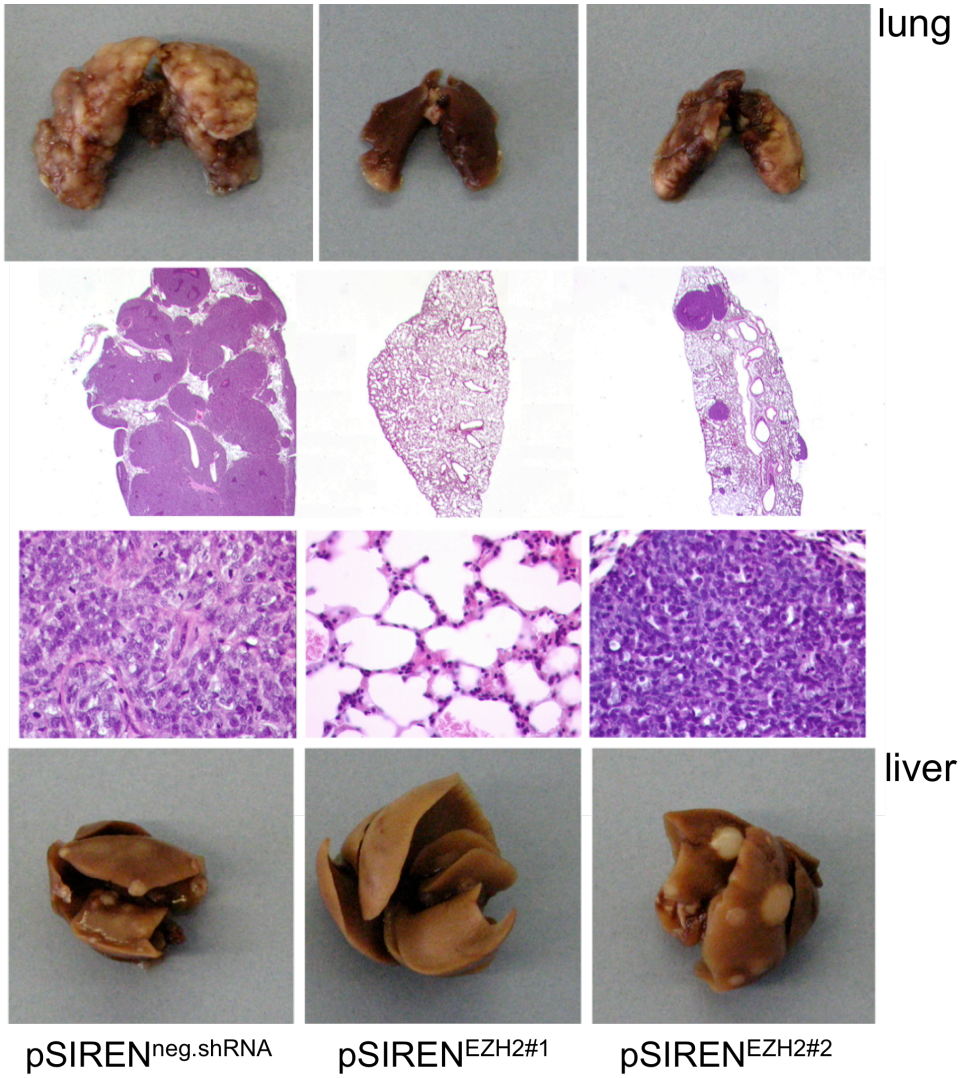


**Figure 14: Affected organs of Rag2$^{-/-}\gamma c^{-/-}$ mice after intravenous injection of pSIREN$^{EZH2}$ and pSIREN$^{neg.shRNA}$ infected A673 ET cells.** Representative lungs (upper panel) and livers (lower panel) of 1 out of 4 mice per group are shown. **Middle panel:** H&E (hematoxylin and eosin) staining of paraffin embedded lungs (magnification 12 x and 400 x, respectively).

The histologic examination of the lungs confirmed these findings (Figure 14 middle panel). Even though the size of pSIREN$^{EZH2\#2}$-induced liver metastases exceeded the size of those of pSIREN$^{neg.shRNA}$ (see Figure 14 lower panel), immunohistochemistry of liver sections demonstrated that EZH2 protein was still reduced in pSIREN$^{EZH2}$-derived metastases as compared to controls (Figure 15).

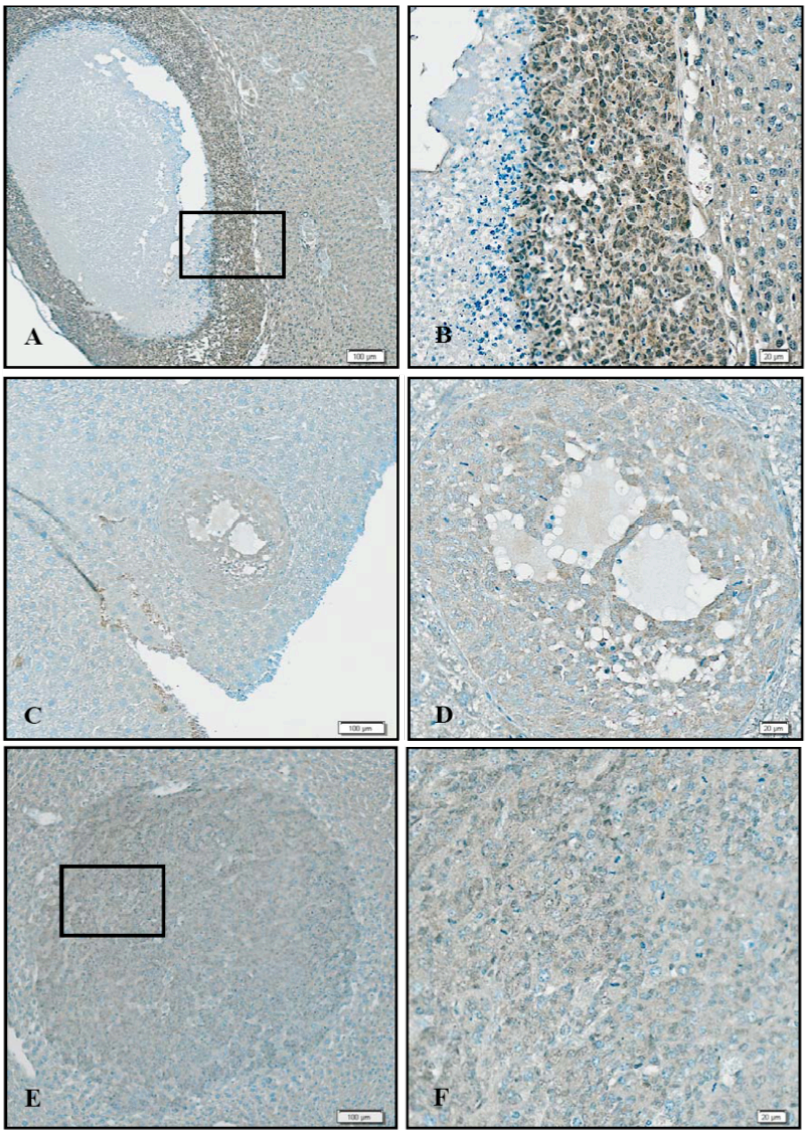


**Figure 15:**
**EZH2 staining (brown) of paraffin embedded liver sections from Rag2$^{-/-}$γc$^{-/-}$ mice after intravenous injection of pSIREN$^{EZH2}$ – and pSIREN$^{neg.shRNA}$ – infected A673 cells.** IHC was executed according to standard procedures with a rabbit polyclonal EZH2 antibody (Abgent ; 1:30).
**A, B:** pSIREN$^{neg.shRNA}$-derived liver tumor.
**C, D:** pSIREN$^{EZH2\#1}$-derived liver tumor. One mouse microscopically exhibited a single mass in the liver that resembled one small tumor. This tumor was confined to the endothelial lining of the blood vessels indicative for a non-invasive tumor formation
**E, F:** pSIREN$^{EZH2\#2}$-derived liver tumor.
Left panel shows 80x and right panel 300x magnification.
Blue background staining due to subsequent hematoxylin counter staining.

All affected organs and local tumor tissues were analyzed by histo- and immunohistochemistry. Morphology and proliferation as well as CD99 and EZH2 expression of the tumor cells were examined. All tumors showed typical histological characteristics of ET (small-round-blue) and areas of necrosis as well as hemorrhage within the tumor mass. The tumors were characterized by the uniform appearance of densely packed, CD99-positive cells containing round nuclei without distinct cytoplasm outlines. Mitoses were present and numerous in all cases as analyzed by Ki67 staining. No differences in morphology and proliferation were seen between pSIREN$^{neg.shRNA}$- and pSIREN$^{EZH2}$-derived tumors (data not shown).

### 4.1.8. EZH2 siRNA and TSA treated ET cells reveal similar gene expression profiles

To further elucidate the observed growth-inhibiting effect and to identify downstream targets regulated by EZH2, microarray analysis of transiently EZH2 and control siRNA transfected A673 cells, respectively, were performed. In order to examine, whether EZH2-mediated gene regulation requires endogenous histone deacetylase (HDAC) activity, HDAC inhibitor treated ET cells were included in these microarray analyses. The involvement of HDACs was reported by Varambally et al., who showed that EZH2 mediated gene silencing could be reverted by Trichostatin A (TSA) treatment in prostate cancer [142].

Total RNA was isolated from A673 ET cells transiently transfected with EZH2 / control siRNA for 48 h or incubated with 100 nM of the pan-HDAC inhibitor Trichostatin A (TSA) for 24 h (experiments initiated by Sabine Rößler, MD). RNA was prepared and hybridized to an Affymetrix HG U133A microarray (see 3.26.). Subsequently, microarray data were evaluated by significance analysis of microarrays (SAM), discovering 259 genes that were induced after EZH2 siRNA or TSA treatment. Figure 16 shows the 100 most significantly up-regulated genes (left panel). Analyses that include only fold changes greater than 1.7 and conventional t-test values less than 0.05 (p-value) discovered 36 genes, of which 23 were up-regulated and 13 down-regulated (see Figure 16 right panel) compared to control siRNA and DMSO, respectively.

Interestingly, these analyses showed that both EZH2 siRNA and TSA treatment led to an up-regulation of genes involved in cell differentiation, predominantly responsible for neuronal and endothelial differentiation. Among these, epithelial membrane protein (EMP1), annexin A13 (ANXA13) and basonuclin 1 (BNC1) are important for epithelial cell differentiation. EPH receptor B2 (EPHB2), glial fibrillary acidic protein (GFAP), growth associated protein 43 (GAP43), SRY (sex determining region Y)-box 11 (SOX11), activated leukocyte cell adhesion molecule (ALCAM), protocadherin 11 X-linked / Y-linked (PCDH11X/Y) are involved in nervous system development. In contrast, amongst others the nerve growth factor receptor (NGFR), described as an essential marker of neuroectodermal stem cells [143], was down-regulated after EZH2 siRNA and TSA treatment (see Figure 16 right panel).

The analyses also showed, that EZH2 expression is not influenced by TSA treatment. Analyzed control cells as well as TSA treated cells revealed comparable levels of EZH2 expression (right panel, red arrow). The microarray results additionally confirm a reduction of EZH2 expression upon EZH2 siRNA treatment, as controlled before by qRT-PCR analyses.

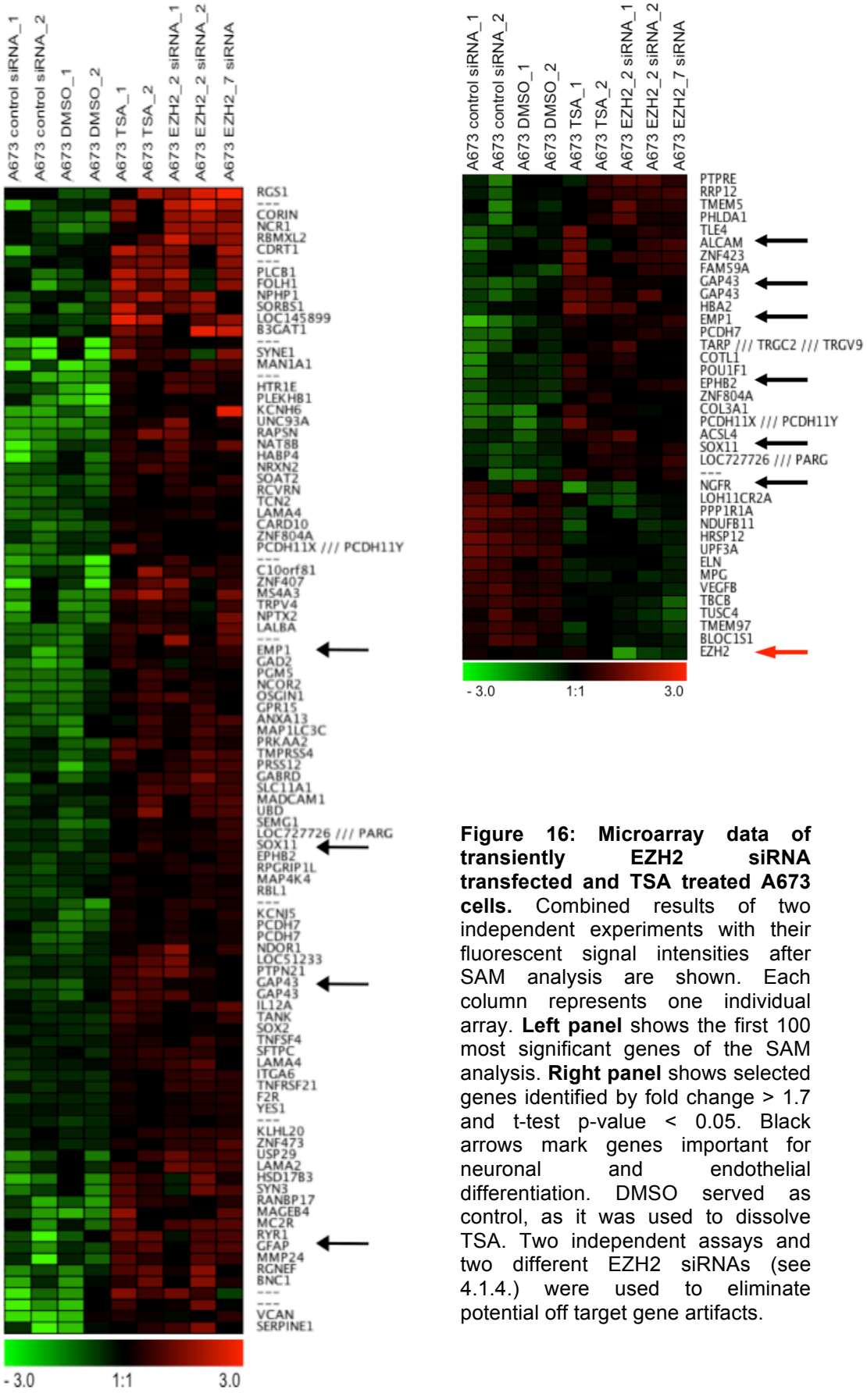


**Figure 16: Microarray data of transiently EZH2 siRNA transfected and TSA treated A673 cells.** Combined results of two independent experiments with their fluorescent signal intensities after SAM analysis are shown. Each column represents one individual array. **Left panel** shows the first 100 most significant genes of the SAM analysis. **Right panel** shows selected genes identified by fold change > 1.7 and t-test p-value < 0.05. Black arrows mark genes important for neuronal and endothelial differentiation. DMSO served as control, as it was used to dissolve TSA. Two independent assays and two different EZH2 siRNAs (see 4.1.4.) were used to eliminate potential off target gene artifacts.

### 4.1.9. Knock down of EZH2, EED and SUZ12 results in similar modulations of differentiation genes

To verify the microarray data, gene expression of different EZH2 siRNA treated ET cell lines was analyzed by qRT-PCR using specific *EPHB2*, *EMP1*, *GAP43* and *NGFR* gene expression assays. Additionally, embryonic ectoderm development (EED) and suppressor of zeste (SUZ12), the two other main components of the polycomb repressive complex 2 (PRC2), were transiently knocked down, to determine whether EZH2 regulates gene expression via PRC2.

To knock down EED and SUZ12, different siRNAs were tested by transient transfection (see 3.2.) in different ET cell lines. As shown in Figure 17 (bottom panel), EED_6 siRNA treatment resulted in a down-regulation of EED mRNA levels to 8-22%, while SUZ12_6 siRNA treatment reduced SUZ12 mRNA levels down to 8-16% compared to control siRNA treated cells.

Results in Figure 17 show that EZH2, EED as well as SUZ12 knock down in A673 and MHHES1 cells increased EPHB2, EMP1 and GAP43 mRNA levels up to 1.5-6-fold, while NGFR mRNA levels were reduced to 60-30% compared to corresponding controls ET cell lines, emphasizing PRC2 mediated regulation of these genes.

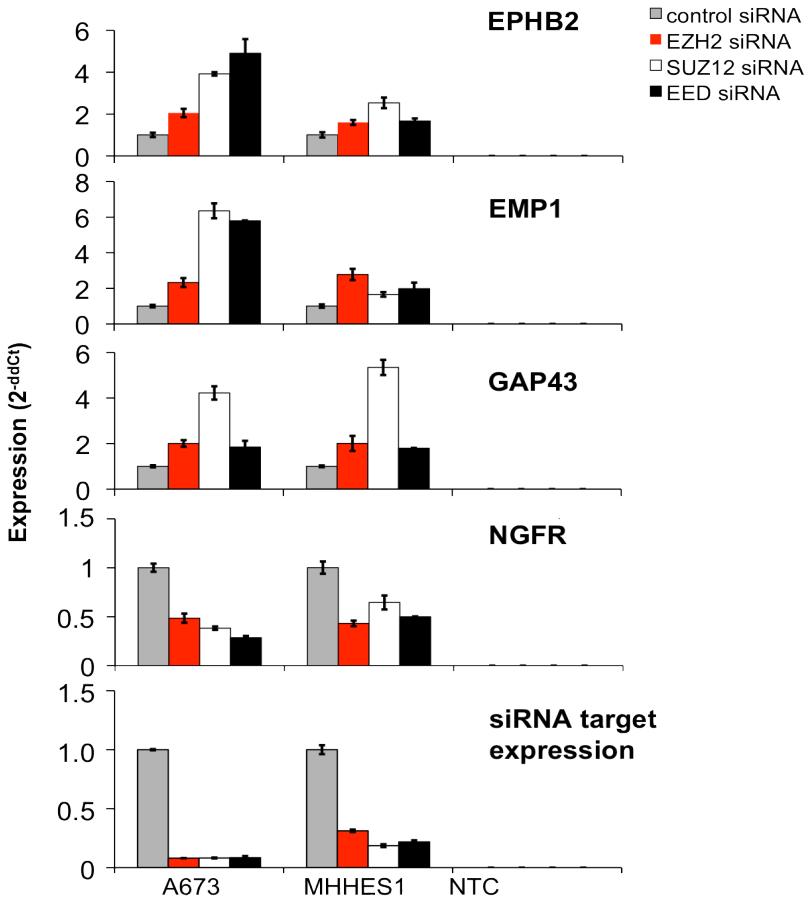


**Figure 17: Verification of microarray data.** Expression of endothelial and neuronal differentiation genes in EZH2, EED or SUZ12 suppressed ET cell lines, respectively. 60 h after transient siRNA transfection, RNA of A673 and MHHES1 ET cells was isolated and corresponding cDNA was analyzed by qRT-PCR. Target gene expression after siRNA-mediated suppression of EZH2, SUZ12 and EED mRNA levels compared to treatment with control siRNA is shown. NTC, non-template control ($H_2O$).

### 4.1.10. EED and SUZ12 are not over-expressed in primary ET and ET cell lines

Additionally, microarray data (see 4.1.1.) were analyzed to test whether the PRC2 components EED and SUZ12 are similarly over-expressed in ET compared to healthy tissues, as observed for EZH2 (see Figure 18 upper panel). Furthermore, qRT-PCR analyses of EWS/FLI1 siRNA treated ET cells were performed to examine whether EWS/FLI1 fusion protein similarly influences EED and SUZ12 expression (see Figure 18 lower panel). However, these analyses revealed, that amongst PRC2 components only EZH2 expression is increased in ET and influenced by the EWS/FLI1 fusion protein.

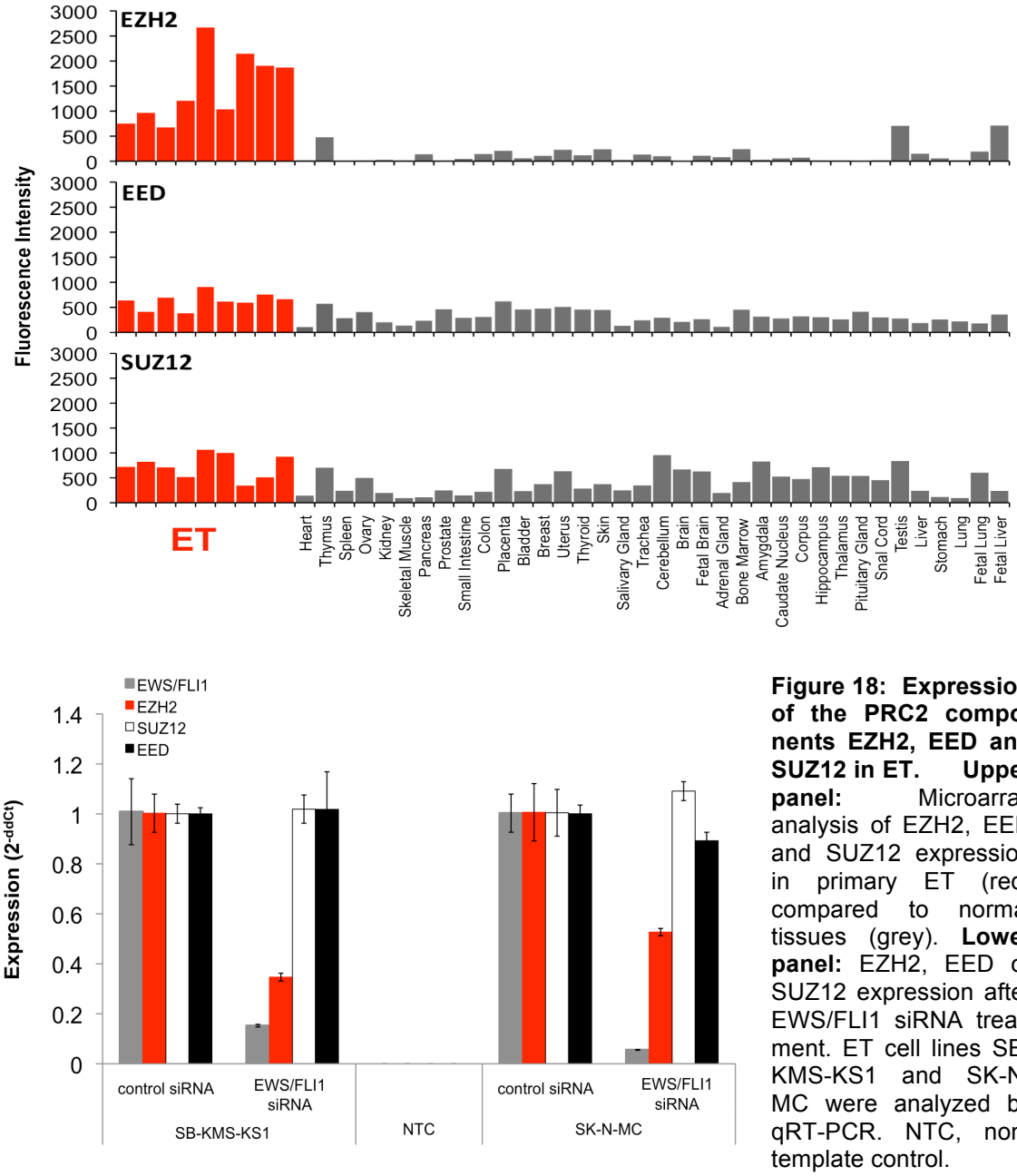


**Figure 18: Expression of the PRC2 components EZH2, EED and SUZ12 in ET. Upper panel:** Microarray analysis of EZH2, EED and SUZ12 expression in primary ET (red) compared to normal tissues (grey). **Lower panel:** EZH2, EED or SUZ12 expression after EWS/FLI1 siRNA treatment. ET cell lines SB-KMS-KS1 and SK-N-MC were analyzed by qRT-PCR. NTC, non-template control.

### 4.1.11. EZH2 knock down inhibits expression of stem cell genes

Both, microarray analysis (4.1.8.) and qRT-PCR analysis (4.1.9) revealed a reduced NGFR expression after EZH2 suppression. To further investigate the mechanism of this regulation through EZH2, NGFR expression of EZH2 over-expressing A673 ET cells (pMSCVneo$^{EZH2}$, see 3.4.) was quantified by qRT-PCR. Furthermore, to distinguish between EZH2- or EWS/FLI1-mediated *NGFR* gene regulation, respectively, EWS/FLI1 expression of A673 cells was stably knocked down by retroviral gene transfer of an appropriate shRNA construct (pSIREN$^{EWS/FLI1}$, see 3.3.) before ectopic induction of EZH2 expression. Results demonstrate (Figure 19) that only over-expression of EZH2 resulted in an increase of NGFR mRNA levels (up to 2.3-fold in three different pMSCVneo$^{EZH2}$ clones compared to controls), while a direct regulation of NGFR expression via EWS/FLI1 was not observed.

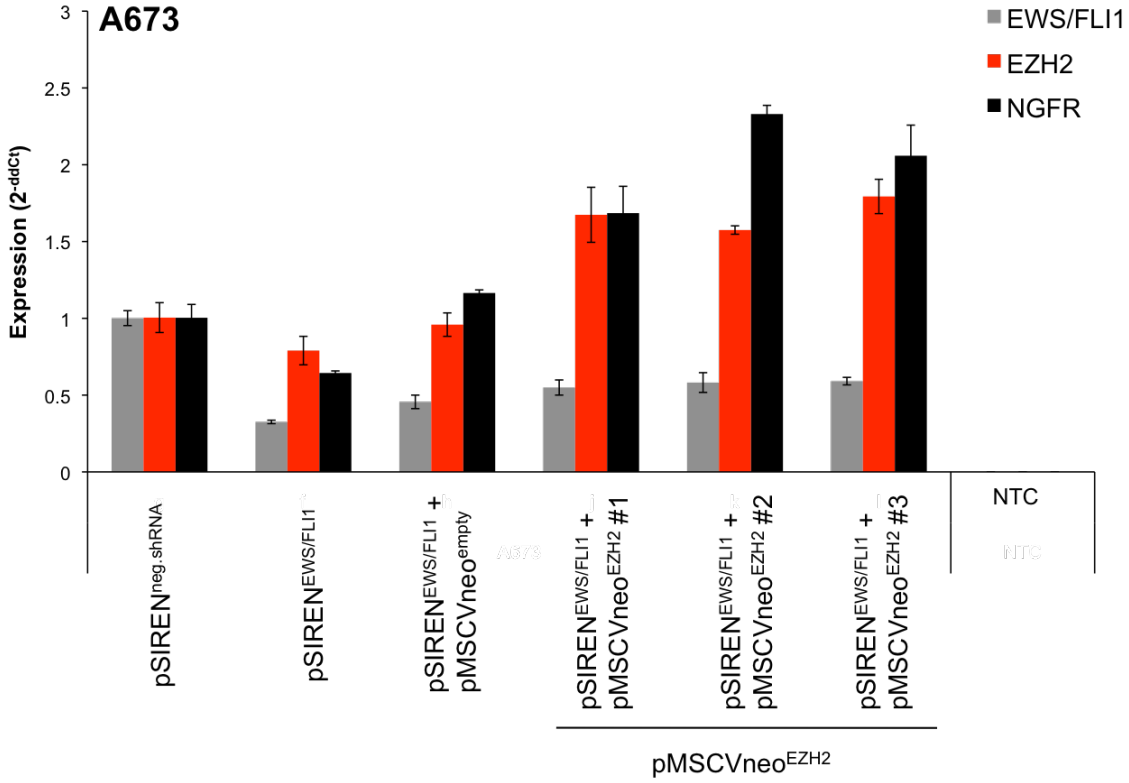


**Figure 19: NGFR expression of A673 ET cells that ectopically express EZH2 after retroviral gene transfer.** NGFR mRNA levels of three different A673 clones with increased EZH2 expression (pMSCVneo$^{EZH2}$ #1,2,3) and control cells were analyzed by qRT-PCR. NTC, non-template control.

Since not only NGFR but also other stem cell markers, including NANOG, are highly expressed in ET (see Figure 20), qRT-PCR analysis was performed to determine the potential influence of EZH2 on the expression level of stem cell markers NANOG and OCT4. Figure 20 demonstrates (upper panel) that transient suppression of EZH2

inhibited NANOG and OCT4 expression in different ET cell lines, similar to the neuroectodermal stem cell marker NGFR (Figure 17).

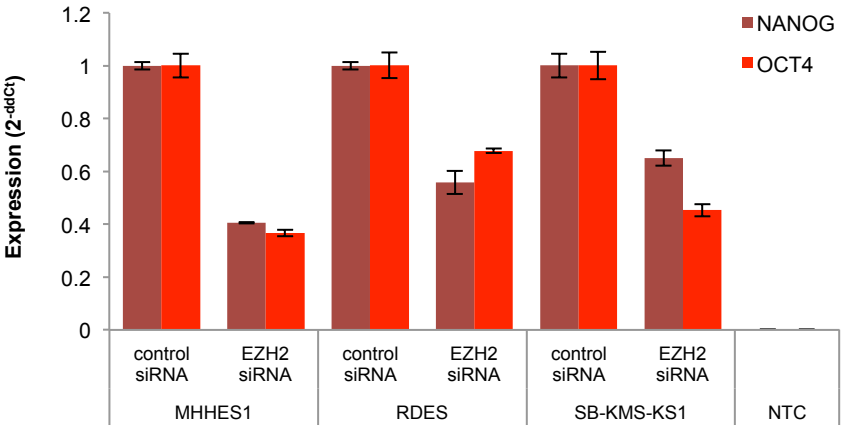


**Figure 20: Expression of stem cell genes in ET. Upper panel:** mRNA levels of OCT4 and NANOG in EZH2 suppressed ET cell lines analyzed by qRT-PCR. NTC, $H_2O$ control **Lower panel:** Microarray analysis of NANOG and NGFR expression in primary ET (red) compared to normal tissue (black).

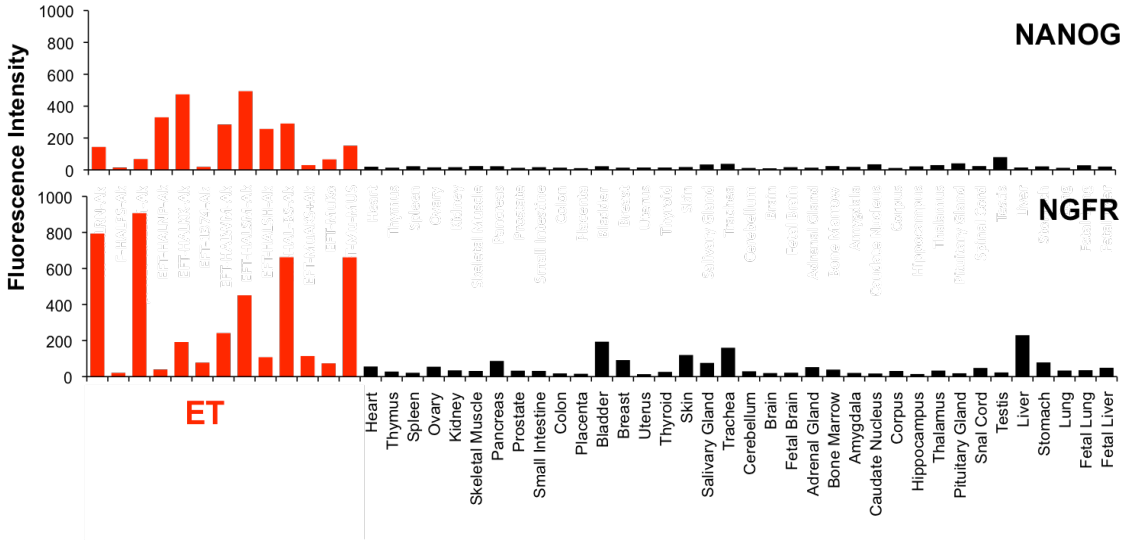


### 4.1.12. HDAC inhibitor treatment increases expression of endothelial and neuronal differentiation genes in different ET cell lines

To further explore the microarray data that revealed an induction of differentiation genes after Trichostatin A (TSA) treatment (see Figure 16), gene expression analyses of TSA treated ET cells were validated by qRT-PCR. Additionally, isolated RNA of ET cells treated with the HDAC inhibitor MS-275 was included in this experiment to specify the type of HDACs involved in this process. While TSA was reported as a pan-HDAC inhibitor, MS-275 specifically inhibits class I HDACs (HDAC1, 2 and 3) and the class II A HDAC9 [144].

TSA as well as MS-275 treatment induced the expression of the endothelial and neuronal differentiation genes *ALCAM*, *EMP1*, *EPHB2*, *GAP43* and *GFAP* up to 12-fold on mRNA level compared to corresponding controls (Figure 21). However, analysis of NGFR expression provided conflicting results, since some ET cell lines showed an induction, whereas others demonstrated a reduction of NGFR mRNA levels after HDAC inhibitor treatment (data not shown).

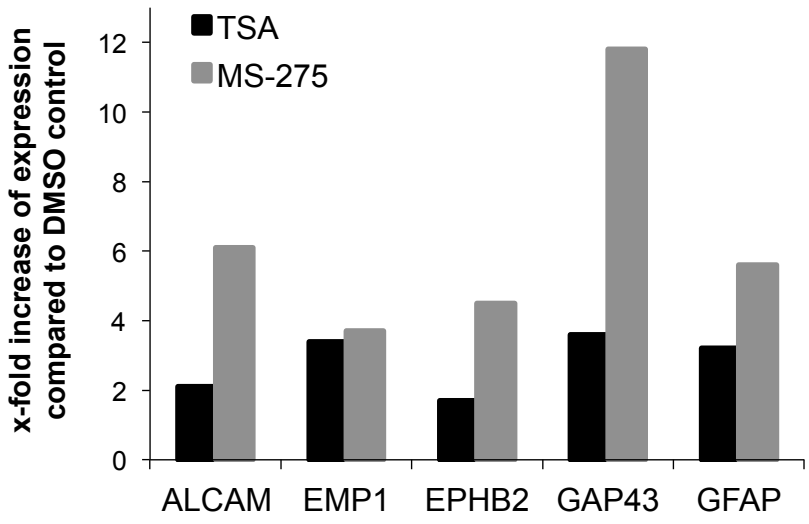


**Figure 21: Induction of differentiation genes after HDAC inhibitor treatment.**
Fold changes of mRNA levels compared to DMSO treated (control) cells are shown. Cells were treated with 100 nM TSA and MS-275 for 24 h, respectively. Gene expression was analyzed by qRT-PCR. Results of SB-KMS-KS1 cells are shown. Induction was confirmed in other ET cell lines.

Furthermore, knock down experiments using specific HDAC1, 2, 3 as well as HDAC9 siRNAs revealed an induction of several differentiation genes after suppression of HDAC2 and HDAC9, but not after HDAC1 and HDAC3 siRNA treatment in different ET cell lines, further specifying the involved HDACs regulating these genes (data not shown). However, HDAC2 as well as HDAC9 knock down consistently led to a reduced expression of GFAP and EMP1.

### 4.1.13. EZH2 knock down alters histone 3 (H3) modifications

Since EZH2 was reported to mediate trimethylation at lysine 27 of histone H3 (H3K27me3), global histone modifications after EZH2 suppression were analyzed by Western blot. In addition to H3K27me3, acetylation of histone H3 was analyzed, since treatment of ET cells with EZH2 siRNA as well as with different histone deacetylase inhibitors led to a similar induction of differentiation genes. Both, transiently and stably transfected ET cell lines revealed a global decrease of H3K27me3 after EZH2 suppression, as exemplarily shown for transiently EZH2 siRNA transfected MHHES1 ET cells in Figure 22. Simultaneously, transient as well as constitutive down-regulation of EZH2 increased the overall acetylation at lysine 9 and lysine 14 of histone H3 (H3K9/14ac). Similarly, an induction of differentiation genes was observed on protein

level: Western blot analyses using a specific anti-GAP43 antibody revealed an increase of GAP43 expression in A673 ET cells after reduced EZH2 expression and increased H3K9/14ac (Figure 22).

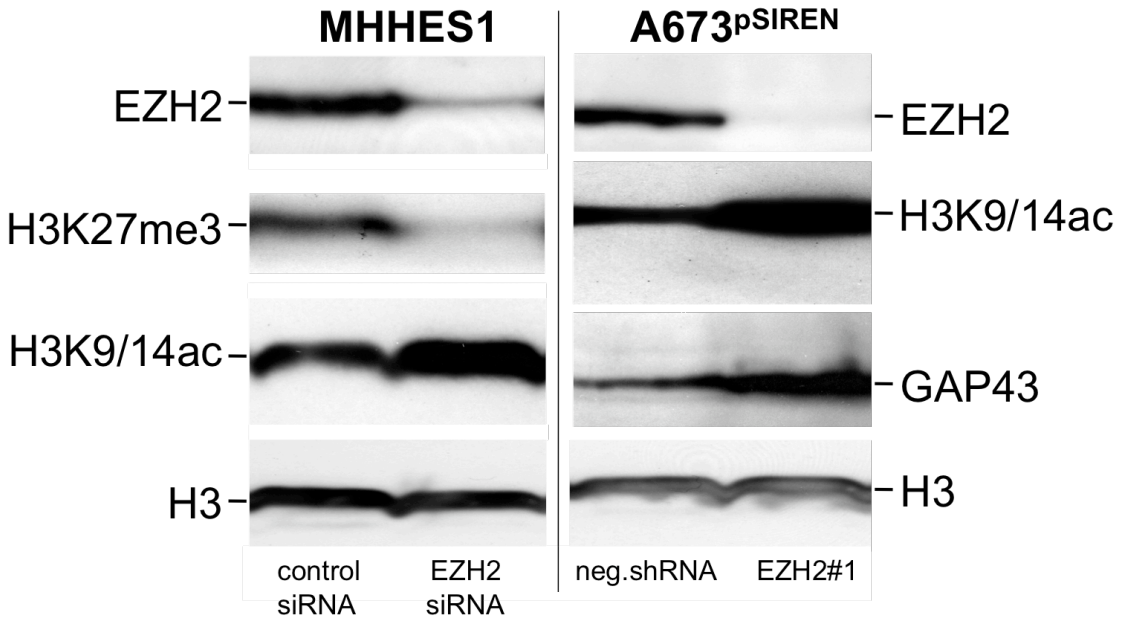


**Figure 22: Detection of histone 3 modifications and GAP43 protein expression after transient and constitutive down-regulation of EZH2 in different ET cell lines by Western blot analyses.** Specific antibodies were used to detect H3K27me3 and H3K9/14ac as well as EZH2 and GAP43 protein of A673 and MHHES1 cells. Detection of histone 3 (H3) protein amounts served as loading control.

Based on these results subsequent ChIP-on-chip analysis (see 3.26.) was carried out to address the question, whether suppression of EZH2 reduces H3K27me3 within the promoter region of these differentiation genes, i.e. whether their regulation is truly based upon an epigenetic mechanism.

A673 cells were transiently transfected with EZH2_7 siRNA to suppress EZH2 expression. 48 h after transfection ChIP assays (see 3.17.) with specific anti-EZH2, anti-H3 and anti-H3K27me3 antibodies as well as an IgG control antibody were carried out to precipitate corresponding genomic fragments. Subsequently, these genomic fragments were hybridized to a promoter microarray containing 50mer oligonucleotides that represented more than 33000 genomic loci. On average, each promoter was represented by three oligonucleotides, that surrounded the transcriptional start site (TSS) of ~ 10000 human genes and 500 microRNAs between – 1500 and + 500 bp. Figure 23 represents changes of promoter H3K27me3 after siRNA-mediated suppression of EZH2. The scatter plot depicts the levels of H3K27me3 compared between EZH2 siRNA and control siRNA treated cells. The red dots indicate gene

promoters that showed reduced H3K27me3 upon EZH2 suppression. All together, 974 genes demonstrated a 1.5-fold or higher reduction of H3K27me3 at their promoter regions and among them *EMP1, EPHB2* as well as *GAP43* were identified. While *GAP43* showed a 3-fold H3K27me3 reduction, *EPHB2* and *EMP1* revealed a 2 and 1.43-fold H3K27me3 reduction at their promoters, respectively (see Table 24).

*EMP1*, *EPHB2* and *GAP43* promoters similarly revealed specific EZH2 binding, which was reduced upon EZH2 suppression. However, H3K27me3 and EZH2 occupancy was not observed at exactly the same loci, as shown in Table 24.

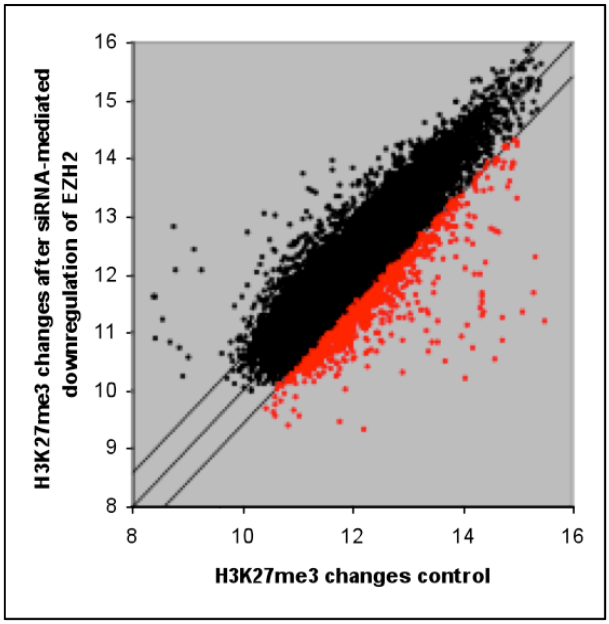


**Figure 23: ChIP-on-chip experiment to analyze H3K27 trimethylation (H3K27me3) at gene promoters.** ChIPs were performed with EZH2 and control siRNA treated A673 cells. Purified genomic fragments were hybridized onto a promoter microarray. The scatter graph demonstrates the promoter H3K27me3 of EZH2 siRNA and control siRNA treated cells. Gene promoters that showed reduced H3K27me3 after EZH2 suppression are marked as red dots.

**Table 24** shows the reduction of H3K27me3 and EZH2 binding upon EZH2 suppression at promoters of the differentiation genes *EMP1*, *EPHB2* and *GAP43* (fold differences of fluorescence intensities between control siRNA and EZH2 siRNA treated cells are shown in bold). The "distance" indicates the relevant position (relative to the TSS) within promoter region.

**Table 24: Results of ChIP-on-chip analysis.**

| Probe ID | gene | Acc.No. | distance | Fold difference EZH2$^{high/low}$ | |
|---|---|---|---|---|---|
| | | | | H3K27me3 | EZH2 binding |
| CM_032207 | *EMP1* | NM_001423 | - 499 | **1.43** | |
| CM_033213 | *EMP1* | NM_001423 | - 177 | | **1.66** |
| CM_005404 | *EPHB2* | D31661 | 301 | **2.02** | |
| CM_005532 | *EPHB2* | NM_004442 | - 134 | | **1.55** |
| CM_007793 | *GAP43* | NM_002045 | 164 | **3.04** | |
| CM_010197 | *GAP43* | NM_002045 | - 121 | | **1.66** |

### 4.1.14. EZH2 knock down induces GFAP expression

Microarray and qRT-PCR analysis similarly revealed an induction of mRNA levels of several genes involved in neuronal differentiation after EZH2 knock down. To examine an induction on protein levels, stably A673 pSIREN$^{EZH2\#1}$- and pSIREN$^{neg.shRNA}$-infected cells were incubated with 0.1 mM butylated hydroxyanisole (BHA) and DMSO for 5 days to induce neuronal differentiation [145]. Since EZH2 knock down increased the mRNA level of the glial fibrillary acidic protein (GFAP), as analyzed by microarray as well as qRT-PCR analysis, a FITC-labeled α-GFAP antibody was used to detect the GFAP protein. GFAP, a structural element of fibrillary astrocytes [146], is exclusively expressed in neuronal tissue and was not detectable in primary ET or ET cell lines under normal conditions (Figure 24). As shown in Figure 25, expression of GFAP protein was detectable in EZH2 suppressed A673 cells, but not in pSIREN$^{neg.shRNA}$-infected A673 cells. However, the phenotype of both, pSIREN$^{EZH2\#1}$- and pSIREN$^{neg.shRNA}$-infected A673 cells changed toward neuronal morphology upon BHA / DMSO treatment (Figure 25 upper panel). This emphasize that complete neuronal differentiation is driven by EZH2 but initial morphological changes are mediated by additional factors.

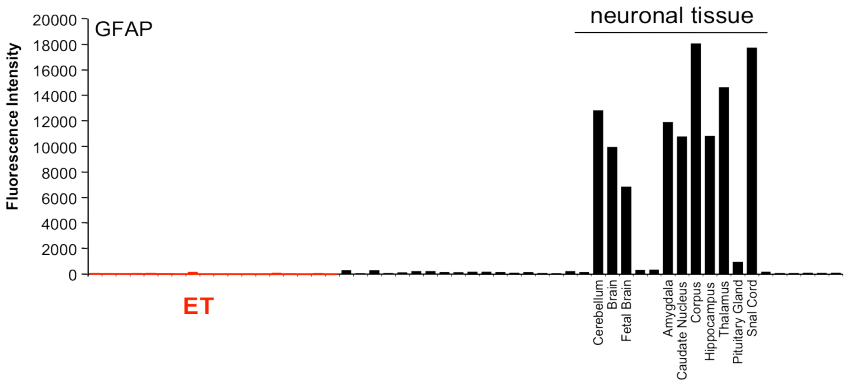


**Figure 24: Microarray analysis of GFAP expression in normal tissue (black) compared to primary ET (red).**

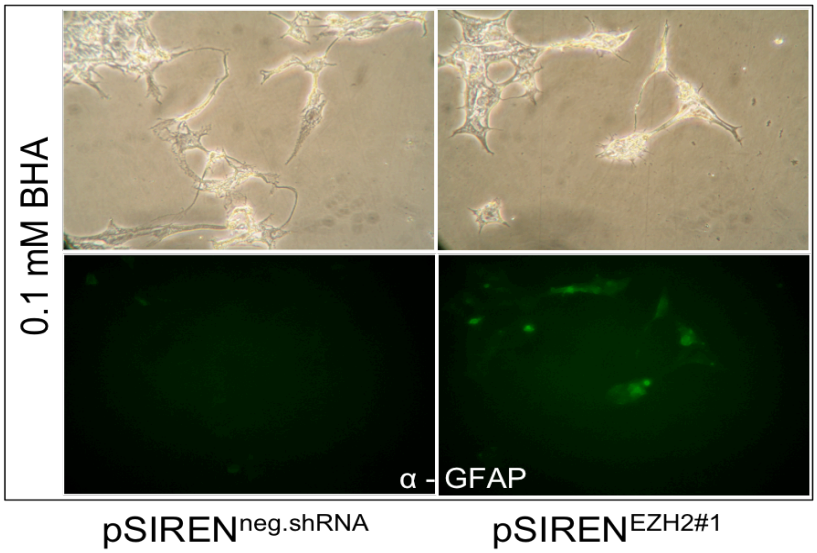


**Figure 25: Immunocytologic analysis of BHA treated pSIREN$^{EZH2\#1}$- and pSIREN$^{neg.shRNA}$-infected A673 cells. Upper panel:** phase contrast microscopy of BHA / DMSO treated cells (20x magnification). **Lower panel:** fluorescence microscopy of these cells (20 x magnification) showing GFAP staining using a FITC-labeled antibody.

### 4.1.15. Knock down of different PRC2 components promotes endothelial tube formation

Microarray and qRT-PCR analysis revealed an increased expression of endothelial differentiation genes after knock down of different PRC2 components. Therefore, the endothelial differentiation potential of ET cell lines influenced by EZH2, EED or SUZ12 suppression, respectively, were examined in tube formation assays. Transiently EZH2, EED, SUZ12 or control siRNA transfected A673 and MHHES1 cells were seeded onto Matrigel Matrix and analyzed for the formation of endothelial tubes by fluorescence microscopy (see 3.20.). This matrix contains laminin, collagen IV and different growth factors and allows the analysis of endothelial differentiation potential, since endothelial cells can differentiate on this matrix and have the ability to form tube-like structures in this assay [147]. Control siRNA transfected A673 and MHHES1 cells were unable to form tubes on Matrigel, while both cell lines acquired the ability to form endothelial tube-like structures after EZH2, EED as well as SUZ12 suppression (Figure 26, left panel). Similarly, no tube formation capacity was observed for parental and stably pSIREN$^{neg.shRNA}$-infected A673 cells, whereas pSIREN$^{EZH2\#1}$-infected A673 cells efficiently formed tubular networks, as shown in the right panel of Figure 26.

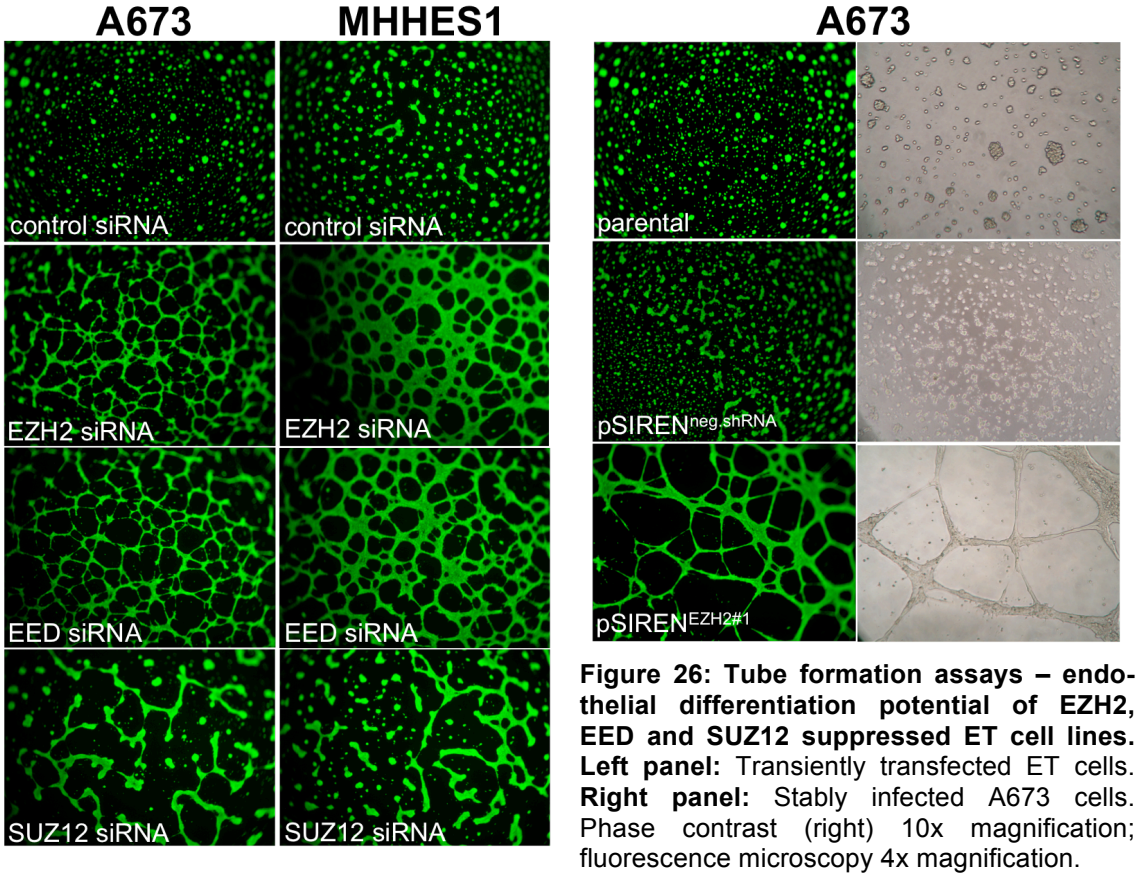


**Figure 26: Tube formation assays – endothelial differentiation potential of EZH2, EED and SUZ12 suppressed ET cell lines. Left panel:** Transiently transfected ET cells. **Right panel:** Stably infected A673 cells. Phase contrast (right) 10x magnification; fluorescence microscopy 4x magnification.

### 4.1.16. Summary - EZH2 blocks expression of differentiation genes and promotes expression of stem cell markers in ET cells

The following schematic diagram represents a summary of the discovered mechanisms, contributing to ET pathogenesis. The ET-specific *EWS/FLI1* chromosomal translocation produces aberrant EWS/FLI1 fusion proteins, that binds to the *EZH2* promoter region. The enhanced expression of the polycomb group protein EZH2, detected in ET by microarray and qRT-PCR analyses, suppresses endothelial and neuronal differentiation genes via PRC2. This silencing of differentiation genes occurs via epigenetic histone modifications, comprising a global as well as a promoter-specific decrease of H3K27me3 and an increase of H3K9/14ac.

Moreover, EZH2 regulates genes typically expressed in stem cells and enhances the growth and metastatic potential of ET cells. *In vivo* experiments revealed a delay of local tumor growth as well as an inhibition of metastatic spread after EZH2 knock down. These data demonstrate that EZH2 is critical for ET pathology by shaping the oncogenicity and the stem cell like ('stemness') phenotype of this tumor entity.

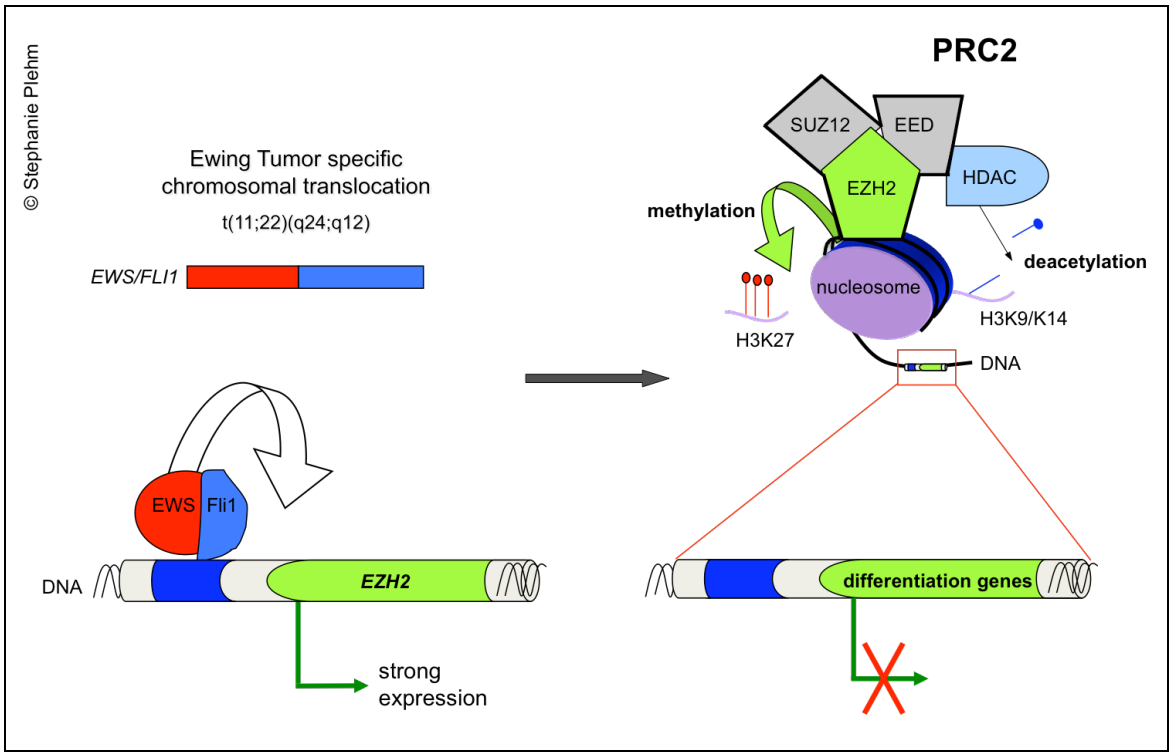


**Figure 27: Schematic diagram that summarizes the role of histone methyltransferase EZH2 in ET pathogenesis.**

## 4.2. Involvement of non-coding RNAs and Argonaute proteins in ET pathogenesis

Although microRNAs (miRNA) were shown to be involved in cancer progression of many tumor entities [148-152], very little is known about the contribution of non-coding RNAs to ET pathogenesis. Since several observations indicate that polycomb group proteins, like EZH2, regulate stemness in normal and cancer cells through epigenetic control of miRNA expression [8], the binding of EZH2 to promoter regions of non-coding RNAs were examined by ChIP-on-chip promoter array analysis.

In addition, two Argonaute proteins (AGO1 and AGO2, also known as eukaryotic translation initiation factor 2C, 1 (EIF2C1) and 2 (EIF2C2)) were separately knocked down in different ET cell lines, to assess the effect of a global inhibition of non-coding RNAs on ET cells. AGO2 plays an important role in mammalian miRNA processing and both Argonaute proteins mediate non-coding RNA-induced gene regulation (see introduction). Furthermore, Argonaute proteins were reported to conduct non-coding RNA-mediated epigenetic gene silencing inter alia by the recruitment of histone-modifying enzymes, including EZH2, to target gene promoters. Thus, the suppression of Argonaute proteins may further elucidate whether non-coding RNAs or Argonaute proteins per se are involved in ET pathogenesis.

### 4.2.1. EZH2 binds to the promoter region of several miRNAs

Data analyses of ChIP-on-chip promoter array experiments performed upon siRNA-mediated EZH2 suppression in A673 cells (see 3.17. and 4.1.13.) revealed a binding of EZH2 to 28 loci, comprising the promoter region of 27 different miRNAs. While a reduced H3K27me3 (more than 1.5-fold) was discovered at six miRNA promoter regions upon EZH2 suppression, 20 miRNA promoters revealed no H3K27me3 reduction upon decreased EZH2 binding. However, among them several miRNAs were reported to be tumor suppressor miRNAs and to be epigenetically silenced in other cancer entities.

The identified EZH2 occupied miRNAs and the corresponding fold changes of reduced H3K27me3 and EZH2 promoter occupancy, respectively, are shown in Table 25 (represented in bold).

**Table 25: EZH2 occupied microRNA (miRNA) promoters and corresponding fold changes of H3K27me3 and EZH2 reduction upon EZH2 suppression.** Results of ChIP-on-chip analysis in ET cell line A673. The "distance" indicates the relevant position (relative to the TSS) within promoter region.

| Probe ID | miRNA | distance | Fold differences $EZH2^{high/low}$ |
|---|---|---|---|
| | | | **H3K27me3 mark** |
| CM_000610 | miRNA-124a-2 | - 514 | **2.05** |
| CM_000182 | miRNA-185 | 0 | **1.60** |
| CM_000670 | miRNA-199a-1 | - 678 | **1.59** |
| CM_000174 | miRNA-423 | 1 | **1.52** |
| CM_000248 | miRNA-497 | - 13 | **2.40** |
| CM_000283 | miRNA-516-4 | - 33 | **1.57** |
| | | | **EZH2 binding** |
| CM_000826 | miRNA-22 | - 1450 | **3.32** |
| CM_000421 | miRNA-29c | - 267 | **2.33** |
| CM_000306 | miRNA-34a | - 86 | **1.80** |
| CM_000458 | miRNA-34b | - 300 | **1.79** |
| CM_000780 | miRNA-99b | - 1079 | **1.95** |
| CM_000684 | miRNA-126 | - 700 | **3.98** |
| CM_000445 | miRNA-129-2 | - 289 | **2.63** |
| CM_000409 | miRNA-152 | - 255 | **2.54** |
| CM_000470 | miRNA-193a | - 305 | **1.52** |
| CM_000541 | miRNA-196b | - 455 | **1.57** |
| CM_000376 | miRNA-199b | - 213 | **1.59** |
| CM_000241 | miRNA-202 | - 11 | **4.29** |
| CM_000054 | miRNA-203 | 64 | **1.83** |
| CM_000472 | miRNA-210 | - 307 | **1.84** |
| CM_000085 | miRNA-210 | 32 | **2.27** |
| CM_000055 | miRNA-219-1 | 64 | **1.53** |
| CM_000420 | miRNA-296 | - 266 | **2.92** |
| CM_000065 | miRNA-345 | 51 | **2.99** |
| CM_000326 | miRNA-365-2 | - 100 | **11.97** |
| CM_000117 | miRNA-499 | 19 | **1.51** |
| CM_000266 | miRNA-507 | - 19 | **2.31** |

### 4.2.2. siRNA and shRNA treatment reduces expression of AGO1 and AGO2 in different ET cell lines

To examine, whether an inhibition of Argonaute proteins has an effect on the phenotype and growth of ET cells, different AGO1 and AGO2 siRNAs were tested in several ET cell lines by transient RNA interference (see Table 11 for specific siRNA target sequences and 3.2. for transient transfection). 48-90 h after transient transfection, RNA was isolated and knock down efficiencies of selected siRNAs were tested by qRT-PCR using specific *AGO1* and *AGO2* gene expression assays. Figure 28 shows the mRNA levels of different ET cells treated with AGO1_3 and AGO2_6 siRNA for 64 h, respectively. These siRNAs showed the best knock down efficiencies of all tested siRNAs, leading to a down-regulation of AGO1 to 25-55% and to a suppression of AGO2 down to 15-30% compared to mRNA levels of control siRNA treated cells.

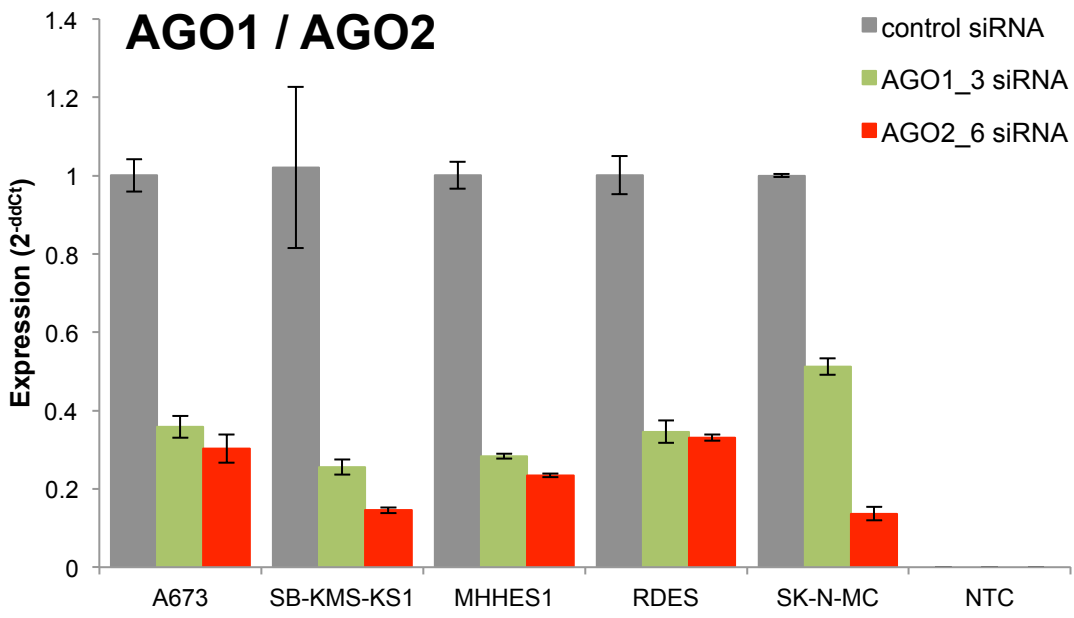


**Figure 28: Transient AGO1 siRNA and AGO2 siRNA transfection in different ET cell lines.** Quantification of AGO1 and AGO2 mRNA levels in AGO1_3 siRNA, AGO2_6 siRNA and control siRNA treated ET cell lines by qRT-PCR. NTC, non-template control.

To generate ET cell lines with constitutive AGO1 or AGO2 knock down, oligonucleotides encoding the target sequence of AGO1_3 siRNA or AGO2_6 siRNA were cloned into the pSIREN RetroQ vector (see Table 12 containing oligonucleotide sequences and 3.3. describing retroviral gene transfer).

As shown in Figure 29, retroviral gene transfer of the pSIREN$^{AGO1}$ construct into A673 cells resulted in a suppression of AGO1 mRNA level down to 18%, while retroviral gene transfer of the pSIREN$^{AGO2}$ construct resulted in a down-regulation of AGO2 expression to ~30% compared to control cells (pSIREN$^{neg.shRNA}$-infected cells).

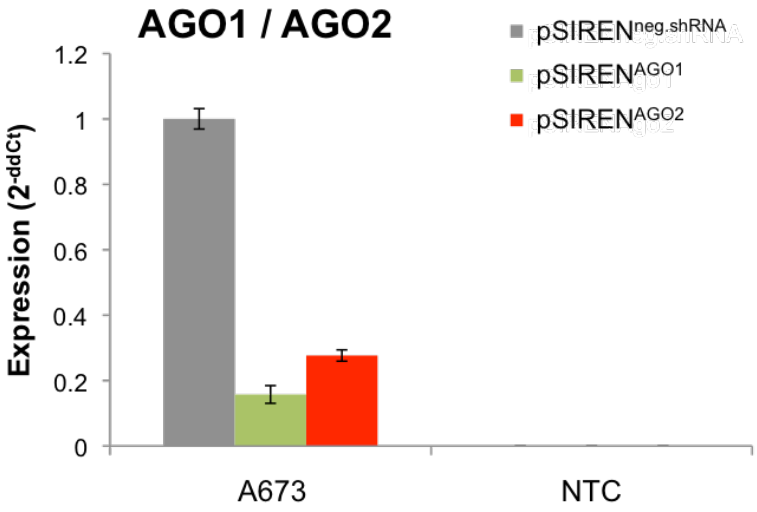


**Figure 29: AGO1 and AGO2 expression of stably infected A673 ET cell line.** A673 ET cells were infected with pSIREN$^{AGO1}$, pSIREN$^{AGO2}$ or pSIREN$^{neg.shRNA}$ (control) construct. Quantification of AGO1 and AGO2 mRNA levels were performed by qRT-PCR. NTC, non-template control.

### 4.2.3. AGO2 knock down reduces the amounts of mature miRNA-221 in ET cells

T.J. Triche reported miRNA-221 to be highly expressed in primary ET [153]. Since Argonaute proteins have important roles in miRNA processing, quantitative expression of mature miRNA-221 was examined after AGO knock down in ET.

First, established ET cell lines were analyzed for miRNA-221 expression using specific miRNA-221 reverse transcription primers and qRT-PCR assays (see 3.11.). Figure 30 (upper panel) shows, that different ET cell lines expressed high levels of mature miRNA-221 in comparison to diverse neuroblastoma and cALL cell lines.

Subsequently, A673, MHHES1 as well as SK-N-MC ET cell lines were transiently transfected with AGO1_3 and AGO2_6 siRNA, respectively. 64 h later, the amount of mature miRNA-221 was quantified by qRT-PCR. As shown in Figure 30 (lower panel), AGO2 knock down reduced the expression level of mature miRNA-221 in all tested ET cell lines. In contrast, suppression of AGO1 had no apparent effect on miRNA-221 processing in A673 and MHHES1 cells, but increased the amount of mature miRNA-221 in SK-N-MC cells as compared to control cells.

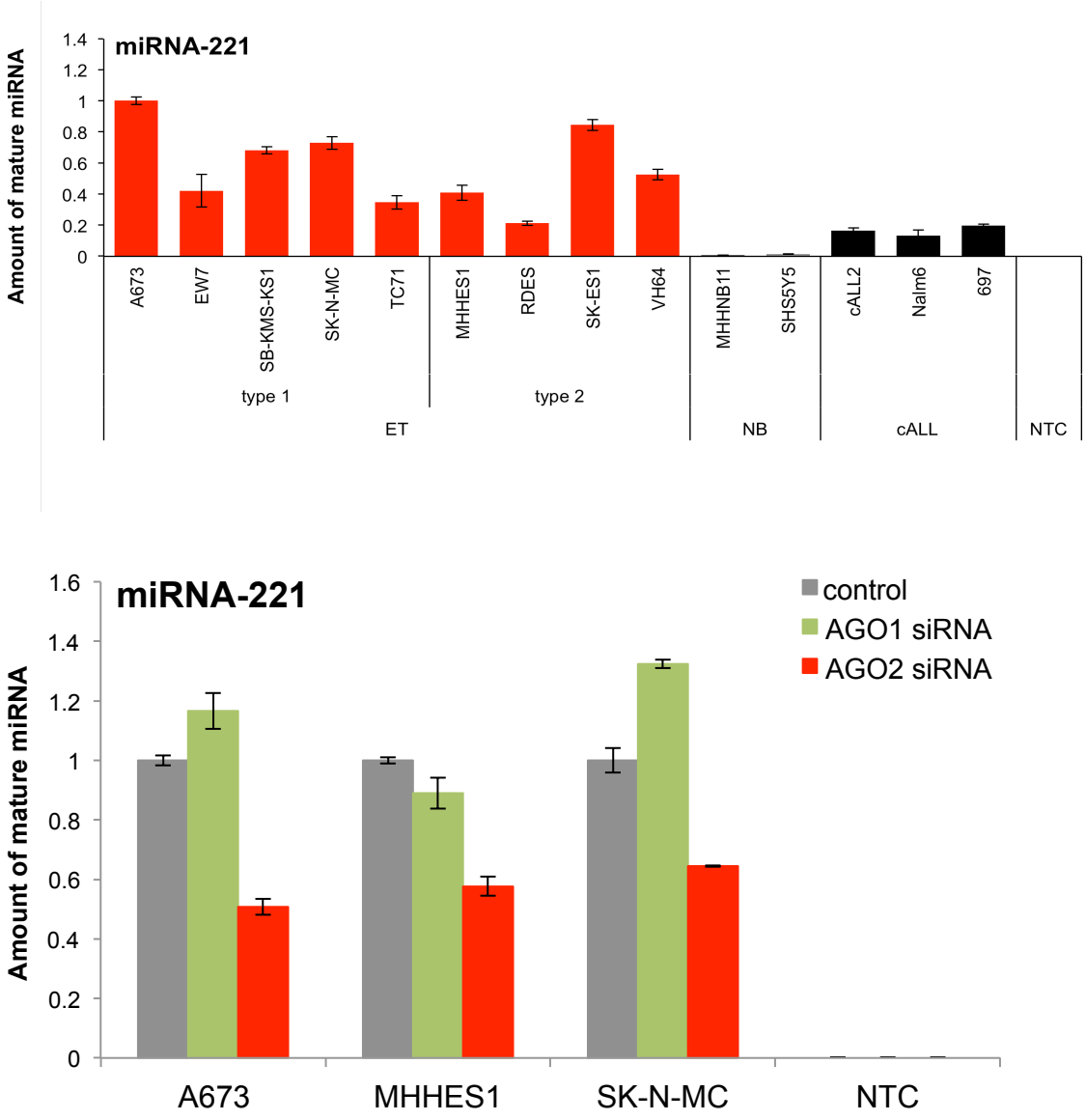


**Figure 30: Quantification of mature microRNA-221 by qRT-PCR. Upper panel:** Amounts of mature miRNA-221 in several ET, neuroblastoma (NB) and cALL cell lines. **Lower panel:** Amounts of mature microRNA-221 in AGO1 and AGO2 suppressed ET cell lines. NTC, non-template control.

### 4.2.4. AGO2 knock down inhibits cell proliferation

To analyze the effect of AGO1 or AGO2 knock down on the proliferation of ET cells *in vitro*, BrdU incorporation assays of A673 cells with a constitutive down-regulation of AGO1 or AGO2, respectively, were performed (see 3.19.).

Figure 31 shows, that stably pSIREN$^{AGO2}$-infected A673 cells exhibit a significantly lower cell proliferation rate than pSIREN$^{neg.shRNA}$-infected A673 cells after 46-63 h (t-test; $p < 0.05$), while the proliferation of pSIREN$^{AGO1}$-infected A673 cells was not significantly changed during considered time period.

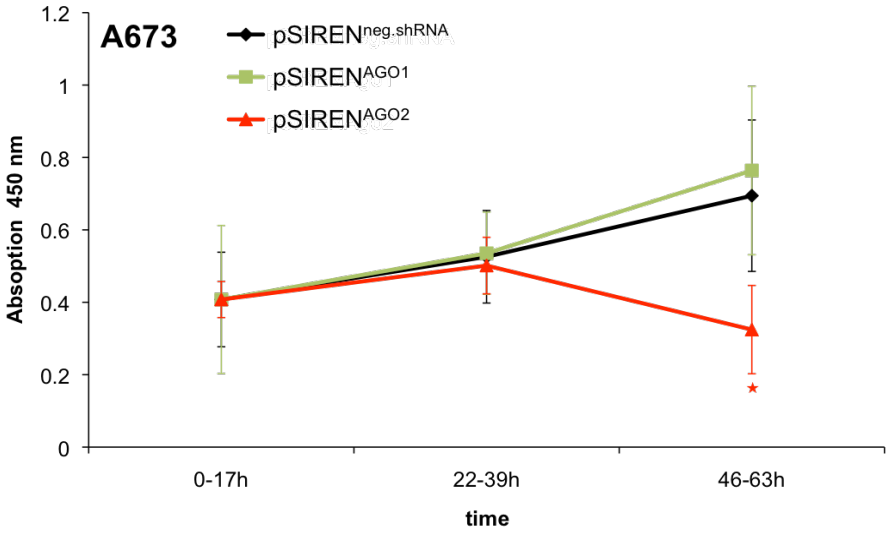


**Figure 31: Proliferation of stably pSIREN$^{AGO}$- and pSIREN$^{neg.shRNA}$-infected A673 cells.** Proliferation was measured by BrdU incorporation assay. Within each time period, cells were incubated with BrdU for 14 h. The error bars indicate standard deviation of octaplicates. ⋆($p<0.05$)

### 4.2.5. Knock down of AGO2 inhibits contact-independent growth *in vitro*

Subsequently, the effect of AGO1 and AGO2 knock down on *in vitro* contact-independent growth of ET was assayed by colony formation assays (see 3.22.). Stably pSIREN$^{neg.shRNA}$-, pSIREN$^{AGO1}$- and pSIREN$^{AGO2}$-infected A673 were tested in duplicates (5 x $10^3$ each) and incubated for 16 days at 37°C (5% $CO_2$) in a humidified atmosphere. As shown in Figure 32, pSIREN$^{AGO2}$-infected A673 cells had a clearly reduced capacity to form colonies compared to pSIREN$^{AGO1}$- and pSIREN$^{neg.shRNA}$-infected A673 cells. A673 pSIREN$^{AGO1}$- and pSIREN$^{neg.shRNA}$-infected cells formed similar numbers of colonies, indicating that AGO1 suppression has no impact on contact-independent growth of A673 ET cells.

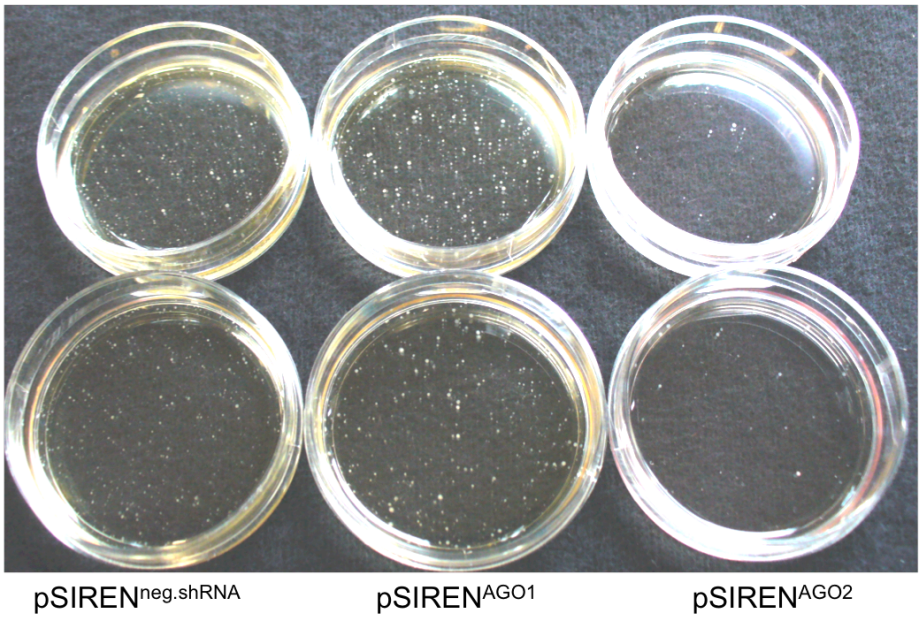


**Figure 32: Colony formation of AGO suppressed and control A673 cells.** pSIREN$^{AGO1}$-, pSIREN$^{AGO2}$-infected as well as control cells were seeded in duplicates into methylcellulose-based media to analyze *in vitro* contact-independent growth.

### 4.2.6. Knock down of AGO2 inhibits, whereas knock down of AGO1 enhances local tumor growth *in vivo*

These *in vitro* results induced experiments to investigate, whether the down-regulation of Argonaute proteins AGO1 and AGO2 has an effect on the tumorigenic growth potential of ET cells *in vivo*. Stably pSIREN$^{AGO1}$- and pSIREN$^{AGO2}$-infected A673 cells as well as the respective controls were injected subcutaneously into the inguinal region of immunodeficient Rag2$^{-/-}\gamma_C^{-/-}$ mice (see 3.24. and Table 18).

As shown in Figure 33, the reduction of AGO2 expression prominently delayed tumor growth, while AGO1 suppression enhanced tumor growth compared to controls (pSIREN$^{neg.shRNA}$-infected A673 cells). 16 days after injection 100% of pSIREN$^{AGO1}$-injected mice showed tumors larger than > 10mm in diameter, while pSIREN$^{neg.shRNA}$-injected mice exhibit none (3 / 5) or only very small tumors (2 / 5) at this time point. 20 days after injection, first small tumors were observed in 2 of 5 pSIREN$^{AGO2}$-injected mice and not until 34 days after injection, 100% of mice injected with A673 pSIREN$^{AGO2}$ cells had tumors larger than > 10mm in diameter.

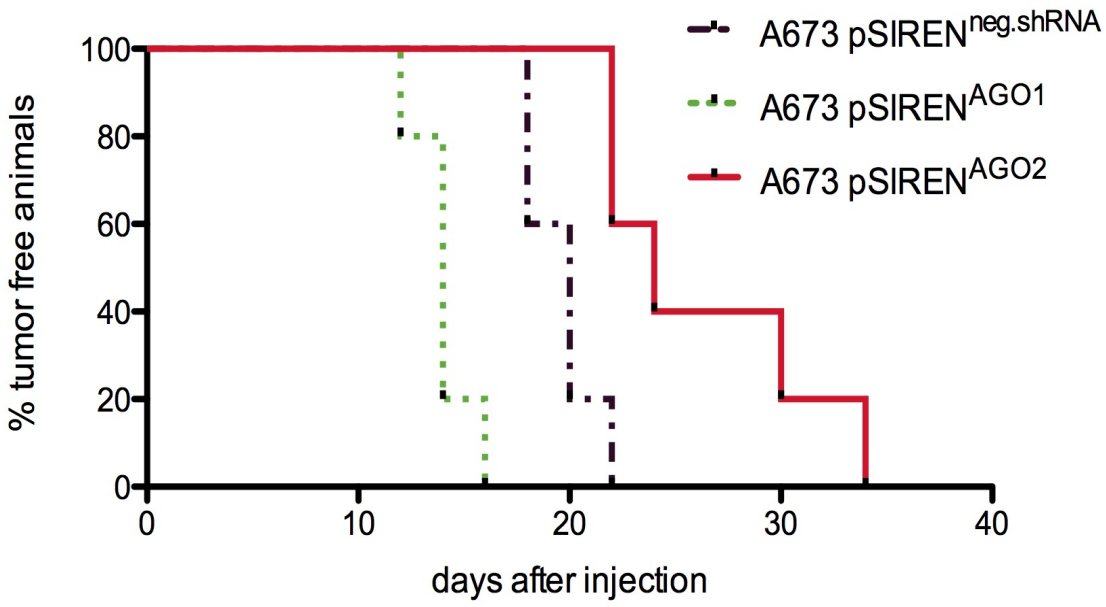


**Figure 33: Kaplan-Meier plot of the local tumor growth experiment.** A673 shRNA infectants (pSIREN$^{neg.shRNA}$, pSIREN$^{AGO1}$ and pSIREN$^{AGO2}$) were injected s.c. into the inguinal region of immunodeficient Rag2$^{-/-}\gamma c^{-/-}$ mice (5 mice / group). Mice with an average tumor size > 10 mm in diameter were considered as positive and were sacrificed.

### 4.2.7. Knock down of AGO2 inhibits, whereas knock down of AGO1 promotes metastatic tumor growth of ET cells

Subsequently, stably pSIREN$^{AGO}$-infected and control A673 cells were injected intravenously into the tail vein of Rag2$^{-/-}\gamma_C^{-/-}$ mice (see 3.24. and Table 18), to investigate the effect of Argonaute proteins AGO1 and AGO2 on metastatic behavior of ET cells. Similar to local tumor growth, macroscopic (Figure 34) and microscopic (Figure 35) analyses showed that all A673 pSIREN$^{neg.shRNA}$- as well as pSIREN$^{AGO1}$-injected animals developed metastases of the lungs and liver, while A673 pSIREN$^{AGO2}$-infected A673 cells lost their ability to metastasize to the lung. Similar to the observations for local tumor growth, mice injected with AGO1 suppressed A673 cells had a stronger affection of the lungs and liver compared to controls. Moreover, only pSIREN$^{AGO1}$-injected mice developed metastases in the kidneys (2/4). However, AGO2 suppressed A673 cells also strongly metastasized into the liver.

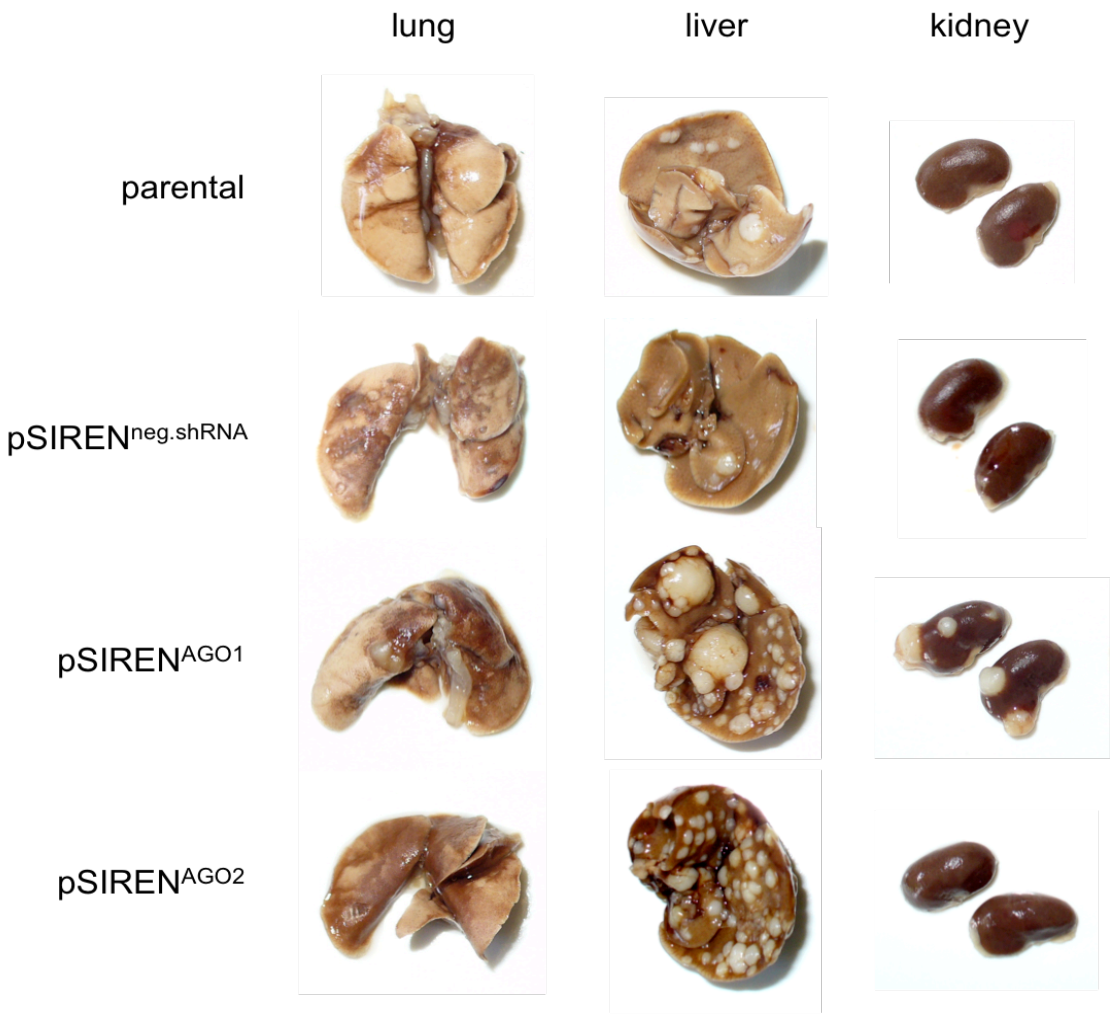


**Figure 34: Affected organs of Rag2$^{-/-}\gamma c^{-/-}$ mice after intravenous injection of pSIREN$^{AGO1}$-, pSIREN$^{AGO2}$-, pSIREN$^{neg.shRNA}$-infected and parental A673 cells.** Representative lungs (left), livers (middle) and kidneys (right) of 1 out of 4 mice per group are shown.

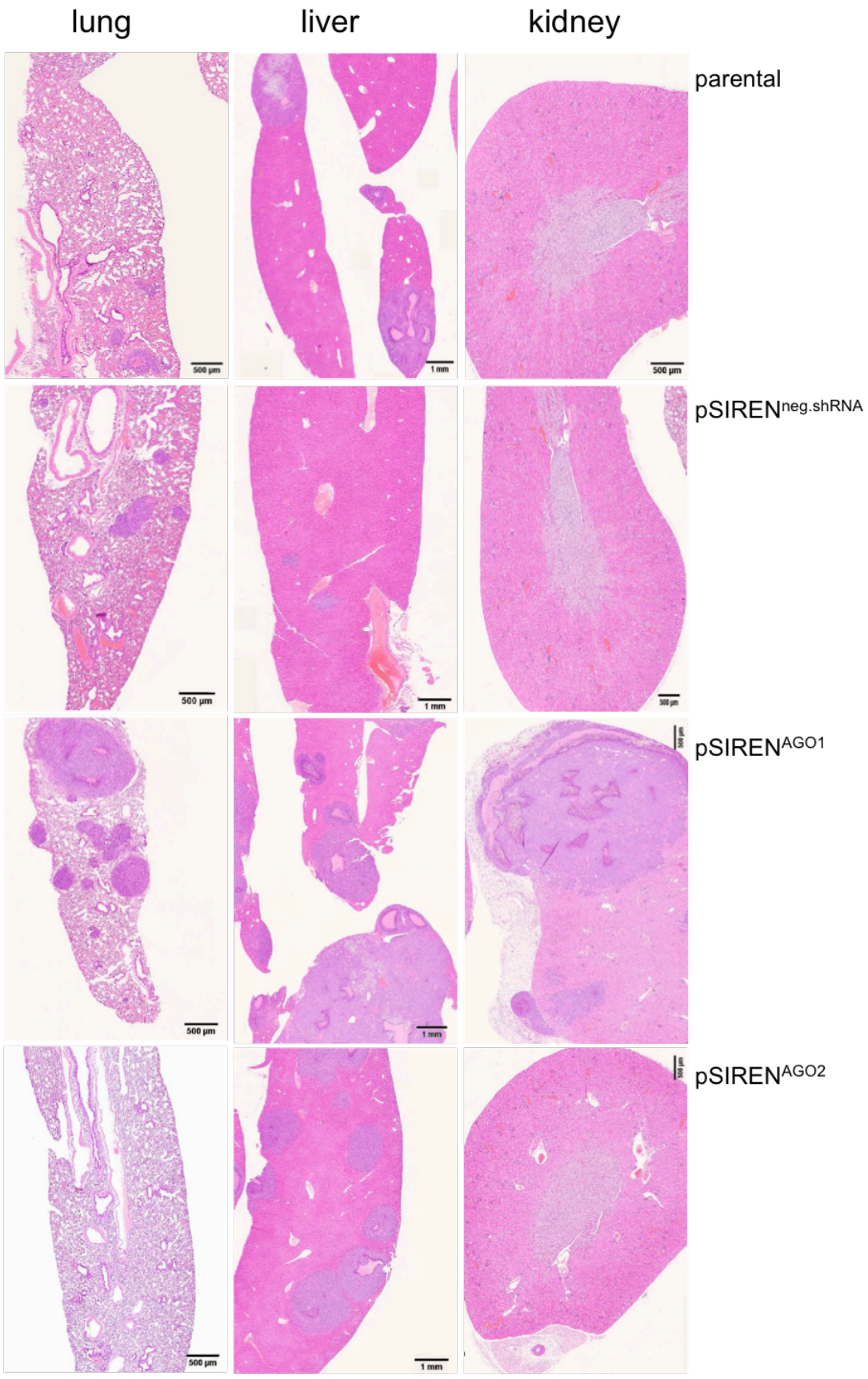


**Figure 35: Hematoxylin and Eosin staining of paraffin embedded lung, liver and kidney sections from Rag2$^{-/-}$γc$^{-/-}$ mice after intravenous injection of pSIREN$^{AGO1}$- , pSIREN$^{AGO2}$-, pSIREN$^{neg.shRNA}$-infected and parental A673 cells.** One representative section of the lungs, liver and kidney is shown (1 out of 4 per group).

### 4.2.8. Knock down of AGO2 inhibits, whereas knock down of AGO1 promotes invasive growth of ET cells

To further elucidate the basis of the observed metastatic phenotypes of ET cells after AGO1 and AGO2 knock down, analyses of invasive growth were performed using the BioCoat™ Angiogenesis System *in vitro* invasion assays. This assay allows to analyze whether AGO1 and AGO2 influence tumor invasiveness. A673 pSIREN$^{AGO1}$-, pSIREN$^{AGO2}$- and pSIREN$^{neg.shRNA}$-infectants were cultured for 48 h on BioCoat Invasion plates. Cells that invaded Matrigel and migrated to the other side of the membrane were stained with Calcein AM fluorescent dye and counted by fluorescence microscopy. As shown in Figure 36, pSIREN$^{AGO1}$-infected A673 cells exhibited a considerably increased invasive capacity than pSIREN$^{neg.shRNA}$-infected A673 cells, while pSIREN$^{AGO2}$-infected cells almost completely lost their ability to cross the Matrigel barrier.

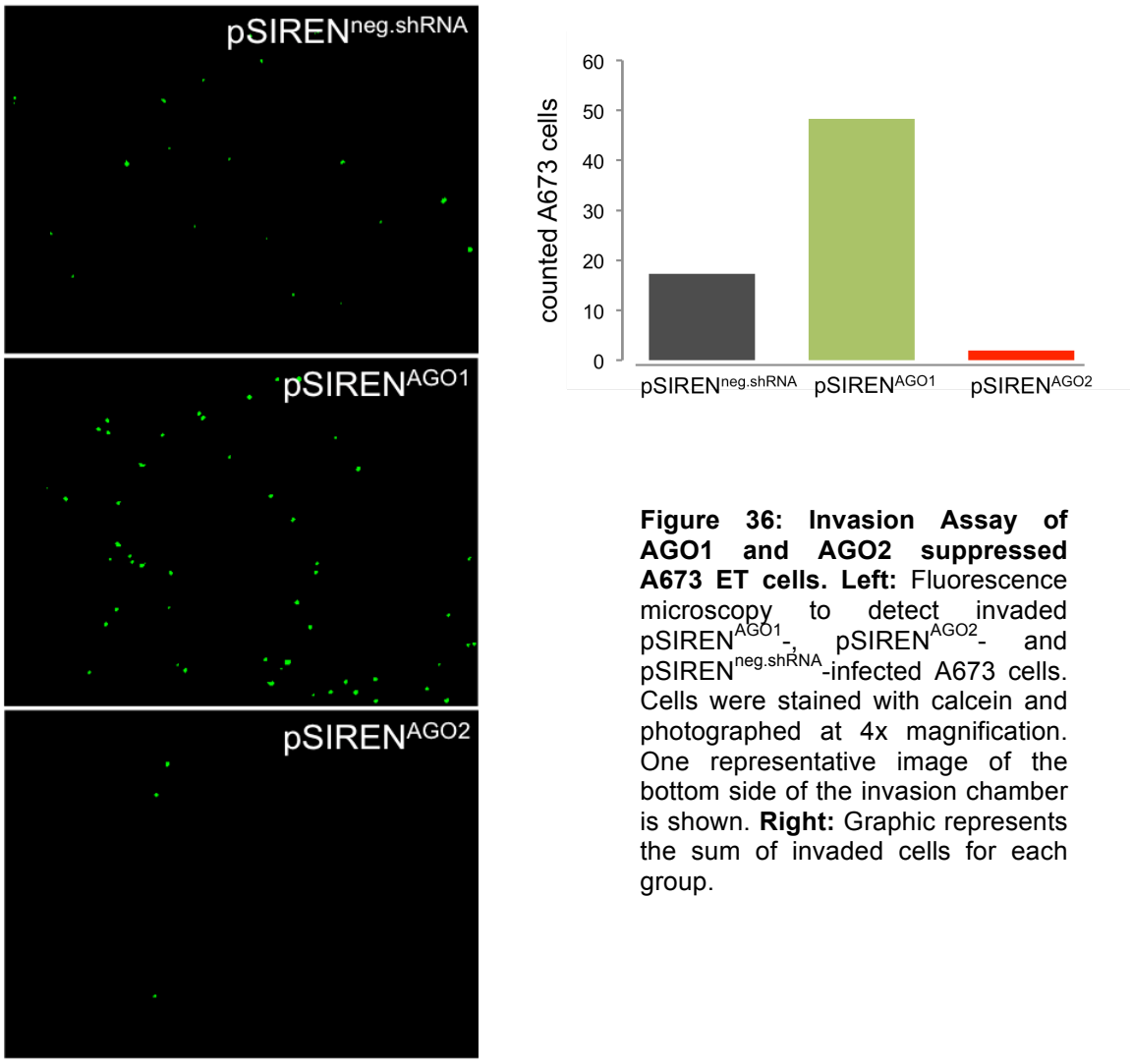


**Figure 36: Invasion Assay of AGO1 and AGO2 suppressed A673 ET cells. Left:** Fluorescence microscopy to detect invaded pSIREN$^{AGO1}$-, pSIREN$^{AGO2}$- and pSIREN$^{neg.shRNA}$-infected A673 cells. Cells were stained with calcein and photographed at 4x magnification. One representative image of the bottom side of the invasion chamber is shown. **Right:** Graphic represents the sum of invaded cells for each group.

### 4.2.9. Knock down of AGO1 inhibits tube formation capacity

Since the so far observed properties of AGO2 suppressed ET cells resembled those of ET cells after EZH2 knock down (see chapter 4.1.), tube formation assays were performed to analyze, whether AGO2 suppression similarly induces a more differentiated ET phenotype.

First, tube formation assays (see 3.20.) with transiently AGO1, AGO2 and control siRNA treated SK-N-MC, A673 and MHHES1 ET cells were carried out. Previous experiments demonstrated, that parental SK-N-MC, A673 as well as MHHES1 ET cells exhibited no tube formation capabilities in this Matrigel assay. Different from results obtained with these cells after EZH2 knock down, neither SK-N-MC nor A673 or MHHES1 cells formed tubes after AGO1 or AGO2 knock down (Figure 37). Similar results were observed for A673 cells with constitutive AGO1 and AGO2 knock down (data not shown).

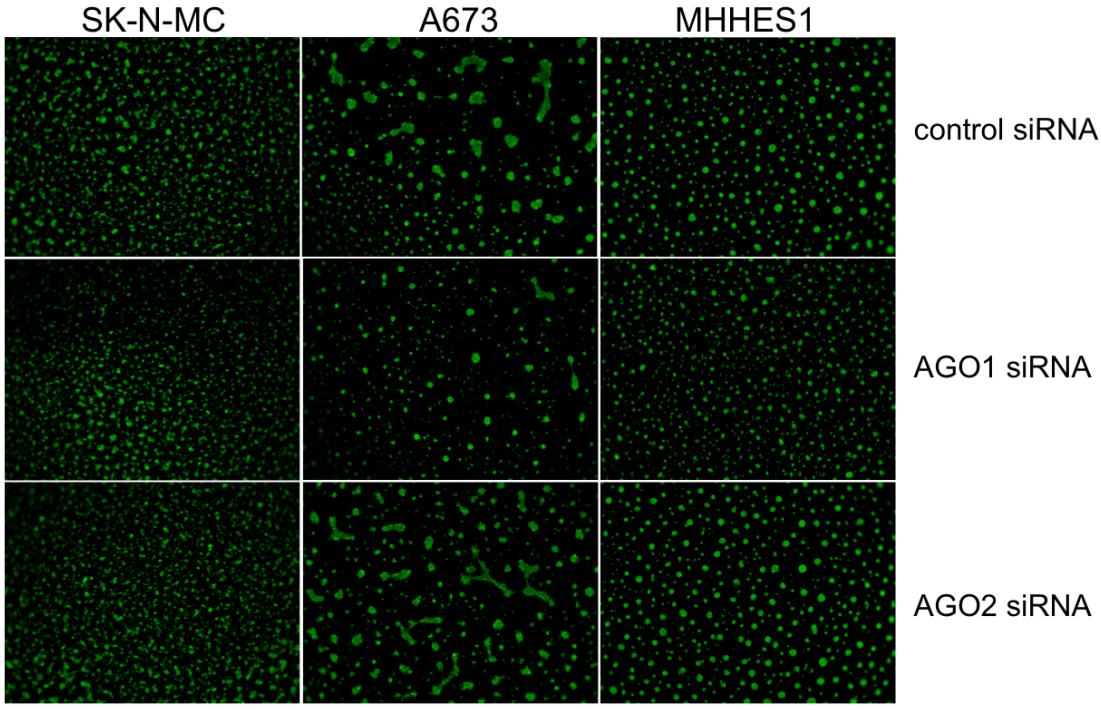


**Figure 37: Tube formation assays of different AGO1, AGO2 and control siRNA treated SK-N-MC, A673 and MHHES1 ET cell lines.** 64 h after transient siRNA transfection, 5 x $10^4$ cells / well were seeded onto Matrigel and incubated for 24 h at 37°C (5% $CO_2$) in a humidified atmosphere. Pictures of Calcein AM stained cells are shown (at 4 x magnification).

Next, tube formation assays with transiently AGO1, AGO2 and control siRNA treated SK-ES1, SB-KMS-KS1 and RDES ET cells were performed. These ET cell lines form tube-like structures on Matrigel, which was demonstrated previously. Figure 38 shows,

that these ET cells lines exhibited tube formation capacity after both, control siRNA as well as AGO2 siRNA treatment. Interestingly, AGO1 suppressed ET cells lost the ability of tube formation (middle panel). Pictures of Matrigel assays showed a diffuse distribution of single cells after AGO1 knock down, while control and AGO2 siRNA treated cells formed organized structures in all tested ET cell lines (Figure 38).

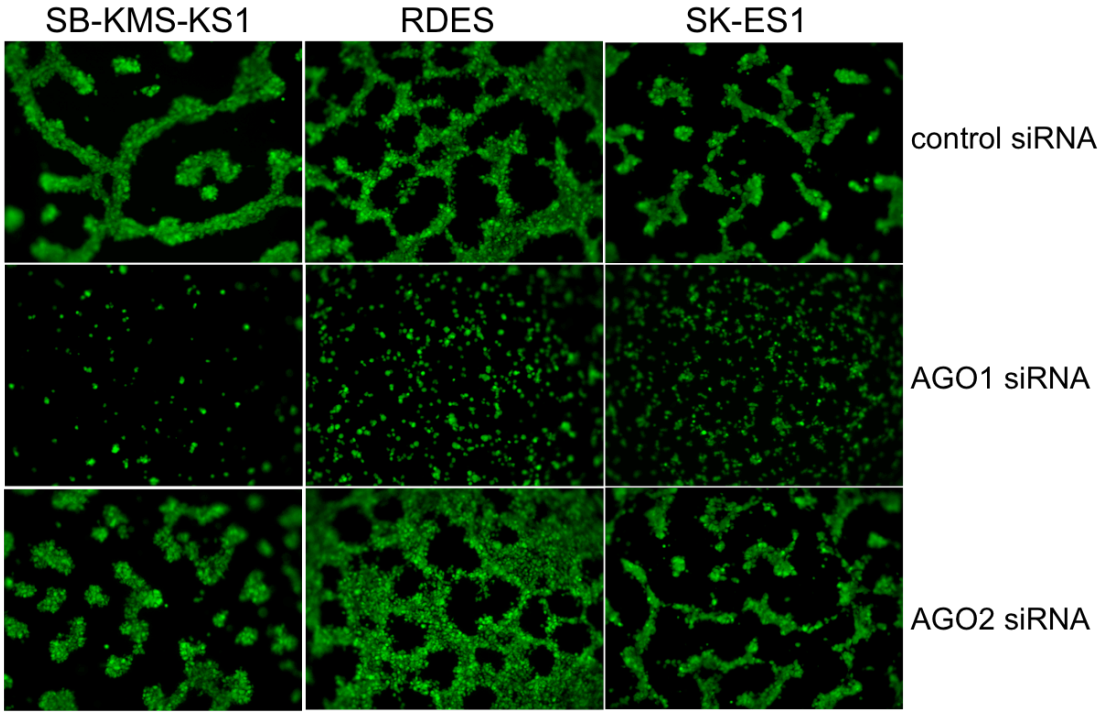


**Figure 38: Tube formation assays of different AGO1, AGO2 and control siRNA treated SB-KMS-KS1, RDES and SK-ES1 ET cell lines.** 64 h after transient siRNA transfection, 5 x $10^4$ cells per well were seeded onto Matrigel and incubated for 24 h at 37°C (5% $CO_2$) in a humidified atmosphere. Calcein AM stained cells are shown (at 10 x magnification).

### 4.2.10. Knock down of AGO1 increases expression of stem cell genes in different ET cell lines

To identify possible downstream targets of Argonaute proteins in ET and to understand the phenotypic changes observed after AGO knock down, microarray analyses with transiently AGO1 siRNA and AGO2 siRNA transfected ET cells were performed. First evaluations of microarray results, including fold change values greater than 2 and conventional t-test values less than 0.01 (p-value), discovered 904 genes that were up and 132 genes that were down regulated in A673 upon AGO1 suppression. Similarly, AGO2 knock down resulted in an up-regulation of 828 and down-regulation of 127 genes.

Among others, expression of PROM1 (Prominin 1, also known as CD133) and ABCG2 (ATP-binding cassette, sub-family G (WHITE), member 2) was induced after knock down of AGO1 in A673 ET cells. The *PROM1* gene encodes a pentaspan transmembrane protein, that is expressed in embryonic and adult stem cells as well as cancer stem cells [154]. It is thought to maintain stem cell properties by suppressing differentiation. ABCG2 is a membrane-associated xenobiotic transporter that is expressed in a wide variety of stem cells [155].

To verify these microarray data, PROM1 and ABCG2 expression in different AGO1 and AGO2 suppressed ET cells was analyzed by qRT-PCR. Additionally, expression analyses of the stem cell markers NGFR and OCT4 upon AGO1 and AGO2 suppression were included. Figure 39 shows that siRNA-mediated suppression of AGO1 increased NGFR, PROM1 and ABCG2 mRNA levels up to 1.5-3-fold compared to controls. In contrast, mRNA levels of the stem cell markers ABCG2 and OCT4 were suppressed by 60% after knock down of AGO2 (data not shown).

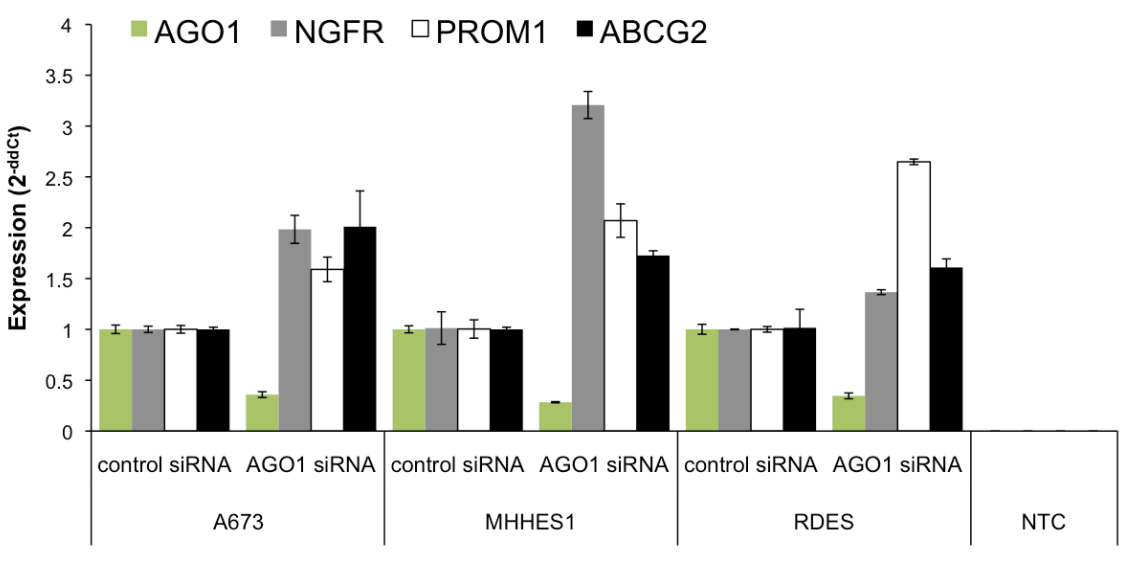


**Figure 39: Expression of NGFR, PROM1 and ABCG2 in different AGO1 suppressed ET cell lines.** The mRNA levels of respective genes were analyzed by qRT-PCR. NTC, non-template ($H_2O$) control.

To prove an induction of NGFR and PROM1 on protein level, transiently AGO1 siRNA transfected ET cells were analyzed by flow cytometry using specific FITC-labeled NGFR and APC-labeled PROM1 antibodies. 64 h after AGO1 or control siRNA transfection, respectively, MHHES1, RDES and SK-ES1 ET cells were analyzed by flow cytometry (see 3.13).

As exemplified for MHHES1 cells, suppression of AGO1 increased NGFR and PROM1 protein levels (Figure 40). The overlaid signals of AGO1 suppressed cells (green line) and control cells (purple area) illustrate the shift towards higher fluorescence intensities of AGO1 suppressed cells in comparison to control cells (Figure 40 lower panel).

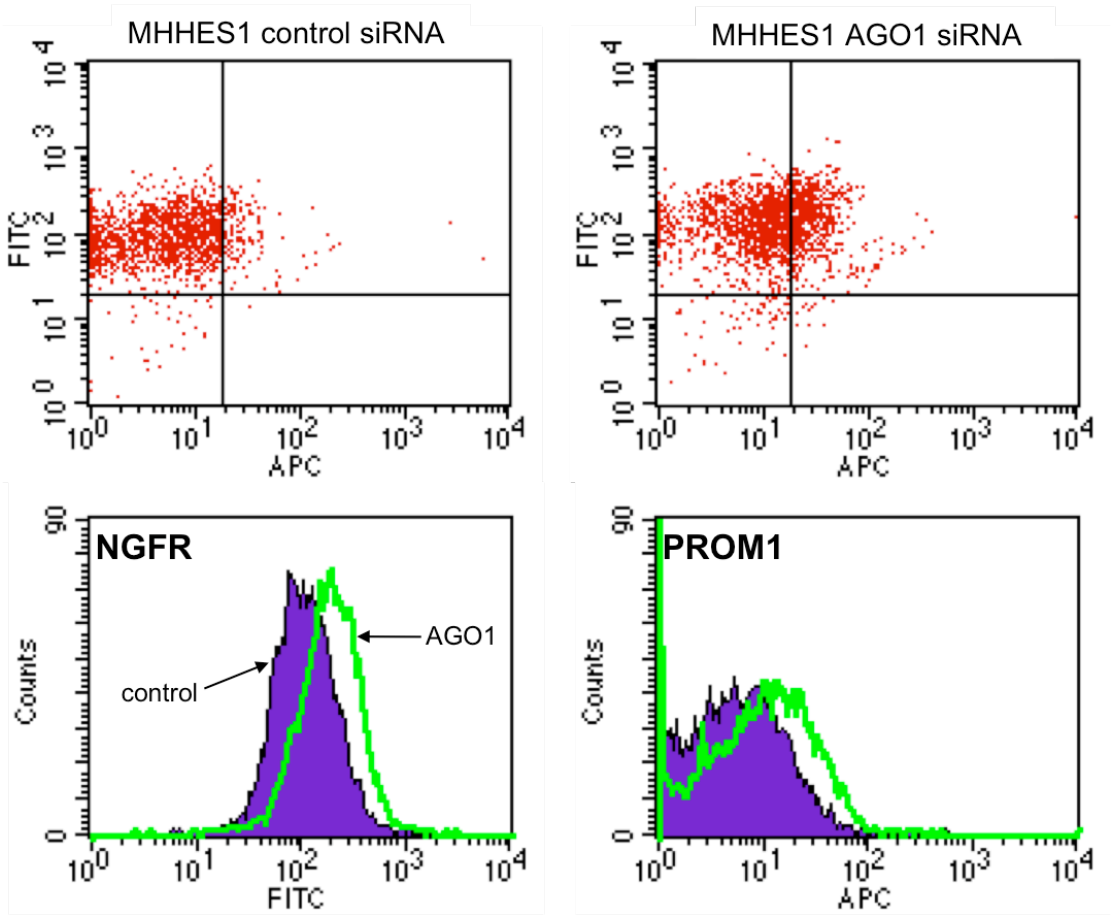


**Figure 40: Detection of NGFR and PROM1 protein expression in MHHES1 ET cells after AGO1 suppression by flow cytometry.** In each measurement 20.000 events were counted. FITC = NGFR protein; APC = PROM1 protein (CD133). **Upper panel**: Density dot plots that depict 10% of cell counts in two-parameter histograms. **Lower panel**: Overlay histograms, green line = signal of AGO1 siRNA treated cells; purple area = signal of control siRNA treated cells. Indicated are the counts per channel. Similarly, flow cytometry analysis confirmed increased protein expression of NGFR and PROM1 in AGO1 suppressed RDES and SK-ES1 ET cell lines, respectively.

### 4.2.11. EZH2 knock down decreases AGO2 expression

Since both, EZH2 as well as AGO2 knock down revealed similar phenotypic changes in several *in vitro* and *in vivo* assays, AGO2 expression levels of different EZH2 siRNA treated ET cells were examined by qRT-PCR and Western blot. As shown in Figure 41, both analyses revealed decreased AGO2 expression after siRNA-mediated EZH2 suppression. Furthermore, suppression of AGO1 led to an increase of AGO2 mRNA

levels in several analyzed ET cell lines. However, expression of AGO1 was not influenced after EZH2 suppression and neither AGO1 nor AGO2 suppression affected EZH2 expression (data not shown).

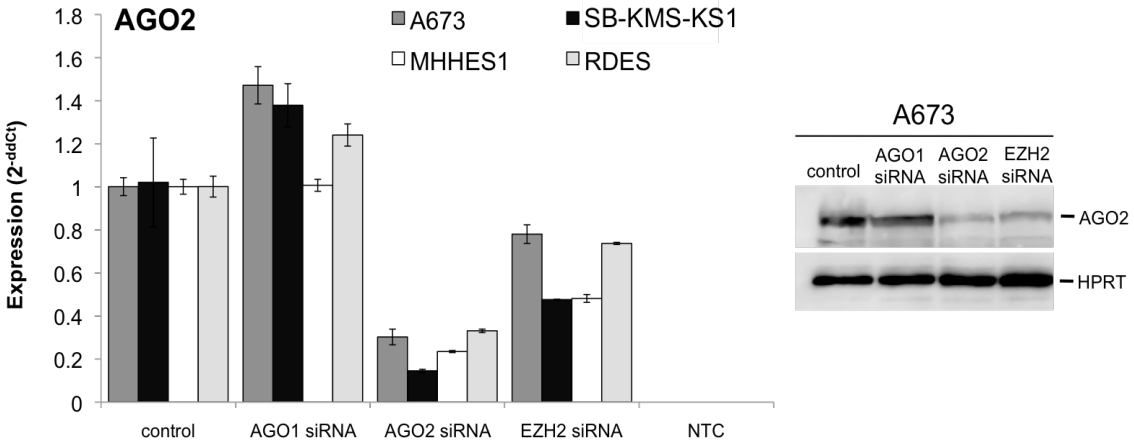


**Figure 41: Quantification of AGO2 on mRNA and protein level in EZH2-suppressed ET cell lines. Left:** AGO2 expression 64 h after transient siRNA transfection, NTC, non-template control. **Right:** Western blot analysis of corresponding A673 whole cell lysates. HPRT; loading control.

Subsequently, microarray data of EZH2 siRNA and AGO2 siRNA treated ET cells were compared to identify potential target genes that were regulated by both proteins. Interestingly, this comparison revealed several genes to be similarly influenced after EZH2 or AGO2 suppression, respectively. With regard to the regulation of differentiation genes, no endothelial marker, but genes typically expressed in neuronal cells, like *neurexin 2* (*NRXN2*) and *neuron navigator 3* (*NAV3*) were induced by both siRNAs. Furthermore, mRNA levels of NCOR2 (nuclear receptor co-repressor 2), SERPINE1 (serpin peptidase inhibitor, clade E, member 1, also known as PAI1) and the potential tumor suppressors RASSF4 (Ras association RalGDS/AF-6 domain family member 4) were up-regulated after EZH2 or after AGO2 suppression. However, further analysis (qRT-PCR) is required to verify these microarray data.

### 4.2.12. AGO1 and AGO2 knock down does not affect global histone H3 modifications

Since Argonaute proteins were also reported to regulate gene expression via histone modifications [92, 94, 156, 157], analyses of histone 3 (H3) modifications upon AGO1 and AGO2 knock down were performed by Western blot. Both, “active” (H3K9/14ac

and H3K4me2/me3) as well as “inactive” (H3K27me3 and H3K9me3) chromatin marks were analyzed using corresponding antibodies.

Different ET cell lines were transiently transfected with AGO1, AGO2 and control siRNA, respectively. 64 h after transfection, whole cell lysates were prepared for Western blot analyses (see 3.12.) and H3 proteins were separated using 12.5% SDS-PAGE. Antibodies were incubated at appropriate dilutions (see Table 7) with the PVDF membranes and histone modifications were visualized using an HRP-labeled goat-anti-rabbit antibody. EZH2 suppressed RDES cells served as an internal control, while detection of H3 served as loading control.

Overall, SB-KMS-KS1, A673 as well as MHHES1 cells showed no clear alteration of histone 3 (H3) marks after AGO1 and AGO2 knock down as compared to controls (Figure 42). RDES cells, in contrast, revealed controversial results, since “active” as well as “inactive” marks were increased after AGO2 knock down.

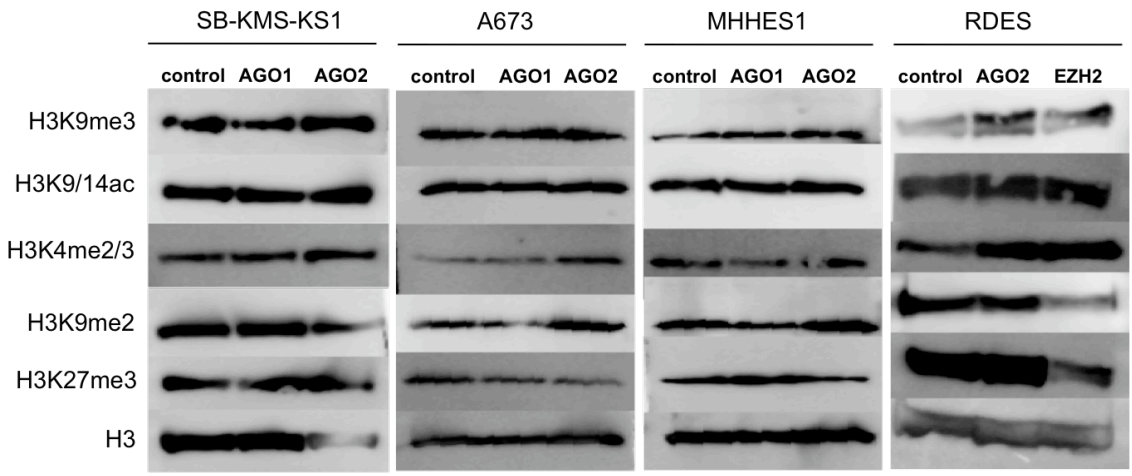


**Figure 42: Analysis of histone 3 modifications upon AGO1 and AGO2 suppression in different ET cell lines.** “Active” histone marks (H3K9/14ac and H3K4me2/me3) as well as “inactive” marks (H3K27me3 and H3K9me3) were examined by Western blot analyses.

### 4.2.13. Summary – Argonaute proteins are involved in ET pathology

ChIP-on-chip analyses revealed EZH2 and H3K27me3 occupancy at several promoter regions of putative tumor suppressor as well as oncogenic miRNA in ET. MiRNAs belongs to the group of non-coding RNAs, which are key regulators of i.e. normal cell differentiation as well as proliferation and are involved in tumor progression of a variety of other cancer types.

To assess, whether non-coding RNAs and Argonaute proteins per se are involved in ET pathogenesis, Argonaute protein 1 (AGO1) and Argonaute protein 2 (AGO2) were separately knocked down in several ET cell lines. These experiments showed that AGO2, but not AGO1 knock down reduced the amount of mature miRNA-221, which is highly expressed in primary ET tissue (as reported by Triche et al. [153]) as well as in parental ET cell lines.

Furthermore, AGO1 suppression accelerated tumor growth and promoted metastatic spread of ET cells in immunodeficient mice, and was associated by augmented invasive growth as analyzed by *in vitro* invasion assays. In contrast, delayed local tumor growth was observed for AGO2 suppressed ET cells. Additionally, AGO2 silenced ET cells lost their ability to metastasize to the lungs, combined with a prominently reduced invasive growth and colony formation capacity *in vitro*.

While AGO2 suppressed ET cell lines revealed no phenotypic changes in endothelial tube formation assays, knock down of AGO1 resulted in a less differentiated phenotype, that inhibited tube formation on Matrigel. In addition, microarray as well as qRT-PCR analyses detected an increased expression of stem cell markers, such as NGFR, PROM1 and ABCG2 in AGO1 siRNA treated ET cells.

AGO2 siRNA and EZH2 siRNA treated ET cells exhibited similar phenotypic changes and qRT-PCR and Western blot analysis revealed a decreased expression of AGO2 after siRNA-mediated EZH2 suppression. The expression of AGO1 was not affected by EZH2 suppression, and neither AGO1 nor AGO2 suppression influenced the expression of EZH2.

# 5. Discussion

## 5.1. Role of PcG protein EZH2 in Ewing Tumor (ET) pathogenesis

The reciprocal t(11,22)(q24;q12) chromosomal translocation is present in about 85% of ET and generates the EWS/FLI1 fusion protein [117, 158]. This aberrant transcription factor is pathognomonic for the disease by altering the gene expression pattern and thus mediating the pathogenesis of ET [109, 159]. Several transcription factors that regulate cell differentiation, such as *runt-related transcription factor 2* (*RUNX2*) [160], *GLI family zinc finger 1* [161] and *inhibitor of DNA binding 2* (*ID2*) [162] were reported to be direct target genes of EWS/FLI1. Additionally, EWS/FLI1 activates genes involved in cell proliferation and survival (e.g. *insulin-like growth factor 1* (*IGF1*), *v-myc myelocytomatosis viral oncogene homolog* (*MYC*), *NK2 homeobox 2* (*NKX2.2*), *T-LAK cell-originated protein kinase* (*TOPK*)) and inhibits tumor suppressors including the *cyclin-dependent kinase inhibitor 1C* (*CDKN1C p57kip*), the *transforming growth factor, beta receptor II* (*TGFßR2*) and the *insulin-like growth factor binding protein 3* (*IGFBP3*), thus preventing growth arrest, senescence and apoptosis [163].

This study shows for the first time, that EWS/FLI1 increases the EZH2 expression in ET, thereby employing epigenetic mechanisms to promote and maintain stemness and tumorigenicity of ET cells.

### 5.1.1. EWS/FLI1 fusion protein regulates EZH2 expression

DNA microarray analysis revealed *enhancer of zeste, Drosophila, homolog 2* (*EZH2*), but not the EZH2 homolog *EZH1* (data not shown), to be up-regulated in primary ET as compared to 133 normal tissues of diverse origin [128]. Furthermore, EZH2 mRNA levels of ET cell lines were prominently increased compared to those of other small-round-blue pediatric tumor cell lines (cALL and neuroblastoma), as analyzed by qRT-PCR (Fig. 3, 4).

*In vitro* and *in vivo* binding assays were used to examine, whether *EZH2* is a direct target of the EWS/FLI1 fusion protein. *FLI1* encodes a member of the ETS protein family, a group of winged helix-loop-helix transcription factors sharing a DNA-binding domain with specificity for GGAA/T core motifs, thereby recruiting the EWS/FLI1 fusion protein to target gene promoters [164, 165]. This canonical GGAA/T recognition motif was found to be present in several copies throughout the *EZH2* promoter region. ABCD assays using synthetic oligonucleotides as well as ChIP-qRT-PCR analyses revealed a binding of EWS/FLI1 to this sequence motif within the *EZH2* promoter *in vitro* and *in*

*vivo*. Additionally, the ChIP-qRT-PCR analysis showed that the endogenous EWS/FLI1 most prominently bound to the evolutionary conserved ets recognition site located -1081 bp upstream of the *EZH2* transcriptional start site (Fig. 7, 8). Both assays identified *EZH2* as a direct target of the EWS/FLI1 fusion protein, suggesting that EWS/FLI1 regulates EZH2 expression in ET. Previous studies, that showed a binding of EWS/FLI1 to the GGAA/T recognition site within promoter regions of *TGFßR2*, *serine/threonine/tyrosine interacting-like 1* (*STYXL1*) and *protein-tyrosine phosphatase 1* (*PTPL1*), resulting in an up-regulation of corresponding gene expression measured by luciferase assays [166, 167], indicate that this recognition sequence is a common target of EWS/FLI1.

Quantification of EZH2 expression in the absence or presence of EWS/FLI1-specific siRNA as well as upon ectopic expression of EWS/FLI1 in mesenchymal stem cells (MSC), confirmed a regulation of EZH2 expression by EWS/FLI1. When the EWS/FLI1 expression was suppressed by 90%, a decrease of EZH2 mRNA levels down to 30-50% was observed in several ET cell lines. Ectopic expression of EWS/FLI1 fusion protein in MSCs, in turn, increased EZH2 expression that appeared to be dose-dependent, since the MSC cell clones with the strongest EWS/FLI1 induction showed the highest (more than threefold) up-regulation of EZH2 expression (Fig. 5, 6).

Overall, these analyses validate a regulation of *EZH2* gene expression by the aberrant EWS/FLI1 fusion protein, leading to an increased amount of EZH2 mRNA level in ET.

### 5.1.2. EWS/FLI1 mediates transformation and growth of ET via EZH2 over-expression

To examine the effect of EZH2 on tumor growth *in vivo*, EZH2 suppressed ET cells were injected into BALB/c $Rag2^{-/-}\gamma c^{-/-}$mice. Although these mice are immunodeficient, they develop no endogenous tumors [168]. This enables the analysis of tumor growth and metastatic behavior of xenografted cancer cells [169].

The *in vivo* experiments showed delayed local tumor growth and a strong inhibition of metastasis upon EZH2 suppression (Fig. 13, 14). The inhibiting effect on local tumor growth was similarly observed by Riggi et al., who locally injected EZH2 suppressed A673 ET cells into immunocompromised mice [170]. In this thesis work, in addition, an EZH2 dose-dependent inhibition of invasive growth was observed, whereby intravenously injected ET cells with a strongly suppressed EZH2 expression (down to 20% compared to control cells; EZH2#1) completely lost their ability to metastasize into the lungs and liver. Although ET cells with a lower reduction of EZH2 expression (40%

compared to control cells; EZH2#2) still metastasized into pulmonary and hepatic tissue, the lungs of these mice exhibited smaller and considerably reduced numbers of metastases (Fig. 14). The hepatic tissue, however, was less colonized by “EZH2#2 cells” but showed metastases that exceeded the size of tumor nodules developed by control ET cells (Fig. 14 and Fig. 44 see Appendix 10.2.). Since histologic examinations revealed a continuous suppression of EZH2 in these metastases (Fig. 15), loss of EZH2 suppression could not explain this observation. However, the strong formation of metastases could be due to the structure of hepatic tissue. The liver capillaries (liver sinusoids) are surrounded by a discontinuous endothelium composed of liver sinusoidal endothelial cells (LSEC) [171]. The presence of open pores lacking a membrane and a basal lamina underneath the endothelium enable the exchange of macromolecules, solutes and fluids between the vasculature and surrounding tissues [171]. As liver sinusoids lack a sustained endothelial lining, tumor cells that were unable to invade into lung tissue might have been passively transported into the liver tissue, where they were able to form metastases.

However, these experiments demonstrated that the EWS/FLI1-mediated over-expression of EZH2 induces growth and a transformed phenotype (anchorage-independent growth and invasive phenotype), suggesting that EZH2 acts as an oncogene in ET. EZH2 was shown to be highly up-regulated in a variety of tumors, including breast [172], prostate [142] and bladder cancer [173]. Furthermore, EZH2 was reported to be a marker of aggressive breast and prostate cancer and to be most significantly increased at advanced stages of a disease as well as in patients with poor prognosis [29, 142, 174].

The highly malignant phenotype is reflected in human ET patients, where approximately 25% have detectable metastases in the lung and/or bone and/or bone marrow at initial diagnosis. Furthermore, patients with metastasis in bone or bone marrow have a very poor prognosis with a less than 27% change of cure [109-111].

### 5.1.3. EWS/FLI1 employs epigenetic mechanisms to maintain tumorigenicity and stemness of ET cells

The histone methyltransferase EZH2 is part of the human polycomb repressive complex 2 (PRC2). In addition to EZH2, other core components of PCR2 include EED, SUZ12 and the histone-binding protein RbAp46/48 [175]. EZH2 exhibits a SET domain, which is active when complexed with at least two of its non-catalytic partners, and mediates gene repression via di- and trimethylation of histone 3 at lysine 27 (H3K27me2/me3) [35, 176]. During normal development, EZH2 has a key role in cell

fate transition by maintaining stem cell expression signatures and regulating stem cell renewal as well as differentiation [46, 177-179].

The delayed tumor growth as well as the inhibition of contact-independent growth *in vitro* after EZH2 suppression (Fig. 12) cannot be explained by altered proliferative behavior or cell death, since no induction of apoptosis or reduced cell proliferation of EZH2-suppressed ET cells was observed (Fig. 11). To further elucidate the involved mechanisms mediating the EZH2-promoted tumorigenicity, microarray analyses were performed to identify EZH2 target genes. Histone deacetylase (HDAC) inhibitor (TSA) treated ET cells were included in these analyses to compare their expression pattern with that of EZH2 siRNA-treated ET cells. The microarray analyses showed that both treatments induce expression of genes involved in endothelial as well as neuronal differentiation, such as *EMP1*, *EPHB2*, *GAP43* and *GFAP* (Fig. 16). The induction of these genes upon TSA treatment indicates that HDACs are involved in EZH2-mediated gene regulation. Furthermore, the observed re-expression of differentiation genes upon EZH2 suppression suggests a reversible inactivation of genes by EZH2 in ET cells. This is in contrast to observations in colon cancer that demonstrated an irreversible inactivation of tumor suppressor genes even after EZH2 knock down, adhered via respective promoter DNA methylation [180]. However, already Varambally et al. observed that EZH2-mediated gene silencing could be reverted in prostate cancer cells by the treatment with HDAC inhibitor TSA [142], since PRC2 complexes may interact through EED with HDAC2 to mediate their suppressive activity [32]. Subsequent experiments revealed, that not only treatment with the pan-HDAC inhibitor TSA but also with the more specific HDAC inhibitor MS-275, inhibiting only class I HDACs (HDAC1, 2 and 3) and the class II A HDAC9 [144], led to a similar induction of differentiation genes (Fig. 21).

Since both, SUZ12 and EED are essential for the histone methyltransferase activity of EZH2, several knock down experiments were performed to examine the requirement for SUZ12 and EED in EZH2-mediated inactivation of differentiation genes in ET. Microarray data revealed that SUZ12 and EED are not over-expressed in primary ET compared to normal tissues (Fig. 18). Similar results were also reported for prostate and breast cancer, since patient samples revealed EZH2, but not EED over-expression [142, 174]. Furthermore, suppression of EWS/FLI1 did not result in a reduction of SUZ12 or EED expression, as observed for EZH2 expression (Fig. 18). These analyses substantiate, that amongst PRC2 components only EZH2 is regulated by EWS/FLI1 in ET.

However, suppression of EED and SUZ12, using specific EED and SUZ12 siRNAs, revealed an induction of the same differentiation genes as observed upon EZH2 suppression (Fig. 17). In addition, EZH2, EED as well as SUZ12 suppressed ET cells efficiently formed tubular networks in endothelial tube formation assays, while parental and control cells showed no tube formation capacity (Fig. 26). These results show that the re-activation of endothelial differentiation genes on the transcriptional level also lead to a more differentiated phenotype of ET cells, enabling the formation of endothelial tube-like structures after EZH2 knock down. Similarly, after induction of neuronal differentiation by BHA [145], only EZH2 suppressed ET cells showed induced protein expression of GFAP, a structural element of fibrillary astrocytes [146] that is exclusively expressed in neuronal tissue (Fig. 24, 25). Vice versa these analyses suggest, that endothelial as well as neuronal differentiation genes are suppressed by PRC2-mediated gene silencing in ET.

Interestingly, microarray analyses of EZH2 suppressed ET cells also revealed a direct or indirect regulation of stem cell markers (Fig. 16). qRT-PCR analyses validated, that the neuroectodermal stem cell marker NGFR [143] as well as the transcription factors NANOG and OCT4 (also known as POU5F1) were down-regulated upon EZH2 suppression (Fig. 17, 20). Since no mechanism for a PRC2-mediated or EZH2-mediated gene activation is described in the literature so far, further experiments to examine the influence of EZH2 on *NGFR* expression were performed. Ectopic expression of EZH2 in A673 ET cells resulted in an increase of NGFR mRNA levels (Fig. 19), indicating a regulation of *NGFR* expression by EZH2. In addition, promoter arrays revealed a binding of EZH2 protein to the *NGFR* promoter DNA region (- 212 bp upstream of the *NGFR* transcriptional start site) and a reduced EZH2 occupancy upon EZH2 suppression (data not shown). Interestingly, a simultaneous reduction of H3K27me3 within the *NGFR* promoter region was not detectable upon EZH2 suppression. Similarly, only 294 out of the 2593 gene promoters revealed a significant reduction (more than 1.5-fold) of H3K27me3 upon reduced EZH2 binding. However, further experiments are necessary to substantiate these results. Likewise, comparable results were observed by Kirmizis et al. [51] who suggested SUZ12 (one of the essential PRC2 components) to have a role in both, transcriptional repression and activation of target genes. SUZ12 is over-expressed in colon cancer and siRNA-mediated depletion of SUZ12 resulted in an activation as well as inhibition of several genes. ChIP-on-chip analyses showed a direct recruitment of SUZ12 to promoter regions of genes, that were up-regulated as well as down-regulated upon SUZ12 suppression and reduced H3K27me3 was only observed at previously silenced target gene promoters.

Consistently, a simultaneous reduction of EZH2 protein binding and H3K27me3 was observed at promoter regions of previously silenced and, upon EZH2 suppression reactivated differentiation genes. As shown in Tab. 24, a reduced H3K27me3 were observed at loci upstream (e.g. *EMP1*) or downstream (e.g. *EPHB2*, *GAP43*) of the transcriptional start site (TSS). These findings are consistent with results of other groups demonstrating an enrichment of H3K27me3 and an EZH2-mediated gene regulation via H3K27me3 at sites proximal and distal of the TSS [46, 50, 181, 182]. The observed induction of differentiation genes upon EZH2 suppression may be a direct result of reduced promoter EZH2 binding and H3K27me3, since H3K27me3 marks inactive chromatin and silenced gene promoters, respectively. However, reductions of EZH2 binding at exactly the same loci that revealed reduced H3K27me3 were not observed in this analysis (compare corresponding positions “distances” within promoter regions shown in Tab. 24). A “not precise overlap” of the H3K27me3 and the EZH2 binding site within target gene promoters was also reported by others [51, 183]. Tiwari et al. noticed that EZH2 transcriptionally regulates multiple genes simultaneously by mediating long-range chromosomal interactions [183]. They showed that EZH2 acts as a cis/trans regulatory element, thereby mediating H3K27 histone modifications of spatially adjacent chromatin regions (physical proximity by chromatin looping).

Western blot analyses in addition suggested a simultaneous, EZH2-mediated regulation of multiple genes via broad H3K27 modifications, since the suppression of EZH2 led to a very efficient and global reduction of the associated heterochromatin mark H3K27me3 (Fig. 22). The concurrent global increase of the “active” H3K9/14ac histone mark upon EZH2 suppression, further validates the participation of HDAC activity in PRC2-mediated epigenetic gene silencing in ET.

An inverse correlation of H3K27me3 and H3K9/14ac and the presence of both, repressive H3K27me3 and active H3K9/14 marks (so called bivalent chromatin) at gene promoters of cancer cells as well as stem cells were observed by others [54, 181, 184]. In embryonic stem cells, this bivalent chromatin marks silence developmentally regulated genes while keeping them poised for activation [14, 15, 43, 47, 185].

Taken together, these findings indicate that ET cells use a conserved developmental mechanism to maintain their undifferentiated phenotype. The inhibition of differentiation genes as well as the induction of genes typically expressed in stem cells by EZH2, underlines that EZH2 might play a central role in the pathology of ET, described as poorly differentiated and aggressive tumors [186-188]. This study showed, that the aberrant EWS/FLI1 fusion protein employs PRC2-mediated epigenetic mechanisms to preserve the stem cell like character of ET cells. This stemness phenotype seems to

contribute to the highly aggressive phenotype of ET cells, since EZH2 suppressed ET cells completely lost their ability to colonize lungs of immunocompromised mice. This is in line with previous reports, that i) showed EZH2 to be a marker of aggressive breast, prostate, bladder as well as gastric cancers and ii) demonstrated that tumors with stem cell like gene expression profiles (characterized by deregulation of the polycomb system) are very aggressive and are more likely to resist multiagent chemotherapies [8, 189-191].

Additionally, these results revealed that the EZH2-mediated gene regulation in ET is not necessarily associated with promoter DNA methylation, which is in contrast to reports of other tumor entities [55, 192] but in line with previous findings in prostate and colon cancer cells [54, 142]. Why this undifferentiated phenotype is a reversible state in ET and is not manifest by irreversible DNA methylation is not understood, but may be advantageous for the tumorigenic capacity of this tumor.

The mechanism, how PRC2 may induce the expression of target genes remains unclear. Besides the fact, that several groups showed an inhibition of various genes upon EZH2, EED as well as SUZ12 suppression by microarray analyses, Kirmizis et al., Bracken et al. as well as Pasini et al. reported PRC2 occupancy at activated gene promoters [30, 46, 51, 52]. Additionally, Pasini et al. observed that these genes were not activated in Suz12−/− mouse embryonic stem (ES) cells, suggesting that PRC2 has a direct role in the transcriptional activation of these targets. Furthermore, the authors demonstrated a binding of PRC2 to *Nanog* and *Oct4* promoter regions. It was also reported that NANOG and OCT4 together with PcG proteins bind at many repressed target genes [43] and that OCT4 maintains stem cell self-renewal of ES and tumor cells by recruiting PRC2 to certain genes that otherwise promote differentiation [44]: suggesting that a regulation of NANOG and OCT4 expression by PRC2 may be a possible mechanism in ET.
However, whether the induction of NANOG and OCT4 is a consequence of the stem cell like phenotype or is necessary to maintain stemness in ET requires further investigations.

### 5.1.4. Histogenesis of ET - EZH2 suppressed ET cells cluster with neuronal tissue, MSCs and endothelial cells

The histogenetic origin of ET is still under debate. ET cells display mesenchymal, neuroectodermal as well as endothelial features [113-115], suggestive for either a mesenchymal or a neuroectodermal origin. Since ET display no specific histological

phenotype that enables a correlation to a putative cell of origin, the comparison of its expression profile via microarray analysis might provide further informations.
Microarray analyses comparing ET-specific gene expression profiles with a wide spectrum of normal tissues, identified a relationship of ET to fetal, neural as well as endothelial cells [128]. This led to the conclusion, that primitive neural crest-derived progenitors at the transition to mesenchymal and endothelial differentiation are transformed into ET. In this study, cluster analyses revealed that the expression signature of EZH2 suppressed ET cells clustered with expression profiles of neuronal tissue, mesenchymal stem cells (MSC) and endothelial cells (see Appendix 9.1.). Riggi et al. argued [193] that MSCs display the required intrinsic tolerance for the transforming potential of EWS/FLI1, which can induce partial neuroectodermal differentiation of primary MSCs indicating that ET do not necessarily arise from a neuroectodermal precursor to explain their primitive neuroectodermal phenotype. Furthermore, two studies suggested that a significant portion of MSCs may originate from neuroepithelium and neural crest stem cells [194, 195], while the similarities between ET and endothelial cells might be explained by the observation, that hematopoietic stem cells can generate MSCs [196]. These studies provided evidence that ET may derive from a MSC of hematopoietic or neuroectodermal origin that maintains dual plasticity.

### 5.1.5. Clinical implications – epigenetic therapy including EZH2 blockage

The discovery of the cell of origin and the generation of a proper ET animal model, which is still lacking, are urgent goals for the development of new alternative drugs and treatment approaches. However, this study indicates that EZH2 per se and EZH2-mediated epigenetic modifications might be promising novel pharmacological targets for ET therapy. Furthermore, since EZH2 expression correlates with tumor aggressiveness in a wide variety of cancers and serves as an independent prognostic factor in the progression and prognosis of breast and prostate cancer, EZH2 may also provide a prognostic marker in ET.

Epigenetic therapies aim to pharmacologically reactivate abnormally silenced genes in cancer patients to reverse the tumorigenic properties. A variety of such epigenetic modifiers, namely DNA methylation inhibitors and HDAC inhibitors, are currently tested in clinical trials [197-202]. These epigenetic drugs can reverse aberrant epigenetic gene silencing *in vivo,* as demonstrated by Gore et al. who showed, that the combinatorial treatment with a DNA methyltransferase inhibitor and a HDAC inhibitor (HDACi) decreased DNA methylation and increased histone acetylation in patients with

myelodysplastic syndrome and acute myeloid leukemia, which was accompanied with hematological improvement [203].

Since HDACs also seem to be involved in PRC2-mediated gene silencing in ET, such a combinatorial treatment might be a new therapeutic modality for ET patients. The synthetic benzidamide MS-275 is an attractive HDACi candidate, since it retains HDACi activity when administered orally in mice [200]. This efficient HDACi activity is mediated by the targeting of the $Zn^{2+}$ ion in the catalytic domain of the $Zn^{2+}$-dependent HDACs [204]. MS-275 potently inhibits cell growth and the tumorigenic potential of different ET cell lines *in vitro* and *in vivo* [205-207] and the authors proposed MS-275 as a novel treatment strategy for ET either applied as monotherapy or in combination, based on its potential to enhance the efficacy of other anticancer agents. However, specific inhibitors of EZH2 have not yet been described. A promising inhibitory agent of PRC2 is deazaneplanocin A (DZNep), which acts through an indirect mechanism. Tan et al. demonstrated that DZNep reactivates PRC2-silenced genes, which lead to cell death of many cancer cell types tested, without affecting normal cells [208]. This is an important observation, since EZH2 is also expressed (albeit clearly weaker than in ET) in normal tissue (see Fig. 3).

Nevertheless, since these types of inhibitors could affect many processes that require either methyl transferase or acetylase activity, unspecific adverse effects have to be evaluated and minimized by the development of more specific inhibitors.

## 5.2. Involvement of non-coding RNAs and Argonaute proteins in ET pathogenesis

Although microRNAs (miRNA) were shown to be involved in cancer progression of many tumor entities [148-152], very little is known about the participation of non-coding RNAs in ET pathogenesis. Non-coding RNAs are involved in fundamental processes such as development, differentiation, cell proliferation and apoptosis [209, 210]. The observation that polycomb group proteins, like EZH2, regulate stemness in normal and cancer cells via an epigenetic control of miRNA expression [8], suggest a possible role for non-coding RNAs in ET pathogenesis.

This study shows for the first time, that EZH2 and the repressive mark H3K27me3 occupy promoter regions of putative tumor suppressor miRNAs as well as oncogenic miRNAs in ET. Furthermore, it was observed that knock down of Argonaute proteins, which are essential for miRNA processing and non-coding RNA-mediated gene regulation, led to changes in phenotype and tumorigenic potential of ET cells *in vitro* and *in vivo*.

### 5.2.1. EZH2 binds to promoter regions of putative tumor suppressor miRNAs and oncogenic miRNAs

The ChIP-on-chip analyses performed in this study revealed a H3K27me3 occupancy and a binding of EZH2 to promoters of several miRNAs (Tab. 25). Many of these miRNAs were reported to act as tumor suppressors (14 / 26) and are epigenetically silenced (8 / 26) in a number of other tumor entities [211-214],[213, 215-221]. Only two of them, miRNA-507 and miRNA-516-4 have not been described in the literature so far. However, knowledge about biological functions of individual miRNAs and their regulation is still scarce and a possible involvement of these miRNAs in tumor progression and their possible regulation through epigenetic mechanisms in different cancer types, still need to be investigated.

Upon EZH2 suppression, a significantly reduced H3K27me3 at promoter regions of six miRNAs was observed. Except for the “unknown” miRNA-516-4, all of these miRNAs were reported to be suppressed in different tumors (miRNA-124a-2, miRNA-199a-1, miRNA-423) [222-224] or to have potential roles as tumor suppressor miRNAs (miRNA-185, miRNA-497) [211, 212].

Among those miRNAs that revealed a reduced EZH2 binding but no significant H3K27me3 reduction at their promoters upon EZH2 suppression are miRNA-34a,

miRNA-34b, miRNA-126, miRNA-129-2, miRNA-193a, miRNA-196b as well as miRNA-203. These miRNAs were reported to be tumor suppressor miRNAs and to be epigenetically silenced in other tumor entities. In addition, all of these miRNAs had methylated CpG island promoters and their expression could be reactivated upon treatment with DNA methyltransferase inhibitors alone or in combination with HDACi [213, 215-221]. This is interesting, because EZH2 may similarly mediate gene silencing by the recruitment of DNA methyltranferases (DNMT) and subsequent *de novo* CpG methylation at target promoters [56, 225]. It is assumed that the EZH2 SET domain is involved in DNMT recruitment and that EZH2 pre-marks certain genes to become abnormally hyper-methylated and silenced in cancer cells [55, 192, 226-229]. However, whether these miRNAs are epigenetically silenced in a similar way in ET and whether this occurs via promoter DNA methylation (which may explain the unchanged H3K27me3) warrants further investigations. Though, experimental artefacts may not be excluded at this stage, since only 6 out of 26 miRNA promoters showed significantly reduced H3K27me3 upon EZH2 suppression.

MiRNAs that exhibited reduced EZH2 binding upon EZH2 suppression included miRNA-22, miRNA-29c, miRNA-99b, miRNA-152, miRNA-199b, miRNA-202 and miRNA-296 [230-236]. While the ectopic expression of miRNA-22, miRNA-29c or miRNA-199b inhibits cell proliferation and the tumorigenic potential of tumor cells [237-239], the biological functions and effects of the other miRNAs were not examined in the corresponding tumor entities and remain unknown.

Interestingly, the EZH2-bound miRNA-219-1 and miRNA-499 were reported to control cell differentiation of oligodendrocytes and cardiomyocytes, respectively, and were highly up-regulated in differentiated cells [240-242]. In addition, miRNA-203 was shown to repress stemness by promoting epithelial differentiation [243, 244].

Taken together, the binding of EZH2 to promoter regions of miRNAs, which inhibit cell proliferation or induce cell differentiation, suggested that EZH2 may also suppresses critical miRNAs to enhance tumorigenicity and to maintain stemness of ET cells.

In contrast, EZH2 binding too was observed at promoter regions of miRNAs that were reported to be up-regulated in tumor cells, such as miRNA-210, miRNA-345 and miRNA-365-2. The hypoxia-regulated miRNA-210 has an important role in cell survival under hypoxic conditions and its over-expression in head and neck as well as pancreatic tumors is associated with poor survival [245-247]. In addition, miRNA-210 is linked to aggressiveness and metastatic spread in breast cancer [248]. MiRNA-345 is highly expressed in malignant mesothelioma [224], while miRNA-365-2 belongs to the miRNA cluster miR-193b-365 that is over-expressed in multiple myeloma [249].

Similarly, miRNA-345 seems to be associated with acquired resistance of breast cancer cells to cisplatin [250] and with the malignant transformation to oral carcinoma [251]. Enhanced survival under hypoxic conditions, drug resistance and aggressiveness are important features of aggressive tumors, such as ET. Since EZH2 occupancy was also observed at active gene promoters (discussed in 5.1.3.), an up-regulation of these miRNAs in ET cells seems to be possible.

However, whether these miRNAs are indeed deregulated in ET by EZH2 requires further investigations. So far, no ET-specific miRNA expression profile was published, while such profiles are already available for many other cancer types. Due to a lack of proper probe sets, the Affymetrix microarrays used in this study did not include miRNA expression. Therefore, the expression analysis of respective miRNAs in primary ET versus normal tissues or upon EZH2 siRNA and HDAC inhibitor treatment was impossible. Further experiments, such as miRNA array analyses upon EZH2 knock down, DNMT and HDAC inhibition with subsequent RT-PCR analyses as well as functional analyses of miRNAs using synthetic miRNAs mimics or miRNA inhibitors (anti-miRNAs / antagomirs) are planned. These experiments would help to elucidate, whether and how non-coding RNAs are involved in ET pathogenesis and whether EZH2 de facto regulates miRNA expression in this disease.

Several studies demonstrated EZH2 to be a direct target of miRNA-26a and miRNA-101 and deregulation of both miRNAs led to an over-expression of EZH2 in different tumor entities [64, 67, 252-256]. Thereupon, several experiments addressed the question, whether EZH2 is additionally regulated by miRNAs in ET. The comparison of the amounts of mature miRNA-26a between ET and neuroblastoma as well as cALL cell lines (with considerably weaker EZH2 expression, Fig. 4) showed equal amounts of miRNA-26a in all tested cell lines, and neither suppression of EWS/FLI1 in different ET cell lines nor ectopic expression of EWS/FLI1 in MSC influenced the amount of miRNA-26a. Additionally, siRNA-mediated knock down of AGO1, AGO2 and of TAR (HIV-1) RNA binding protein 2 TARBP2 (three essential proteins that are required for miRNA processing and RNA-mediated gene silencing in humans [74, 78, 257]) did not affect EZH2 expression on mRNA or protein levels, respectively (data not shown). These results further substantiate our initial observation, that the EWS/FLI1 fusion protein directly regulates EZH2 expression in ET.

### 5.2.2. MiRNA-221 is highly expressed in ET

MiRNA-221 has been implicated in tumor progression and is over-expressed in a variety of tumor entities, including aggressive chronic lymphocytic leukemia's [258, 259], acute myeloid leukemia [260], glioma [261], aggressive non-small cell lung cancer [262], hepatocellular carcinoma [262-264], atypical teratoid-rhabdoid tumors [265], prostate cancer [266, 267], cutaneous melanomas [268], breast cancer [269], thyroid papillary carcinomas [270], bladder cancer [271] and pancreatic adenocarcinoma [272]. Several studies showed miRNA-221 to be an oncogenic miRNA, activating the serine/threonine protein kinase (Akt) pathway [261, 262] and inhibiting different tumor suppressors, such as CDKN1C p57kip, PTEN (phosphatase and tensin homolog), p27 (26S proteasome regulatory subunit p27**)** and TIMP3 (TIMP metallopeptidase inhibitor 3), that contribute to the development of an invasive phenotype, characteristic for highly malignant cancer cells [262, 263, 273]. Furthermore, several studies showed that inhibition of miRNA-221 induces cell apoptosis and decreases tumor growth *in vivo* [258, 274-276], while over-expression of miRNA-221 increases cell proliferation, invasion and tumor growth of different cancer cells [261, 262].

Since miRNA-221 was also reported to be up-regulated in primary ET tissue [153], RT-PCR analyses were performed to quantify the amounts of mature miRNA-221 in different ET cell lines. These analyses revealed a high amount of miRNA-221 also in ET cell lines when compared to other pediatric tumor cell lines (Fig. 30). While expression of miRNA-221 was nearly undetectable in neuroblastoma cell lines, cALL and ET cell lines expressed mature miRNA-221. However, several ET cell lines had a 2 to 4 times higher amount of miRNA-221 as compared to cALL. These results and the observed decreased tumorigenicity of ET cells upon AGO2-mediated reduction of mature miRNA-221 (discussed in the next chapter), hint to an involvement of miRNA-221 also in ET pathogenesis.

### 5.2.3. Loss of Argonaute protein 2 reduces the amount of mature miRNA-221 in ET

Riggi et al. recently reported miRNA-145 as the first miRNA to be involved in ET pathogenesis and to be regulated by EWS/FLI1. They showed, that EWS/FLI1-mediated repression of miRNA-145 contributes to an initiation of MSC reprogramming towards ET cells [83]. To assess the effect of a general inhibition of non-coding RNAs on phenotype and tumorigenic potential of ET cells, two Argonaute proteins (AGO1 and AGO2) were separately knocked down in different ET cell lines. Argonaute proteins,

especially Argonaute protein 2, play important roles in mammalian miRNA processing as well as in mediating small RNA-induced gene regulation [74, 89, 92]. In addition, Argonaute proteins were reported to direct non-coding RNA-mediated epigenetic gene silencing inter alia by the recruitment of histone-modifying enzymes, including EZH2, to target gene promoters [93-95, 277]. Thus, suppression of Argonaute proteins may elucidate if non-coding RNAs and thus Argonaute proteins are involved in ET pathogenesis.

To examine whether siRNA-mediated inhibition of AGO1 and AGO2 interfere with processing of mature miRNA in ET cells, quantification of mature miRNA-221 was performed by RT-PCR analysis. These analyses revealed reduced amounts of mature miRNA-221 in different ET cell lines upon AGO2 knock down, but not upon AGO1 knock down (Fig. 30), suggesting a role of AGO2 in miRNA maturation and/or the stabilization of miRNAs in ET. Consistently, previous reports showed that AGO2, but not of AGO1, is essential for miRNA maturation [77, 257, 278]. Diederichs and Haber observed strongly reduced expression of different miRNAs in murine embryonic fibroblasts (MEFs) derived from Ago2 knockout mice. Rescue experiments demonstrated increased expression of mature miRNAs in Ago2 reconstituted MEFs, while the ectopic expression of Ago1 only partially compensated for Ago2 deficiency [77].

Knock down of AGO2 reduced proliferation, colony formation and invasiveness of ET cells *in vitro* (Fig. 31, 32, 36). Furthermore, suppression of AGO2 impaired local tumor growth (Fig. 33) and inhibited metastasis into the lungs *in vivo* (Fig. 34, 35). Metastasis into the liver may be due to tumor cells that were unable to invade pulmonary tissue and have been passively transported through the porous barrier of liver tissue, where they grew to metastases (as discussed in 5.1.2.).

The inhibition of mature miRNA-221 levels upon AGO2 suppression may directly mediate these phenotypic changes, since miRNA-221-suppressed cancer cells show similar phenotypic and tumorigenic changes [261, 262] (discussed in 5.2.2.). However, AGO2 knock down only results in a suppression of miRNA-221 down to 50-60%. Thus, involvement of additional miRNAs or proteins is likely. AGO2 knock down experiments in myeloma cells enhanced expression of the cyclin-dependent kinase inhibitors (*p21* and *p27*) and caspases (*caspase-3, -8, -9*), which significantly decreased cell viability [279].

SAM analyses of microarray data of AGO2-suppressed A673 and MHHES1 ET cells revealed an up-regulation of 42 genes (q-value ≥ 0.2%) and a down-regulation of 83 genes (q-value ≥ 0.2%). A down-regulation of several genes upon AGO2 suppression

was observed by others [280] and may be due to an indirect regulation (enhanced activation of inhibitors) or a direct effect, since an Argonaute-mediated translational activation was previously reported [281]. Enhanced expression of cyclin-dependent kinase inhibitors or caspases was not observed, instead, the mRNA level of the tumor suppressor RASSF4 (Ras association (RalGDS/AF-6) domain family member 4) was found to be strongly induced in AGO2 suppressed ET cells. *RASSF4* is epigenetically silenced in several cancer types and ectopic expression enhances apoptosis and reduces cell proliferation [282-284]. The reduced tumorigenic potential of AGO2 suppressed ET cells may also arise from enhanced differentiation, since RT-PCR analyses revealed an inhibition of the stem cell markers *ABCG2* and *OCT4*. Additionally, microarray analyses further illustrated an up-regulation of genes typically expressed in neuronal cells, such as *neurexin 2* (*NRXN2*) and *neuron navigator 3* (*NAV3*). This induction of neuronal markers, but not of endothelial markers, may also explain the phenotype of AGO2 suppressed ET cells observed in endothelial tube formation assays (Fig. 37, 38).

Nevertheless, further analyses are required to verify the microarray data and to clarify the involvement of miRNA-221 and Argonaute 2 protein in ET pathogenesis.

### 5.2.4. AGO2 expression is reduced upon EZH2 suppression

EZH2 suppression and AGO2 suppression inhibits metastatic spread and local tumor growth *in vivo*. Therefore expression of commonly regulated target genes of both proteins was analyzed. Interestingly, analysis of EZH2 siRNA-treated ET cells exhibited reduced expression of AGO2 on mRNA and protein levels (Fig. 41). Vice versa expression of EZH2 was not changed after AGO2 knock down (data not shown). Comparison of microarray data (genes identified by SAM analyses) revealed a significant regulation of similar target genes upon both, EZH2 and AGO2 suppression. A total of 19 genes were commonly up-regulated, while 9 genes were down-regulated in both, EZH2 and in AGO2 siRNA-treated ET cells. The tumor suppressors *RASSF4* and *NCOR2* (*nuclear receptor co-repressor 2*) as well as the neuronal markers *NRXN2* and *NAV3* belong to the group of commonly up-regulated genes. Interestingly, ChIP-on-chip analysis showed neither reduced H3K27me3 nor diminished EZH2 binding at promoter regions of *NAV3* and *NCOR2* upon EZH2 suppression. Furthermore, no EZH2 or H3K27me3 occupancy was observed at *SERPINE1* (*serpin peptidase inhibitor, clade E, member 1*) and *NRXN2* promoter regions, indicating that these genes are indirect targets of EZH2. Since AGO2 was reported to regulate post-transcriptional as well as transcriptional gene silencing [77, 92, 156], these results

suggest that EZH2 may employ RNA-dependent mechanisms to enhance tumorigenicity of ET cells, too.

However, further investigations are required to make clear, whether EZH2 regulates AGO2 expression directly or indirectly and to characterize the genes involved in the phenotypic and tumorigenic changes observed upon EZH2 and AGO2 suppression.

### 5.2.5. Knock down of AGO1 enhances stemness of ET cells

In contrast to AGO2 knock down, AGO1 suppressed ET displayed enhanced metastatic spread and tumor growth *in vivo* (Fig. 33, 34, 35), associated by an increased invasive growth as analyzed by *in vitro* invasion assays (Fig. 36). Furthermore, AGO1 knock down inhibits formation of endothelial-like structures on Matrigel (Fig. 38).

Expression analyses of endothelial as well as vasculogenic mimicry markers were performed to address the question, why some parental ET cell lines have the capability to form tubes and others do not. *De novo* generation of micro vascular channels by aggressive tumor cells without participation of endothelial cells (independent of angiogenesis) was termed “vasculogenic mimicry“. Vasculogenic mimicry is associated with high expression of EPHA2 (EPH receptor A2), VECAD2 (vascular endothelial cadherin 2) and TFPI (tissue factor pathway inhibitor) [285-287]. While expression of these vasculogenic mimicry markers were similar in different ET cell lines, the endothelial marker EPHB2 exhibited the strongest expression in ET cell lines that display tube formation capacities (data not shown). EPHB2 was reported to induce capillary sprout formation in *in vitro* angiogenesis assays [288], which may explain the different phenotypes of ET cell lines. However, reduced expression of EPHB2 was neither observed in RDES and SB-KMS-KS1 cells (with tube formation capability) nor in A673 and MHHES1 cells (without tube formation capability) upon AGO1 suppression.

Instead, the expression of the stem cell markers NGFR, PROM1 (also known as CD133) and ABCG2 was increased after suppression of AGO1 in these ET cell lines, as examined by microarray, qRT-PCR and FACS analysis (Fig. 39, 40). While NGFR was reported to be a marker of neuroectodermal stem cells [143], ABCG2 and PROM1 are expressed in a wide variety of stem cells [154, 155]. Several studies demonstrated an expression of both markers on putative cancer stem cells of different tumor entities [289-294], including ET [295, 296]. ABCG2 and PROM1 positive cancer cells revealed enhanced invasive as well as tumorigenic potential *in vitro* and *in vivo* [289-294, 297-299]. These findings suggest that the induction of *ABCG2* and *PROM1* enhances the

stemness phenotype of AGO1-suppressed ET cells, thus promoting local and invasive growth *in vitro* and *in vivo*.

Interestingly, the tumorigenic potential of ET cells correlates with the NGFR expression. Less tumorigenic ET cells expressed low levels of NGFR (see chapter 5.1.3. for discussion of NGFR suppression upon EZH2 suppression), while the strongly tumorigenic AGO1-suppressed ET cells exhibited increased NGFR expression. Since EZH2 expression was not influenced after AGO1 suppression, an up-regulation of NGFR due to increased EZH2 expression upon AGO1 suppression was excluded. RT-PCR analysis showed enhanced NGFR mRNA levels upon AGO1 suppression, indicating that the up-regulation of NGFR expression may be due to reduced transcriptional repression rather than diminished translational repression. Janowski et al. reported that AGO1 associates with promoter DNA and mediates transcriptional gene silencing (TGS) in mammalian cells [92]. It was shown that AGO1 regulates TGS through the binding to small non-coding RNAs as well as long antisense RNAs, that are complementary to promoter DNA and mRNA, respectively, and by recruiting histone methyltransferases to corresponding DNA sequences [92, 94, 300]. Interestingly, *NGFR* antisense RNA was detected in ET cells by the use of specific antisense primers (data not shown), suggesting that AGO1 may regulate NGFR expression via non-coding RNA-mediated transcriptional gene silencing. Since Kim et al. proposed that AGO1 recruits histone methyltransferases, such as EZH2, thus mediating H3K27me3 and H3K9me2 histone modifications at several gene promoters [94], Western blot analyses were performed to analyze global changes in histone modifications upon AGO1 suppression. No obvious changes of different histone marks were observed between control siRNA- and AGO1 siRNA-treated cells on global levels (Fig. 42), indicating that AGO1-mediated gene silencing does not necessarily require histone modifications, as also reported by Janowski et al. [92]. Another explanation could be that these histone modifications only occur at several specific gene promoters, which is not detectable by global Western blot analyses.

Further investigations are needed to address the questions, how AGO1 induces *ABCG2*, *PROM1* and *NGFR* gene expression in ET cells and why these genes are not induced in parental cells, even though this induction would lead to phenotypic changes that obviously enhance tumorigenicity of ET cells. The observation that AGO1 is involved in repression of stem cell activities in *Drosophila*, thereby contributing to the control of a balance between ovarian germ line stem cell self-renewal and differentiation [301], may be a possible answer to this question.

However, these results further support the assumption, that stemness is rather a state than a fate of cancer cells and that stemness features are preserved via epigenetic mechanisms. Cellular plasticity, mediated by epigenetic mechanisms, plays an essential role in cancer development, since differentiated cells can acquire cancer stem cell properties [302-305]. Both, EZH2 protein and Argonaute proteins regulate stem cell marker and differentiation genes, thereby most likely controlling the maintenance of stemness and tumorigenicity in ET.

### 5.2.6. Argonaute proteins as potential biomarkers and therapies based on synthetic miRNA mimics or antagomirs

Argonaute proteins are potential biomarkers for prostate, esophageal and colon cancer, due to an increased AGO1 and / or AGO2 expression in tumorigenic rather than in adjacent benign tissues [306, 307]. In primary ET samples, AGO1 or AGO2 expression levels are similar to those of normal tissues of diverse origin (expression analyses of 11 ET and 133 normal tissue samples using DNA microarrays, data not shown), indicating that Argonaute proteins do not seem to be suitable biomarkers for ET. However, since the cell of origin of ET is still unknown, the expression of Argonaute proteins in ET tissues was not matched to the appropriate corresponding non-tumorigenic tissue. This aspect should be considered.

In contrast, EZH2 protein and miRNA-221 are highly expressed in primary ET samples and ET cell lines. Over-expression of EZH2 and miRNA-221, respectively, enhances tumorigenicity of a variety of cancer cells, therefore both molecules are potential targets for the development of non-coding RNA-based anti-cancer drugs. Synthetic antisense oligonucleotides, encoding sequences that are complementary to mature oncogenic miRNAs (called antagomirs) as well as synthetic miRNAs (called miRNA mimics) that repress the expression of oncogenic proteins, are promising therapeutic agents to block tumor progression [308, 309]. Krützfeldt et al. used the first chemically engineered oligonucleotides (antagomir-122) to specifically and effectively silence miRNA-122 expression in mice and they showed a suppression of miRNA-122 in several tissues for more than 23 days after one intravenous injection [310]. Furthermore, intravenous injection of a PBS-formulated locked-nucleic-acid (LNA)-modified oligonucleotide complementary to miRNA-122 (SPC3649) effectively antagonized the liver-expressed miRNA-112 in African green monkeys and suppressed Hepatitis C virus (HCV) viremia in chronically HCV infected chimpanzees [311, 312]. As a result, SPC3649 reaches human clinical trials (as first miRNA therapeutic). Additionally, SPC2996, EZN2968 and EZN3042, inhibitors of tumor-associated BCL2

(B-cell CLL/lymphoma 2) mRNA, HIF1A (hypoxia inducible factor 1, alpha subunit) mRNA and Survivin mRNA, respectively, will be checked in future clinical trials for treatment of a variety of human solid and non-solid tumors (Santaris Pharma).

LNA drugs complementary to the oncogenic miRNA-221 or miRNA mimics, that effectively silence EZH2 protein by targeting EZH2 mRNA (similar to endogenous miRNA-101 or miRNA-26a), may be an alternative therapeutic approach for treatment of ET in the future.

# 6. Summary

The Ewing Family of Tumors (ET) is the second most common malignancy of bone and soft tissue in children and young adults and comprise of poorly differentiated and highly malignant tumor cells of uncertain histogenesis. ET are characterized by the presence of chromosomal translocations that fuse the *EWSR1* gene on chromosome 22 with different *ETS* genes. The most common fusion (in 85% of cases) results in the generation of the EWS/FLI1 fusion protein, which acts as an aberrant transcription factor. This thesis work shows for the first time, that EWS/FLI1 regulates the expression of the histone methyltransferase EZH2 (enhancer of zeste, *Drosophila*, homolog 2), thereby employing epigenetic mechanisms to promote and maintain an undifferentiated and highly malignant phenotype of ET. *EZH2* is strongly over-expressed in primary ET tissue as well as in established ET lines and further experimental evidence revealed an EWS/FLI1-dependent expression of *EZH2* in ET and mesenchymal stem cells. Furthermore, chromatin-IP analyses demonstrated a binding of the EWS/FLI1 fusion protein to conserved ETS recognition sites within the *EZH2* promoter region *in vivo*. EZH2 is part of the human polycomb repressive complex 2 (PRC2) and requires at least two of its non-catalytic partners, EED and SUZ12 (not deregulated in ET), to mediate gene repression via di- and trimethylation of histone 3 at lysine 27 (H3K27me2/me3). RNA interference-mediated knock down of EZH2 inhibited contact-independent growth *in vitro* as well as metastatic spread of ET cells, and resulted in delayed local tumor growth in immunodeficient mice. Subsequent analysis revealed a PRC2-mediated repression of endothelial and neuronal differentiation genes in ET cells that was reversible and required HDAC activity. Additionally, an EZH2-dependent regulation of stem cell markers, including NGFR was observed. This study, in addition, demonstrates for the first time, that EZH2 and the repressive mark H3K27me3 occupy promoter regions of putative tumor suppressor as well as oncogenic miRNAs, and that the oncogenic miRNA-221, which is highly expressed in ET cells, is processed in the presence of Argonaute (AGO) protein 2. Moreover, knock down of AGO1 and 2, which are key players in miRNA processing and non-coding RNA-induced gene regulation, also influenced the expression of stem cell and differentiation genes. While AGO2 suppressed ET cells exhibited less contact-independent and invasive growth *in vitro* as well as reduced metastatic potential and delayed local tumor growth in immunodeficient mice, AGO1 knock down resulted in opposite phenotypic changes and was associated with increased expression of the stem cell markers NGFR, ABCG2 and PROM1. Taken together, this study demonstrates the pivotal role of EZH2 in ET pathogenesis and indicates the critical

involvement of Argonaute proteins and non-coding RNAs for maintaining the highly malignant and reversible stemness phenotype. These results open the avenue for new therapeutic modalities, i.e. the implementation of epigenetic drugs or miRNA therapeutics, specifically targeting oncogenic miRNAs or proteins, such as miRNA-221 or EZH2.

# 7. Zusammenfassung

Bei Kindern und jungen Erwachsenen stellt die Familie der Ewing Tumore (ET) die zweithäufigste maligne Erkrankung des Knochens und Weichgewebes dar. Sie bestehen aus wenig differenzierten und hoch malignen Tumorzellen von unklarer Histogenese und sind charakterisiert durch chromosomale Translokationen, die in einer Fusion des *EWSR1* Gen auf Chromosom 22 mit verschiedenen *ETS* Genen resultieren. Die häufigste Fusion (in 85% der Fälle) führt zur Bildung des Fusionsproteins EWS/FLI1, welches als aberranter Transkriptionsfaktor fungiert. Diese Arbeit zeigt zum ersten Mal, dass EWS/FLI1 die Expression der Histon-Methyltransferase EZH2 (enhancer of zeste, *Drosophila*, homolog 2) reguliert und dadurch epigenetische Mechanismen zur Begünstigung und Erhaltung eines undifferenzierten und hoch malignen ET-Phänotyps nutzt. EZH2 ist sowohl in primärem ET Gewebe also auch in etablierten ET Zelllinien stark überexprimiert und verschiedene Experimente zeigten eine EWS/FLI1-abhängige Expression von EZH2 in ET und mesenchymalen Stammzellen. Zudem konnte durch Chromatin-IPs eine Bindung von EWS/FLI1 an konservierte ETS Erkennungssequenzen innerhalb des *EZH2* Promotors *in vivo* nachgewiesen werden. EZH2 ist Teil des humanen polycomb repressive complex 2 (PRC2) und benötigt mindestens zwei der nicht-katalytischen Partner, wie EED und SUZ12 (nicht dereguliert in ET) zur Inaktivierung von Genen über Di- und Trimethylierungen am Lysin 27 des Histon 3 (H3K27me2/me3). Ein RNA-Interferenz-vermittelter EZH2 knock down inhibierte sowohl das kontakt-unabhängige Wachstum *in vitro* also auch die Metastasierung von ET Zellen und resultierte in einem verzögerten lokalen Tumorwachstum in immundefizienten Mäusen. Anschließende Analysen deckten eine reversible PRC2-vermittelte Repression von endothelialen und neuronalen Differenzierungsgenen in ET Zellen auf, die HDAC Aktivität benötigt. Zusätzlich konnte eine EZH2-abhängige Regulation von Stammzellmarkern, wie NGFR, nachgewiesen werden. Diese Arbeit zeigt zudem zum ersten Mal, dass EZH2 und H3K27me3 Promotorregionen von putativen Tumor supprimierenden als auch onkogenen microRNAs (miRNA) besetzen und dass miRNA-221, eine onkogene miRNA die in ET stark exprimiert wird, in Anwesenheit des Argonaute (AGO) Protein 2 prozessiert wird. Außerdem beeinflusste ein knock down von AGO1 und 2, welche essentiell für die miRNA Prozessierung und nicht-kodierende RNA-vermittelte Genregulation sind, ebenfalls die Expression von Stammzell- und Differenzierungsgenen. Während AGO2 supprimierte ET Zellen ein geringeres kontakt-unabhängiges und invasives Wachstum *in vitro* als auch ein vermindertes Metastasierungspotential und verzögertes lokales Tumorwachstum in

immundefizienten Mäusen aufwiesen, resultierte ein knock down von AGO1 in genau gegensätzliche phänotypische Veränderungen, verbunden mit einer verstärkten Expression der Stammzellmarker NGFR, ABCG2 und PROM1. Diese Arbeit demonstriert die zentrale Rolle von EZH2 in der ET Pathogenese und zeigt die Beteiligung von Argonaute Proteinen und nicht-kodierenden RNAs zur Erhaltung des hoch malignen und reversiblen Stammzell-Phänotyps auf. Diese Ergebnisse eröffnen neue Behandlungsmodalitäten, wie etwa die Anwendung epigenetischer Medikamente oder von microRNA Therapeutika, welche zielgerichtet gegen onkogene miRNAs oder Proteine wie miRNA-221 oder EZH2 wirken.

# 8. References


1. Herman, J.G. and S.B. Baylin, *Gene silencing in cancer in association with promoter hypermethylation.* N Engl J Med, 2003. **349**(21): p. 2042-54.
2. Weber, M., et al., *Distribution, silencing potential and evolutionary impact of promoter DNA methylation in the human genome.* Nat Genet, 2007. **39**(4): p. 457-66.
3. Egger, G., et al., *Epigenetics in human disease and prospects for epigenetic therapy.* Nature, 2004. **429**(6990): p. 457-63.
4. Esteller, M., *Epigenetics in cancer.* N Engl J Med, 2008. **358**(11): p. 1148-59.
5. Feinberg, A.P., H. Cui, and R. Ohlsson, *DNA methylation and genomic imprinting: insights from cancer into epigenetic mechanisms.* Semin Cancer Biol, 2002. **12**(5): p. 389-98.
6. Reik, W. and A. Lewis, *Co-evolution of X-chromosome inactivation and imprinting in mammals.* Nat Rev Genet, 2005. **6**(5): p. 403-10.
7. Fuks, F., *DNA methylation and histone modifications: teaming up to silence genes.* Curr Opin Genet Dev, 2005. **15**(5): p. 490-5.
8. Gieni, R.S. and M.J. Hendzel, *Polycomb group protein gene silencing, non-coding RNA, stem cells, and cancer.* Biochem Cell Biol, 2009. **87**(5): p. 711-46.
9. Alvarez-Venegas, R. and Z. Avramova, *SET-domain proteins of the Su(var)3-9, E(z) and trithorax families.* Gene, 2002. **285**(1-2): p. 25-37.
10. Sims, R.J., 3rd, K. Nishioka, and D. Reinberg, *Histone lysine methylation: a signature for chromatin function.* Trends Genet, 2003. **19**(11): p. 629-39.
11. Jenuwein, T., *The epigenetic magic of histone lysine methylation.* FEBS J, 2006. **273**(14): p. 3121-35.
12. Jenuwein, T. and C.D. Allis, *Translating the histone code.* Science, 2001. **293**(5532): p. 1074-80.
13. McGarvey, K.M., et al., *Defining a chromatin pattern that characterizes DNA-hypermethylated genes in colon cancer cells.* Cancer Res, 2008. **68**(14): p. 5753-9.
14. Bernstein, B.E., et al., *A bivalent chromatin structure marks key developmental genes in embryonic stem cells.* Cell, 2006. **125**(2): p. 315-26.
15. Azuara, V., et al., *Chromatin signatures of pluripotent cell lines.* Nat Cell Biol, 2006. **8**(5): p. 532-8.
16. Mikkelsen, T.S., et al., *Genome-wide maps of chromatin state in pluripotent and lineage-committed cells.* Nature, 2007. **448**(7153): p. 553-60.
17. Rada-Iglesias, A., et al., *Histone H3 lysine 27 trimethylation in adult differentiated colon associated to cancer DNA hypermethylation.* Epigenetics, 2009. **4**(2): p. 107-13.
18. Schwartz, Y.B. and V. Pirrotta, *Polycomb complexes and epigenetic states.* Curr Opin Cell Biol, 2008. **20**(3): p. 266-73.
19. Balch, C., et al., *Epigenetic "bivalently marked" process of cancer stem cell-driven tumorigenesis.* Bioessays, 2007. **29**(9): p. 842-5.
20. Ben-Porath, I., et al., *An embryonic stem cell-like gene expression signature in poorly differentiated aggressive human tumors.* Nat Genet, 2008. **40**(5): p. 499-507.
21. Zhang, K. and S.Y. Dent, *Histone modifying enzymes and cancer: going beyond histones.* J Cell Biochem, 2005. **96**(6): p. 1137-48.
22. Santos-Rosa, H. and C. Caldas, *Chromatin modifier enzymes, the histone code and cancer.* Eur J Cancer, 2005. **41**(16): p. 2381-402.
23. Feinberg, A.P. and B. Tycko, *The history of cancer epigenetics.* Nat Rev Cancer, 2004. **4**(2): p. 143-53.
24. Esteller, M. and J.G. Herman, *Cancer as an epigenetic disease: DNA methylation and chromatin alterations in human tumours.* J Pathol, 2002. **196**(1): p. 1-7.
25. Jiang, G., et al., *Effects of long-term low-dose cadmium exposure on genomic DNA methylation in human embryo lung fibroblast cells.* Toxicology, 2008. **244**(1): p. 49-55.

26. Schneider, R., A.J. Bannister, and T. Kouzarides, *Unsafe SETs: histone lysine methyltransferases and cancer.* Trends Biochem Sci, 2002. **27**(8): p. 396-402.

27. Iyer, N.G., H. Ozdag, and C. Caldas, *p300/CBP and cancer.* Oncogene, 2004. **23**(24): p. 4225-31.

28. Wang, G.G., C.D. Allis, and P. Chi, *Chromatin remodeling and cancer, Part I: Covalent histone modifications.* Trends Mol Med, 2007. **13**(9): p. 363-72.

29. Simon, J.A. and C.A. Lange, *Roles of the EZH2 histone methyltransferase in cancer epigenetics.* Mutat Res, 2008. **647**(1-2): p. 21-9.

30. Bracken, A.P., et al., *EZH2 is downstream of the pRB-E2F pathway, essential for proliferation and amplified in cancer.* EMBO J, 2003. **22**(20): p. 5323-35.

31. Margueron, R., et al., *Ezh1 and Ezh2 maintain repressive chromatin through different mechanisms.* Mol Cell, 2008. **32**(4): p. 503-18.

32. van der Vlag, J. and A.P. Otte, *Transcriptional repression mediated by the human polycomb-group protein EED involves histone deacetylation.* Nat Genet, 1999. **23**(4): p. 474-8.

33. Margueron, R., et al., *Role of the polycomb protein EED in the propagation of repressive histone marks.* Nature, 2009. **461**(7265): p. 762-7.

34. Pasini, D., et al., *Suz12 is essential for mouse development and for EZH2 histone methyltransferase activity.* EMBO J, 2004. **23**(20): p. 4061-71.

35. Cao, R. and Y. Zhang, *SUZ12 is required for both the histone methyltransferase activity and the silencing function of the EED-EZH2 complex.* Mol Cell, 2004. **15**(1): p. 57-67.

36. Shen, X., et al., *EZH1 mediates methylation on histone H3 lysine 27 and complements EZH2 in maintaining stem cell identity and executing pluripotency.* Mol Cell, 2008. **32**(4): p. 491-502.

37. Ringrose, L. and R. Paro, *Polycomb/Trithorax response elements and epigenetic memory of cell identity.* Development, 2007. **134**(2): p. 223-32.

38. Brown, J.L. and J.A. Kassis, *Spps, a Drosophila Sp1/KLF family member, binds to PREs and is required for PRE activity late in development.* Development, 2010. **137**(15): p. 2597-602.

39. Woo, C.J., et al., *A region of the human HOXD cluster that confers polycomb-group responsiveness.* Cell, 2010. **140**(1): p. 99-110.

40. Sing, A., et al., *A vertebrate Polycomb response element governs segmentation of the posterior hindbrain.* Cell, 2009. **138**(5): p. 885-97.

41. Soshnikova, N. and D. Duboule, *Epigenetic temporal control of mouse Hox genes in vivo.* Science, 2009. **324**(5932): p. 1320-3.

42. Simon, J.A. and R.E. Kingston, *Mechanisms of polycomb gene silencing: knowns and unknowns.* Nat Rev Mol Cell Biol, 2009. **10**(10): p. 697-708.

43. Lee, T.I., et al., *Control of developmental regulators by Polycomb in human embryonic stem cells.* Cell, 2006. **125**(2): p. 301-13.

44. Squazzo, S.L., et al., *Suz12 binds to silenced regions of the genome in a cell-type-specific manner.* Genome Res, 2006. **16**(7): p. 890-900.

45. Endoh, M., et al., *Polycomb group proteins Ring1A/B are functionally linked to the core transcriptional regulatory circuitry to maintain ES cell identity.* Development, 2008. **135**(8): p. 1513-24.

46. Bracken, A.P., et al., *Genome-wide mapping of Polycomb target genes unravels their roles in cell fate transitions.* Genes Dev, 2006. **20**(9): p. 1123-36.

47. Boyer, L.A., et al., *Polycomb complexes repress developmental regulators in murine embryonic stem cells.* Nature, 2006. **441**(7091): p. 349-53.

48. Schoeftner, S., et al., *Recruitment of PRC1 function at the initiation of X inactivation independent of PRC2 and silencing.* EMBO J, 2006. **25**(13): p. 3110-22.

49. Cao, Q., et al., *Repression of E-cadherin by the polycomb group protein EZH2 in cancer.* Oncogene, 2008. **27**(58): p. 7274-84.

50. Yang, X., et al., *CDKN1C (p57) is a direct target of EZH2 and suppressed by multiple epigenetic mechanisms in breast cancer cells.* PLoS One, 2009. **4**(4): p. e5011.

51. Kirmizis, A., et al., *Silencing of human polycomb target genes is associated with methylation of histone H3 Lys 27.* Genes Dev, 2004. **18**(13): p. 1592-605.

52. Pasini, D., et al., *The polycomb group protein Suz12 is required for embryonic stem cell differentiation.* Mol Cell Biol, 2007. **27**(10): p. 3769-79.

53. Shi, B., et al., *Integration of estrogen and Wnt signaling circuits by the polycomb group protein EZH2 in breast cancer cells.* Mol Cell Biol, 2007. **27**(14): p. 5105-19.

54. Kondo, Y., et al., *Gene silencing in cancer by histone H3 lysine 27 trimethylation independent of promoter DNA methylation.* Nat Genet, 2008. **40**(6): p. 741-50.

55. Schlesinger, Y., et al., *Polycomb-mediated methylation on Lys27 of histone H3 pre-marks genes for de novo methylation in cancer.* Nat Genet, 2007. **39**(2): p. 232-6.

56. Vire, E., et al., *The Polycomb group protein EZH2 directly controls DNA methylation.* Nature, 2006. **439**(7078): p. 871-4.

57. Klose, R.J. and A.P. Bird, *Genomic DNA methylation: the mark and its mediators.* Trends Biochem Sci, 2006. **31**(2): p. 89-97.

58. Esteller, M., et al., *A gene hypermethylation profile of human cancer.* Cancer Res, 2001. **61**(8): p. 3225-9.

59. Bracken, A.P., et al., *The Polycomb group proteins bind throughout the INK4A-ARF locus and are disassociated in senescent cells.* Genes Dev, 2007. **21**(5): p. 525-30.

60. Nevins, J.R., *Toward an understanding of the functional complexity of the E2F and retinoblastoma families.* Cell Growth Differ, 1998. **9**(8): p. 585-93.

61. Wu, Z.L., et al., *Polycomb protein EZH2 regulates E2F1-dependent apoptosis through epigenetically modulating Bim expression.* Cell Death Differ, 2010. **17**(5): p. 801-10.

62. Cha, T.L., et al., *Akt-mediated phosphorylation of EZH2 suppresses methylation of lysine 27 in histone H3.* Science, 2005. **310**(5746): p. 306-10.

63. Riising, E.M., et al., *The polycomb repressive complex 2 is a potential target of SUMO modifications.* PLoS One, 2008. **3**(7): p. e2704.

64. Sander, S., et al., *MYC stimulates EZH2 expression by repression of its negative regulator miR-26a.* Blood, 2008. **112**(10): p. 4202-12.

65. Szulwach, K.E., et al., *Cross talk between microRNA and epigenetic regulation in adult neurogenesis.* J Cell Biol, 2010. **189**(1): p. 127-41.

66. Juan, A.H., et al., *Mir-214-dependent regulation of the polycomb protein Ezh2 in skeletal muscle and embryonic stem cells.* Mol Cell, 2009. **36**(1): p. 61-74.

67. Varambally, S., et al., *Genomic loss of microRNA-101 leads to overexpression of histone methyltransferase EZH2 in cancer.* Science, 2008. **322**(5908): p. 1695-9.

68. Fire, A., et al., *Potent and specific genetic interference by double-stranded RNA in Caenorhabditis elegans.* Nature, 1998. **391**(6669): p. 806-11.

69. Mattick, J.S. and I.V. Makunin, *Non-coding RNA.* Hum Mol Genet, 2006. **15 Spec No 1**: p. R17-29.

70. Carninci, P., *RNA dust: where are the genes?* DNA Res, 2010. **17**(2): p. 51-9.

71. Zhang, C., *Novel functions for small RNA molecules.* Curr Opin Mol Ther, 2009. **11**(6): p. 641-51.

72. Malecova, B. and K.V. Morris, *Transcriptional gene silencing through epigenetic changes mediated by non-coding RNAs.* Curr Opin Mol Ther, 2010. **12**(2): p. 214-22.

73. Croce, C.M., *Causes and consequences of microRNA dysregulation in cancer.* Nat Rev Genet, 2009. **10**(10): p. 704-14.

74. Wang, B., et al., *Distinct passenger strand and mRNA cleavage activities of human Argonaute proteins.* Nat Struct Mol Biol, 2009. **16**(12): p. 1259-66.

75. Steitz, J.A. and S. Vasudevan, *miRNPs: versatile regulators of gene expression in vertebrate cells.* Biochem Soc Trans, 2009. **37**(Pt 5): p. 931-5.

76. Ryazansky, S.S. and V.A. Gvozdev, *Small RNAs and cancerogenesis.* Biochemistry (Mosc), 2008. **73**(5): p. 514-27.

77. Diederichs, S. and D.A. Haber, *Dual role for argonautes in microRNA processing and posttranscriptional regulation of microRNA expression.* Cell, 2007. **131**(6): p. 1097-108.

78. Melo, S.A., et al., *A TARBP2 mutation in human cancer impairs microRNA processing and DICER1 function.* Nat Genet, 2009. **41**(3): p. 365-70.

79. Marson, A., et al., *Connecting microRNA genes to the core transcriptional regulatory circuitry of embryonic stem cells.* Cell, 2008. **134**(3): p. 521-33.

80. Rouhi, A., et al., *MiRNAs, epigenetics, and cancer.* Mamm Genome, 2008. **19**(7-8): p. 517-25.

81. Bui, T.V. and J.T. Mendell, *Myc: Maestro of MicroRNAs.* Genes Cancer, 2010. **1**(6): p. 568-575.

82. Schotte, D., et al., *Identification of new microRNA genes and aberrant microRNA profiles in childhood acute lymphoblastic leukemia.* Leukemia, 2009. **23**(2): p. 313-22.

83. Riggi, N., et al., *EWS-FLI-1 modulates miRNA145 and SOX2 expression to initiate mesenchymal stem cell reprogramming toward Ewing sarcoma cancer stem cells.* Genes Dev, 2010. **24**(9): p. 916-32.

84. Fazi, F., et al., *Epigenetic silencing of the myelopoiesis regulator microRNA-223 by the AML1/ETO oncoprotein.* Cancer Cell, 2007. **12**(5): p. 457-66.

85. Hodge, D.R., et al., *Interleukin-6 regulation of the human DNA methyltransferase (HDNMT) gene in human erythroleukemia cells.* J Biol Chem, 2001. **276**(43): p. 39508-11.

86. Fabbri, M., et al., *MicroRNA-29 family reverts aberrant methylation in lung cancer by targeting DNA methyltransferases 3A and 3B.* Proc Natl Acad Sci U S A, 2007. **104**(40): p. 15805-10.

87. Garzon, R., et al., *MicroRNA-29b induces global DNA hypomethylation and tumor suppressor gene reexpression in acute myeloid leukemia by targeting directly DNMT3A and 3B and indirectly DNMT1.* Blood, 2009. **113**(25): p. 6411-8.

88. Noonan, E.J., et al., *miR-449a targets HDAC-1 and induces growth arrest in prostate cancer.* Oncogene, 2009. **28**(14): p. 1714-24.

89. Hock, J. and G. Meister, *The Argonaute protein family.* Genome Biol, 2008. **9**(2): p. 210.

90. Chu, Y., et al., *Involvement of argonaute proteins in gene silencing and activation by RNAs complementary to a non-coding transcript at the progesterone receptor promoter.* Nucleic Acids Res, 2010.

91. Boland, A., et al., *Crystal structure and ligand binding of the MID domain of a eukaryotic Argonaute protein.* EMBO Rep, 2010. **11**(7): p. 522-7.

92. Janowski, B.A., et al., *Involvement of AGO1 and AGO2 in mammalian transcriptional silencing.* Nat Struct Mol Biol, 2006. **13**(9): p. 787-92.

93. Kim, D.H., et al., *MicroRNA-directed transcriptional gene silencing in mammalian cells.* Proc Natl Acad Sci U S A, 2008. **105**(42): p. 16230-5.

94. Kim, D.H., et al., *Argonaute-1 directs siRNA-mediated transcriptional gene silencing in human cells.* Nat Struct Mol Biol, 2006. **13**(9): p. 793-7.

95. Morris, K.V., et al., *Small interfering RNA-induced transcriptional gene silencing in human cells.* Science, 2004. **305**(5688): p. 1289-92.

96. Vasudevan, S., Y. Tong, and J.A. Steitz, *Switching from repression to activation: microRNAs can up-regulate translation.* Science, 2007. **318**(5858): p. 1931-4.

97. Vasudevan, S. and J.A. Steitz, *AU-rich-element-mediated upregulation of translation by FXR1 and Argonaute 2.* Cell, 2007. **128**(6): p. 1105-18.

98. Li, L.C., et al., *Small dsRNAs induce transcriptional activation in human cells.* Proc Natl Acad Sci U S A, 2006. **103**(46): p. 17337-42.

99. Roy, A.L., et al., *Natural mRNA is required for directing Met-tRNA(f) binding to 40S ribosomal subunits in animal cells: involvement of Co-eIF-2A in natural mRNA-directed initiation complex formation.* Biochemistry, 1988. **27**(21): p. 8203-9.

100. Carmell, M.A., et al., *The Argonaute family: tentacles that reach into RNAi, developmental control, stem cell maintenance, and tumorigenesis.* Genes Dev, 2002. **16**(21): p. 2733-42.

101. Koesters, R., et al., *Human eukaryotic initiation factor EIF2C1 gene: cDNA sequence, genomic organization, localization to chromosomal bands 1p34-p35, and expression.* Genomics, 1999. **61**(2): p. 210-8.

102. Adams, B.D., K.P. Claffey, and B.A. White, *Argonaute-2 expression is regulated by epidermal growth factor receptor and mitogen-activated protein kinase signaling and correlates with a transformed phenotype in breast cancer cells.* Endocrinology, 2009. **150**(1): p. 14-23.

103. Li, L., et al., *Argonaute proteins: potential biomarkers for human colon cancer.* BMC Cancer, 2010. **10**: p. 38.

104. Yoo, N.J., et al., *Immunohistochemical analysis of RNA-induced silencing complex-related proteins AGO2 and TNRC6A in prostate and esophageal cancers.* APMIS, 2010. **118**(4): p. 271-6.

105. Zhou, Y., et al., *High-risk myeloma is associated with global elevation of miRNAs and overexpression of EIF2C2/AGO2.* Proc Natl Acad Sci U S A, 2010. **107**(17): p. 7904-9.

106. Lahl, M., V.L. Fisher, and K. Laschinger, *Ewing's sarcoma family of tumors: an overview from diagnosis to survivorship.* Clin J Oncol Nurs, 2008. **12**(1): p. 89-97.

107. Miser, J.S., et al., *Treatment of metastatic Ewing's sarcoma or primitive neuroectodermal tumor of bone: evaluation of combination ifosfamide and etoposide--a Children's Cancer Group and Pediatric Oncology Group study.* J Clin Oncol, 2004. **22**(14): p. 2873-6.

108. Burdach, S. and H. Jurgens, *High-dose chemoradiotherapy (HDC) in the Ewing family of tumors (EFT).* Crit Rev Oncol Hematol, 2002. **41**(2): p. 169-89.

109. Bernstein, M., et al., *Ewing's sarcoma family of tumors: current management.* Oncologist, 2006. **11**(5): p. 503-19.

110. Burdach, S., et al., *Myeloablative radiochemotherapy and hematopoietic stem-cell rescue in poor-prognosis Ewing's sarcoma.* J Clin Oncol, 1993. **11**(8): p. 1482-8.

111. Burdach, S., et al., *Total body MRI-governed involved compartment irradiation combined with high-dose chemotherapy and stem cell rescue improves long-term survival in Ewing tumor patients with multiple primary bone metastases.* Bone Marrow Transplant. **45**(3): p. 483-9.

112. Riggi, N. and I. Stamenkovic, *The Biology of Ewing sarcoma.* Cancer Lett, 2007. **254**(1): p. 1-10.

113. Ewing, J., *Classics in oncology. Diffuse endothelioma of bone. James Ewing. Proceedings of the New York Pathological Society, 1921.* CA Cancer J Clin, 1972. **22**(2): p. 95-8.

114. Ushigome, S., R. Machinami, and P.H. Sorensen, *Ewing sarcoma / primitive neuroectodermal tumors.* WHO Classification of Tumors, Pathology and Genetics, Tumors of Soft Tissue and Bone., ed. U.K. Fletcher CDM, Mertens F (Eds). 2003. 298-300.

115. Schmidt, D., D. Harms, and S. Burdach, *Malignant peripheral neuroectodermal tumours of childhood and adolescence.* Virchows Arch A Pathol Anat Histopathol, 1985. **406**(3): p. 351-65.

116. Weidner, N. and J. Tjoe, *Immunohistochemical profile of monoclonal antibody O13: antibody that recognizes glycoprotein p30/32MIC2 and is useful in diagnosing Ewing's sarcoma and peripheral neuroepithelioma.* Am J Surg Pathol, 1994. **18**(5): p. 486-94.

117. Turc-Carel, C., et al., *Chromosomes in Ewing's sarcoma. I. An evaluation of 85 cases of remarkable consistency of t(11;22)(q24;q12).* Cancer Genet Cytogenet, 1988. **32**(2): p. 229-38.

118. Delattre, O., et al., *Gene fusion with an ETS DNA-binding domain caused by chromosome translocation in human tumours.* Nature, 1992. **359**(6391): p. 162-5.

119. Dockhorn-Dworniczak, B., et al., *[Molecular genetic detection of t(11;22)(q24;12) translocation in Ewing sarcoma and malignant peripheral neuroectodermal tumors].* Pathologe, 1994. **15**(2): p. 103-12.

120. Delattre, O., et al., *The Ewing family of tumors--a subgroup of small-round-cell tumors defined by specific chimeric transcripts.* N Engl J Med, 1994. **331**(5): p. 294-9.

121. Jedlicka, P., *Ewing Sarcoma, an enigmatic malignancy of likely progenitor cell origin, driven by transcription factor oncogenic fusions.* Int J Clin Exp Pathol, 2010. **3**(4): p. 338-47.

122. Uren, A. and J.A. Toretsky, *Ewing's sarcoma oncoprotein EWS-FLI1: the perfect target without a therapeutic agent.* Future Oncol, 2005. **1**(4): p. 521-8.

123. Zucman, J., et al., *Combinatorial generation of variable fusion proteins in the Ewing family of tumours.* EMBO J, 1993. **12**(12): p. 4481-7.

124. Kovar, H., *Context matters: the hen or egg problem in Ewing's sarcoma.* Semin Cancer Biol, 2005. **15**(3): p. 189-96.

125. Huhn, R., et al., *Cleavage of the Ewing tumour-specific EWSR1-FLI1 mRNA by hammerhead ribozymes.* Anticancer Res, 2009. **29**(6): p. 1901-8.

126. Maksimenko, A. and C. Malvy, *Oncogene-targeted antisense oligonucleotides for the treatment of Ewing sarcoma.* Expert Opin Ther Targets, 2005. **9**(4): p. 825-30.

127. Hu-Lieskovan, S., et al., *Sequence-specific knockdown of EWS-FLI1 by targeted, nonviral delivery of small interfering RNA inhibits tumor growth in a murine model of metastatic Ewing's sarcoma.* Cancer Res, 2005. **65**(19): p. 8984-92.

128. Staege, M.S., et al., *DNA microarrays reveal relationship of Ewing family tumors to both endothelial and fetal neural crest-derived cells and define novel targets.* Cancer Res, 2004. **64**(22): p. 8213-21.

129. Giard, D.J., et al., *In vitro cultivation of human tumors: establishment of cell lines derived from a series of solid tumors.* J Natl Cancer Inst, 1973. **51**(5): p. 1417-23.

130. Tomeczkowski, J., et al., *Absence of G-CSF receptors and absent response to G-CSF in childhood Burkitt's lymphoma and B-ALL cells.* Br J Haematol, 1995. **89**(4): p. 771-9.

131. Schlesinger, H.R., et al., *Establishment and characterization of human neuroblastoma cell lines.* Cancer Res, 1976. **36**(9 pt.1): p. 3094-100.

132. van Valen, F., W. Winkelmann, and H. Jurgens, *Expression of functional Y1 receptors for neuropeptide Y in human Ewing's sarcoma cell lines.* J Cancer Res Clin Oncol, 1992. **118**(7): p. 529-36.

133. Goldman, J.P., et al., *Enhanced human cell engraftment in mice deficient in RAG2 and the common cytokine receptor gamma chain.* Br J Haematol, 1998. **103**(2): p. 335-42.

134. Safford, K.M., et al., *Neurogenic differentiation of murine and human adipose-derived stromal cells.* Biochem Biophys Res Commun, 2002. **294**(2): p. 371-9.

135. Eisen, M.B., et al., *Cluster analysis and display of genome-wide expression patterns.* Proc Natl Acad Sci U S A, 1998. **95**(25): p. 14863-8.

136. Sturn, A., J. Quackenbush, and Z. Trajanoski, *Genesis: cluster analysis of microarray data.* Bioinformatics, 2002. **18**(1): p. 207-8.

137. Tusher, V.G., R. Tibshirani, and G. Chu, *Significance analysis of microarrays applied to the ionizing radiation response.* Proc Natl Acad Sci U S A, 2001. **98**(9): p. 5116-21.

138. Moosmann, S., et al., *Milieu-adopted in vitro and in vivo differentiation of mesenchymal tissues derived from different adult human CD34-negative progenitor cell clones.* Cells Tissues Organs, 2005. **179**(3): p. 91-101.

139. Dohjima, T., et al., *Small interfering RNAs expressed from a Pol III promoter suppress the EWS/Fli-1 transcript in an Ewing sarcoma cell line.* Mol Ther, 2003. **7**(6): p. 811-6.

140. Graves, B.J. and J.M. Petersen, *Specificity within the ets family of transcription factors.* Adv Cancer Res, 1998. **75**: p. 1-55.

141. May, W.A., et al., *Ewing sarcoma 11;22 translocation produces a chimeric transcription factor that requires the DNA-binding domain encoded by FLI1 for transformation.* Proc Natl Acad Sci U S A, 1993. **90**(12): p. 5752-6.

142. Varambally, S., et al., *The polycomb group protein EZH2 is involved in progression of prostate cancer.* Nature, 2002. **419**(6907): p. 624-9.

143. Stemple, D.L. and D.J. Anderson, *Isolation of a stem cell for neurons and glia from the mammalian neural crest.* Cell, 1992. **71**(6): p. 973-85.

144. Witt, O., et al., *HDAC family: What are the cancer relevant targets?* Cancer Lett, 2009. **277**(1): p. 8-21.

145. Miao, Z., et al., *Isolation of mesenchymal stem cells from human placenta: comparison with human bone marrow mesenchymal stem cells.* Cell Biol Int, 2006. **30**(9): p. 681-7.

146. Choi, B.H. and R.C. Kim, *Expression of glial fibrillary acidic protein in immature oligodendroglia.* Science, 1984. **223**(4634): p. 407-9.

147. Benelli, R. and A. Albini, *In vitro models of angiogenesis: the use of Matrigel.* Int J Biol Markers, 1999. **14**(4): p. 243-6.

148. Ruan, K., X. Fang, and G. Ouyang, *MicroRNAs: novel regulators in the hallmarks of human cancer.* Cancer Lett, 2009. **285**(2): p. 116-26.

149. Yu, S.L., et al., *Unique MicroRNA signature and clinical outcome of cancers.* DNA Cell Biol, 2007. **26**(5): p. 283-92.

150. Zhang, B., et al., *microRNAs as oncogenes and tumor suppressors.* Dev Biol, 2007. **302**(1): p. 1-12.

151. Schickel, R., et al., *MicroRNAs: key players in the immune system, differentiation, tumorigenesis and cell death.* Oncogene, 2008. **27**(45): p. 5959-74.

152. Lynam-Lennon, N., S.G. Maher, and J.V. Reynolds, *The roles of microRNA in cancer and apoptosis.* Biol Rev Camb Philos Soc, 2009. **84**(1): p. 55-71.

153. Triché, T.J., *Non-coding RNA in the Pathogenesis of Childhood Cancer.* SIOP Education Book, 2008. **Section B**: p. 85-91.

154. Katoh, Y. and M. Katoh, *Comparative genomics on PROM1 gene encoding stem cell marker CD133.* Int J Mol Med, 2007. **19**(6): p. 967-70.

155. Zhou, S., et al., *The ABC transporter Bcrp1/ABCG2 is expressed in a wide variety of stem cells and is a molecular determinant of the side-population phenotype.* Nat Med, 2001. **7**(9): p. 1028-34.

156. Giles, K.E., R. Ghirlando, and G. Felsenfeld, *Maintenance of a constitutive heterochromatin domain in vertebrates by a Dicer-dependent mechanism.* Nat Cell Biol, 2010. **12**(1): p. 94-9; sup pp 1-6.

157. Hawkins, P.G., et al., *Promoter targeted small RNAs induce long-term transcriptional gene silencing in human cells.* Nucleic Acids Res, 2009. **37**(9): p. 2984-95.

158. Lazar, A., et al., *Molecular diagnosis of sarcomas: chromosomal translocations in sarcomas.* Arch Pathol Lab Med, 2006. **130**(8): p. 1199-207.

159. Arvand, A. and C.T. Denny, *Biology of EWS/ETS fusions in Ewing's family tumors.* Oncogene, 2001. **20**(40): p. 5747-54.

160. Li, X., et al., *The Ewing's sarcoma fusion protein, EWS-FLI, binds Runx2 and blocks osteoblast differentiation.* J Cell Biochem, 2010.

161. Zwerner, J.P., et al., *The EWS/FLI1 oncogenic transcription factor deregulates GLI1.* Oncogene, 2008. **27**(23): p. 3282-91.

162. Nishimori, H., et al., *The Id2 gene is a novel target of transcriptional activation by EWS-ETS fusion proteins in Ewing family tumors.* Oncogene, 2002. **21**(54): p. 8302-9.

163. Ordonez, J.L., et al., *Advances in Ewing's sarcoma research: where are we now and what lies ahead?* Cancer Res, 2009. **69**(18): p. 7140-50.

164. Mao, X., et al., *The FLI-1 and chimeric EWS-FLI-1 oncoproteins display similar DNA binding specificities.* J Biol Chem, 1994. **269**(27): p. 18216-22.

165. Arvand, A., et al., *The COOH-terminal domain of FLI-1 is necessary for full tumorigenesis and transcriptional modulation by EWS/FLI-1.* Cancer Res, 2001. **61**(13): p. 5311-7.

166. Siligan, C., et al., *EWS-FLI1 target genes recovered from Ewing's sarcoma chromatin.* Oncogene, 2005. **24**(15): p. 2512-24.

167. Abaan, O.D., et al., *PTPL1 is a direct transcriptional target of EWS-FLI1 and modulates Ewing's Sarcoma tumorigenesis.* Oncogene, 2005. **24**(16): p. 2715-22.

168. Shultz, L.D., F. Ishikawa, and D.L. Greiner, *Humanized mice in translational biomedical research.* Nat Rev Immunol, 2007. **7**(2): p. 118-30.

169. Nanni, P., et al., *High metastatic efficiency of human sarcoma cells in Rag2/gammac double knockout mice provides a powerful test system for antimetastatic targeted therapy.* Eur J Cancer, 2010. **46**(3): p. 659-68.

170. Riggi, N., et al., *EWS-FLI-1 expression triggers a Ewing's sarcoma initiation program in primary human mesenchymal stem cells.* Cancer Res, 2008. **68**(7): p. 2176-85.

171. Braet, F. and E. Wisse, *Structural and functional aspects of liver sinusoidal endothelial cell fenestrae: a review.* Comp Hepatol, 2002. **1**(1): p. 1.

172. Raaphorst, F.M., et al., *Poorly differentiated breast carcinoma is associated with increased expression of the human polycomb group EZH2 gene.* Neoplasia, 2003. **5**(6): p. 481-8.

173. Raman, J.D., et al., *Increased expression of the polycomb group gene, EZH2, in transitional cell carcinoma of the bladder.* Clin Cancer Res, 2005. **11**(24 Pt 1): p. 8570-6.

174. Kleer, C.G., et al., *EZH2 is a marker of aggressive breast cancer and promotes neoplastic transformation of breast epithelial cells.* Proc Natl Acad Sci U S A, 2003. **100**(20): p. 11606-11.

175. Ringrose, L. and R. Paro, *Epigenetic regulation of cellular memory by the Polycomb and Trithorax group proteins.* Annu Rev Genet, 2004. **38**: p. 413-43.

176. Cao, R. and Y. Zhang, *The functions of E(Z)/EZH2-mediated methylation of lysine 27 in histone H3.* Curr Opin Genet Dev, 2004. **14**(2): p. 155-64.

177. Sparmann, A. and M. van Lohuizen, *Polycomb silencers control cell fate, development and cancer.* Nat Rev Cancer, 2006. **6**(11): p. 846-56.

178. Lund, A.H. and M. van Lohuizen, *Polycomb complexes and silencing mechanisms.* Curr Opin Cell Biol, 2004. **16**(3): p. 239-46.

179. Caretti, G., et al., *The Polycomb Ezh2 methyltransferase regulates muscle gene expression and skeletal muscle differentiation.* Genes Dev, 2004. **18**(21): p. 2627-38.

180. McGarvey, K.M., et al., *DNA methylation and complete transcriptional silencing of cancer genes persist after depletion of EZH2.* Cancer Res, 2007. **67**(11): p. 5097-102.

181. Sun, F., et al., *Combinatorial pharmacologic approaches target EZH2-mediated gene repression in breast cancer cells.* Mol Cancer Ther, 2009. **8**(12): p. 3191-202.

182. Zhao, X.D., et al., *Whole-genome mapping of histone H3 Lys4 and 27 trimethylations reveals distinct genomic compartments in human embryonic stem cells.* Cell Stem Cell, 2007. **1**(3): p. 286-98.

183. Tiwari, V.K., et al., *A novel 6C assay uncovers Polycomb-mediated higher order chromatin conformations.* Genome Res, 2008. **18**(7): p. 1171-9.

184. Noer, A., L.C. Lindeman, and P. Collas, *Histone H3 modifications associated with differentiation and long-term culture of mesenchymal adipose stem cells.* Stem Cells Dev, 2009. **18**(5): p. 725-36.

185. Lee, E.R., F.E. Murdoch, and M.K. Fritsch, *High histone acetylation and decreased polycomb repressive complex 2 member levels regulate gene specific transcriptional changes during early embryonic stem cell differentiation induced by retinoic acid.* Stem Cells, 2007. **25**(9): p. 2191-9.

186. de Alava, E. and W.L. Gerald, *Molecular biology of the Ewing's sarcoma/primitive neuroectodermal tumor family.* J Clin Oncol, 2000. **18**(1): p. 204-13.

187. Li, S. and G.P. Siegal, *Small cell tumors of bone.* Adv Anat Pathol, 2010. **17**(1): p. 1-11.

188. Ludwig, J.A., *Ewing sarcoma: historical perspectives, current state-of-the-art, and opportunities for targeted therapy in the future.* Curr Opin Oncol, 2008. **20**(4): p. 412-8.

189. Choi, J.H., et al., *Enhancer of zeste homolog 2 expression is associated with tumor cell proliferation and metastasis in gastric cancer.* APMIS, 2010. **118**(3): p. 196-202.

190. Glinsky, G.V., *"Stemness" genomics law governs clinical behavior of human cancer: implications for decision making in disease management.* J Clin Oncol, 2008. **26**(17): p. 2846-53.

191. Glinsky, G.V., *Genomic models of metastatic cancer: functional analysis of death-from-cancer signature genes reveals aneuploid, anoikis-resistant, metastasis-enabling phenotype with altered cell cycle control and activated Polycomb Group (PcG) protein chromatin silencing pathway.* Cell Cycle, 2006. **5**(11): p. 1208-16.

192. Widschwendter, M., et al., *Epigenetic stem cell signature in cancer.* Nat Genet, 2007. **39**(2): p. 157-8.

193. Riggi, N., M.L. Suva, and I. Stamenkovic, *Ewing's sarcoma origin: from duel to duality.* Expert Rev Anticancer Ther, 2009. **9**(8): p. 1025-30.

194. Takashima, Y., et al., *Neuroepithelial cells supply an initial transient wave of MSC differentiation.* Cell, 2007. **129**(7): p. 1377-88.

195. Lee, G., et al., *Isolation and directed differentiation of neural crest stem cells derived from human embryonic stem cells.* Nat Biotechnol, 2007. **25**(12): p. 1468-75.

196. Ogawa, M., A.C. LaRue, and C.J. Drake, *Hematopoietic origin of fibroblasts/myofibroblasts: Its pathophysiologic implications.* Blood, 2006. **108**(9): p. 2893-6.

197. Drummond, D.C., et al., *Clinical development of histone deacetylase inhibitors as anticancer agents.* Annu Rev Pharmacol Toxicol, 2005. **45**: p. 495-528.

198. Lyko, F. and R. Brown, *DNA methyltransferase inhibitors and the development of epigenetic cancer therapies.* J Natl Cancer Inst, 2005. **97**(20): p. 1498-506.

199. Bolden, J.E., M.J. Peart, and R.W. Johnstone, *Anticancer activities of histone deacetylase inhibitors.* Nat Rev Drug Discov, 2006. **5**(9): p. 769-84.

200. Yoo, C.B. and P.A. Jones, *Epigenetic therapy of cancer: past, present and future.* Nat Rev Drug Discov, 2006. **5**(1): p. 37-50.

201. Dario, L.S., et al., *Chromatin remodeling agents for cancer therapy.* Rev Recent Clin Trials, 2008. **3**(3): p. 192-203.

202. Kuendgen, A. and M. Lubbert, *Current status of epigenetic treatment in myelodysplastic syndromes.* Ann Hematol, 2008. **87**(8): p. 601-11.

203. Gore, S.D., et al., *Combined DNA methyltransferase and histone deacetylase inhibition in the treatment of myeloid neoplasms.* Cancer Res, 2006. **66**(12): p. 6361-9.

204. Pan, L.N., J. Lu, and B. Huang, *HDAC inhibitors: a potential new category of anti-tumor agents.* Cell Mol Immunol, 2007. **4**(5): p. 337-43.

205. Sonnemann, J., et al., *Histone deacetylase inhibitors induce cell death and enhance the apoptosis-inducing activity of TRAIL in Ewing's sarcoma cells.* J Cancer Res Clin Oncol, 2007. **133**(11): p. 847-58.

206. Jaboin, J., et al., *MS-27-275, an inhibitor of histone deacetylase, has marked in vitro and in vivo antitumor activity against pediatric solid tumors.* Cancer Res, 2002. **62**(21): p. 6108-15.

207. Hurtubise, A., M.L. Bernstein, and R.L. Momparler, *Preclinical evaluation of the antineoplastic action of 5-aza-2'-deoxycytidine and different histone deacetylase inhibitors on human Ewing's sarcoma cells.* Cancer Cell Int, 2008. **8**: p. 16.

208. Tan, J., et al., *Pharmacologic disruption of Polycomb-repressive complex 2-mediated gene repression selectively induces apoptosis in cancer cells.* Genes Dev, 2007. **21**(9): p. 1050-63.

209. Bartel, D.P., *MicroRNAs: genomics, biogenesis, mechanism, and function.* Cell, 2004. **116**(2): p. 281-97.

210. Lagos-Quintana, M., et al., *Identification of novel genes coding for small expressed RNAs.* Science, 2001. **294**(5543): p. 853-8.

211. Imam, J.S., et al., *MicroRNA-185 suppresses tumor growth and progression by targeting the Six1 oncogene in human cancers.* Oncogene, 2010. **29**(35): p. 4971-9.

212. Flavin, R.J., et al., *Potentially important microRNA cluster on chromosome 17p13.1 in primary peritoneal carcinoma.* Mod Pathol, 2009. **22**(2): p. 197-205.

213. Lodygin, D., et al., *Inactivation of miR-34a by aberrant CpG methylation in multiple types of cancer.* Cell Cycle, 2008. **7**(16): p. 2591-600.

214. Chim, C.S., et al., *Epigenetic inactivation of the miR-34a in hematological malignancies.* Carcinogenesis. **31**(4): p. 745-50.

215. Chim, C.S., et al., *Epigenetic inactivation of the miR-34a in hematological malignancies.* Carcinogenesis, 2010. **31**(4): p. 745-50.

216. Toyota, M., et al., *Epigenetic silencing of microRNA-34b/c and B-cell translocation gene 4 is associated with CpG island methylation in colorectal cancer.* Cancer Res, 2008. **68**(11): p. 4123-32.

217. Saito, Y., et al., *Epigenetic therapy upregulates the tumor suppressor microRNA-126 and its host gene EGFL7 in human cancer cells.* Biochem Biophys Res Commun, 2009. **379**(3): p. 726-31.

218. Huang, Y.W., et al., *Epigenetic repression of microRNA-129-2 leads to overexpression of SOX4 oncogene in endometrial cancer.* Cancer Res, 2009. **69**(23): p. 9038-46.

219. Kozaki, K., et al., *Exploration of tumor-suppressive microRNAs silenced by DNA hypermethylation in oral cancer.* Cancer Res, 2008. **68**(7): p. 2094-105.

220. Tsai, K.W., et al., *Epigenetic regulation of miR-196b expression in gastric cancer.* Genes Chromosomes Cancer, 2010.

221. Furuta, M., et al., *miR-124 and miR-203 are epigenetically silenced tumor-suppressive microRNAs in hepatocellular carcinoma.* Carcinogenesis, 2010. **31**(5): p. 766-76.

222. Ando, T., et al., *DNA methylation of microRNA genes in gastric mucosae of gastric cancer patients: its possible involvement in the formation of epigenetic field defect.* Int J Cancer, 2009. **124**(10): p. 2367-74.

223. Burnside, J., et al., *Deep sequencing of chicken microRNAs.* BMC Genomics, 2008. **9**: p. 185.

224. Guled, M., et al., *CDKN2A, NF2, and JUN are dysregulated among other genes by miRNAs in malignant mesothelioma -A miRNA microarray analysis.* Genes Chromosomes Cancer, 2009. **48**(7): p. 615-23.

225. Reynolds, P.A., et al., *Tumor suppressor p16INK4A regulates polycomb-mediated DNA hypermethylation in human mammary epithelial cells.* J Biol Chem, 2006. **281**(34): p. 24790-802.

226. Ohm, J.E., et al., *A stem cell-like chromatin pattern may predispose tumor suppressor genes to DNA hypermethylation and heritable silencing.* Nat Genet, 2007. **39**(2): p. 237-42.

227. Villa, R., et al., *Role of the polycomb repressive complex 2 in acute promyelocytic leukemia.* Cancer Cell, 2007. **11**(6): p. 513-25.

228. Esteller, M., *Epigenetic gene silencing in cancer: the DNA hypermethylome.* Hum Mol Genet, 2007. **16 Spec No 1**: p. R50-9.

229. Kondo, Y., et al., *Alterations of DNA methylation and histone modifications contribute to gene silencing in hepatocellular carcinomas.* Hepatol Res, 2007. **37**(11): p. 974-83.

230. Xiong, J., et al., *An estrogen receptor alpha suppressor, microRNA-22, is downregulated in estrogen receptor alpha-positive human breast cancer cell lines and clinical samples.* FEBS J, 2010. **277**(7): p. 1684-94.

231. Stamatopoulos, B., et al., *microRNA-29c and microRNA-223 down-regulation has in vivo significance in chronic lymphocytic leukemia and improves disease risk stratification.* Blood, 2009. **113**(21): p. 5237-45.

232. Wu, W., et al., *Expression profile of mammalian microRNAs in endometrioid adenocarcinoma.* Eur J Cancer Prev, 2009. **18**(1): p. 50-5.

233. Huang, J., et al., *Down-regulated microRNA-152 induces aberrant DNA methylation in hepatitis B virus-related hepatocellular carcinoma by targeting DNA methyltransferase 1.* Hepatology, 2010. **52**(1): p. 60-70.

234. Chao, A., et al., *Decreased expression of microRNA-199b increases protein levels of SET (protein phosphatase 2A inhibitor) in human choriocarcinoma.* Cancer Lett, 2010. **291**(1): p. 99-107.

235. Pizzimenti, S., et al., *MicroRNA expression changes during human leukemic HL-60 cell differentiation induced by 4-hydroxynonenal, a product of lipid peroxidation.* Free Radic Biol Med, 2009. **46**(2): p. 282-8.

236. Corbetta, S., et al., *Differential expression of microRNAs in human parathyroid carcinomas compared with normal parathyroid tissue.* Endocr Relat Cancer, 2010. **17**(1): p. 135-46.

237. Xiong, J., Q. Du, and Z. Liang, *Tumor-suppressive microRNA-22 inhibits the transcription of E-box-containing c-Myc target genes by silencing c-Myc binding protein.* Oncogene, 2010. **29**(35): p. 4980-8.

238. Lang, N., et al., *Effects of microRNA-29 family members on proliferation and invasion of gastric cancer cell lines.* Chin J Cancer, 2010. **29**(6): p. 603-10.

239. Garzia, L., et al., *MicroRNA-199b-5p impairs cancer stem cells through negative regulation of HES1 in medulloblastoma.* PLoS One, 2009. **4**(3): p. e4998.

240. Dugas, J.C., et al., *Dicer1 and miR-219 Are required for normal oligodendrocyte differentiation and myelination.* Neuron, 2010. **65**(5): p. 597-611.

241. Zhao, X., et al., *MicroRNA-mediated control of oligodendrocyte differentiation.* Neuron, 2010. **65**(5): p. 612-26.

242. Sluijter, J.P., et al., *MicroRNA-1 and -499 regulate differentiation and proliferation in human-derived cardiomyocyte progenitor cells.* Arterioscler Thromb Vasc Biol, 2010. **30**(4): p. 859-68.

243. Lena, A.M., et al., *miR-203 represses 'stemness' by repressing DeltaNp63.* Cell Death Differ, 2008. **15**(7): p. 1187-95.

244. Yi, R., et al., *A skin microRNA promotes differentiation by repressing 'stemness'.* Nature, 2008. **452**(7184): p. 225-9.

245. Chen, Z., et al., *Hypoxia-regulated microRNA-210 modulates mitochondrial function and decreases ISCU and COX10 expression.* Oncogene, 2010. **29**(30): p. 4362-8.

246. Gee, H.E., et al., *hsa-mir-210 is a marker of tumor hypoxia and a prognostic factor in head and neck cancer.* Cancer, 2010. **116**(9): p. 2148-58.

247. Greither, T., et al., *Elevated expression of microRNAs 155, 203, 210 and 222 in pancreatic tumors is associated with poorer survival.* Int J Cancer, 2010. **126**(1): p. 73-80.

248. Foekens, J.A., et al., *Four miRNAs associated with aggressiveness of lymph node-negative, estrogen receptor-positive human breast cancer.* Proc Natl Acad Sci U S A, 2008. **105**(35): p. 13021-6.

249. Unno, K., et al., *Identification of a novel microRNA cluster miR-193b-365 in multiple myeloma.* Leuk Lymphoma, 2009. **50**(11): p. 1865-71.

250. Pogribny, I.P., et al., *Alterations of microRNAs and their targets are associated with acquired resistance of MCF-7 breast cancer cells to cisplatin.* Int J Cancer, 2010. **127**(8): p. 1785-94.

251. Cervigne, N.K., et al., *Identification of a microRNA signature associated with progression of leukoplakia to oral carcinoma.* Hum Mol Genet, 2009. **18**(24): p. 4818-29.

252. Wang, H.J., et al., *MicroRNA-101 is down-regulated in gastric cancer and involved in cell migration and invasion.* Eur J Cancer, 2010. **46**(12): p. 2295-303.

253. Cao, P., et al., *MicroRNA-101 negatively regulates Ezh2 and its expression is modulated by androgen receptor and HIF-1alpha/HIF-1beta.* Mol Cancer, 2010. **9**: p. 108.

254. Friedman, J.M., et al., *The putative tumor suppressor microRNA-101 modulates the cancer epigenome by repressing the polycomb group protein EZH2.* Cancer Res, 2009. **69**(6): p. 2623-9.

255. Ciarapica, R., et al., *Deregulated expression of miR-26a and Ezh2 in rhabdomyosarcoma.* Cell Cycle, 2009. **8**(1): p. 172-5.

256. Wong, C.F. and R.L. Tellam, *MicroRNA-26a targets the histone methyltransferase Enhancer of Zeste homolog 2 during myogenesis.* J Biol Chem, 2008. **283**(15): p. 9836-43.

257. Chendrimada, T.P., et al., *TRBP recruits the Dicer complex to Ago2 for microRNA processing and gene silencing.* Nature, 2005. **436**(7051): p. 740-4.

258. Frenquelli, M., et al., *MicroRNA and proliferation control in chronic lymphocytic leukemia: functional relationship between miR-221/222 cluster and p27.* Blood, 2010. **115**(19): p. 3949-59.

259. Calin, G.A., et al., *A MicroRNA signature associated with prognosis and progression in chronic lymphocytic leukemia.* N Engl J Med, 2005. **353**(17): p. 1793-801.

260. Garzon, R., et al., *MicroRNA signatures associated with cytogenetics and prognosis in acute myeloid leukemia.* Blood, 2008. **111**(6): p. 3183-9.

261. Zhang, J., et al., *miR-221/222 promote malignant progression of glioma through activation of the Akt pathway.* Int J Oncol, 2010. **36**(4): p. 913-20.

262. Garofalo, M., et al., *miR-221&222 regulate TRAIL resistance and enhance tumorigenicity through PTEN and TIMP3 downregulation.* Cancer Cell, 2009. **16**(6): p. 498-509.

263. Fornari, F., et al., *MiR-221 controls CDKN1C/p57 and CDKN1B/p27 expression in human hepatocellular carcinoma.* Oncogene, 2008. **27**(43): p. 5651-61.

264. Pineau, P., et al., *miR-221 overexpression contributes to liver tumorigenesis.* Proc Natl Acad Sci U S A, 2010. **107**(1): p. 264-9.

265. Sredni, S.T., et al., *Upregulation of mir-221 and mir-222 in atypical teratoid/rhabdoid tumors: potential therapeutic targets.* Childs Nerv Syst, 2010. **26**(3): p. 279-83.

266. Sun, T., et al., *The role of microRNA-221 and microRNA-222 in androgen-independent prostate cancer cell lines.* Cancer Res, 2009. **69**(8): p. 3356-63.

267. Ambs, S., et al., *Genomic profiling of microRNA and messenger RNA reveals deregulated microRNA expression in prostate cancer.* Cancer Res, 2008. **68**(15): p. 6162-70.

268. Igoucheva, O. and V. Alexeev, *MicroRNA-dependent regulation of cKit in cutaneous melanoma.* Biochem Biophys Res Commun, 2009. **379**(3): p. 790-4.

269. Zhao, J.J., et al., *MicroRNA-221/222 negatively regulates estrogen receptor alpha and is associated with tamoxifen resistance in breast cancer.* J Biol Chem, 2008. **283**(45): p. 31079-86.

270. Visone, R., et al., *MicroRNAs (miR)-221 and miR-222, both overexpressed in human thyroid papillary carcinomas, regulate p27Kip1 protein levels and cell cycle.* Endocr Relat Cancer, 2007. **14**(3): p. 791-8.

271. Lu, Q., et al., *MicroRNA-221 silencing predisposed human bladder cancer cells to undergo apoptosis induced by TRAIL.* Urol Oncol, 2009.

272. Bloomston, M., et al., *MicroRNA expression patterns to differentiate pancreatic adenocarcinoma from normal pancreas and chronic pancreatitis.* JAMA, 2007. **297**(17): p. 1901-8.

273. le Sage, C., et al., *Regulation of the p27(Kip1) tumor suppressor by miR-221 and miR-222 promotes cancer cell proliferation.* EMBO J, 2007. **26**(15): p. 3699-708.

274. Park, J.K., et al., *Antisense inhibition of microRNA-21 or -221 arrests cell cycle, induces apoptosis, and sensitizes the effects of gemcitabine in pancreatic adenocarcinoma.* Pancreas, 2009. **38**(7): p. e190-9.

275. Zhang, C., et al., *Co-suppression of miR-221/222 cluster suppresses human glioma cell growth by targeting p27kip1 in vitro and in vivo.* Int J Oncol, 2009. **34**(6): p. 1653-60.

276. Mercatelli, N., et al., *The inhibition of the highly expressed miR-221 and miR-222 impairs the growth of prostate carcinoma xenografts in mice.* PLoS One, 2008. **3**(12): p. e4029.

277. Djupedal, I. and K. Ekwall, *Epigenetics: heterochromatin meets RNAi.* Cell Res, 2009. **19**(3): p. 282-95.

278. Cifuentes, D., et al., *A novel miRNA processing pathway independent of Dicer requires Argonaute2 catalytic activity.* Science, 2010. **328**(5986): p. 1694-8.

279. Zhou, Y., et al., *High-risk myeloma is associated with global elevation of miRNAs and overexpression of EIF2C2/AGO2.* Proc Natl Acad Sci U S A. **107**(17): p. 7904-9.

280. Schmitter, D., et al., *Effects of Dicer and Argonaute down-regulation on mRNA levels in human HEK293 cells.* Nucleic Acids Res, 2006. **34**(17): p. 4801-15.

281. Iwasaki, S. and Y. Tomari, *Argonaute-mediated translational repression (and activation).* Fly (Austin), 2009. **3**(3): p. 204-6.

282. Steinmann, K., et al., *Frequent promoter hypermethylation of tumor-related genes in head and neck squamous cell carcinoma.* Oncol Rep, 2009. **22**(6): p. 1519-26.

283. Eckfeld, K., et al., *RASSF4/AD037 is a potential ras effector/tumor suppressor of the RASSF family.* Cancer Res, 2004. **64**(23): p. 8688-93.

284. Chow, L.S., et al., *Aberrant methylation of RASSF4/AD037 in nasopharyngeal carcinoma.* Oncol Rep, 2004. **12**(4): p. 781-7.

285. Folberg, R., M.J. Hendrix, and A.J. Maniotis, *Vasculogenic mimicry and tumor angiogenesis.* Am J Pathol, 2000. **156**(2): p. 361-81.

286. Hess, A.R., et al., *Deciphering the signaling events that promote melanoma tumor cell vasculogenic mimicry and their link to embryonic vasculogenesis: role of the Eph receptors.* Dev Dyn, 2007. **236**(12): p. 3283-96.

287. Ruf, W., et al., *Differential role of tissue factor pathway inhibitors 1 and 2 in melanoma vasculogenic mimicry.* Cancer Res, 2003. **63**(17): p. 5381-9.

288. Adams, R.H., et al., *Roles of ephrinB ligands and EphB receptors in cardiovascular development: demarcation of arterial/venous domains, vascular morphogenesis, and sprouting angiogenesis.* Genes Dev, 1999. **13**(3): p. 295-306.

289. Ma, L., et al., *Cancer stem-like cells can be isolated with drug selection in human ovarian cancer cell line SKOV3.* Acta Biochim Biophys Sin (Shanghai), 2010. **42**(9): p. 593-602.

290. Du, Z., et al., *Pancreatic Cancer Cells Resistant to Chemoradiotherapy Rich in "Stem-Cell-Like" Tumor Cells.* Dig Dis Sci, 2010.

291. Bertolini, G., et al., *Highly tumorigenic lung cancer CD133+ cells display stem-like features and are spared by cisplatin treatment.* Proc Natl Acad Sci U S A, 2009. **106**(38): p. 16281-6.

292. Zhu, Z., et al., *Cancer stem/progenitor cells are highly enriched in CD133+CD44+ population in hepatocellular carcinoma.* Int J Cancer, 2010. **126**(9): p. 2067-78.

293. Okamoto, A., et al., *Expansion and characterization of cancer stem-like cells in squamous cell carcinoma of the head and neck.* Oral Oncol, 2009. **45**(7): p. 633-9.

294. Tirino, V., et al., *Detection and characterization of CD133+ cancer stem cells in human solid tumours.* PLoS One, 2008. **3**(10): p. e3469.

295. Suva, M.L., et al., *Identification of cancer stem cells in Ewing's sarcoma.* Cancer Res, 2009. **69**(5): p. 1776-81.

296. Yang, M., et al., *Detection and characterization of side population in Ewing's sarcoma SK-ES-1 cells in vitro.* Biochem Biophys Res Commun, 2010. **391**(1): p. 1062-6.

297. Monzani, E., et al., *Melanoma contains CD133 and ABCG2 positive cells with enhanced tumourigenic potential.* Eur J Cancer, 2007. **43**(5): p. 935-46.

298. Takenobu, H., et al., *CD133 suppresses neuroblastoma cell differentiation via signal pathway modification.* Oncogene, 2010.

299. Jiang, X., et al., *CD133 expression in chemo-resistant Ewing sarcoma cells.* BMC Cancer, 2010. **10**: p. 116.

300. Bayne, E.H., et al., *Stc1: a critical link between RNAi and chromatin modification required for heterochromatin integrity.* Cell, 2010. **140**(5): p. 666-77.

301. Shen, R. and T. Xie, *Stem cell self-renewal versus differentiation: tumor suppressor Mei-P26 and miRNAs control the balance.* Cell Res, 2008. **18**(7): p. 713-5.

302. Kagalwala, M.N., S.K. Singh, and S. Majumder, *Stemness is only a state of the cell.* Cold Spring Harb Symp Quant Biol, 2008. **73**: p. 227-34.

303. Vicente-Duenas, C., et al., *The role of cellular plasticity in cancer development.* Curr Med Chem, 2009. **16**(28): p. 3676-85.

304. Shukla, V., T. Vaissiere, and Z. Herceg, *Histone acetylation and chromatin signature in stem cell identity and cancer.* Mutat Res, 2008. **637**(1-2): p. 1-15.

305. Bapat, S.A., et al., *Multivalent epigenetic marks confer microenvironment-responsive epigenetic plasticity to ovarian cancer cells.* Epigenetics, 2010. **5**(8).

306. Yoo, N.J., et al., *Immunohistochemical analysis of RNA-induced silencing complex-related proteins AGO2 and TNRC6A in prostate and esophageal cancers.* APMIS. **118**(4): p. 271-6.

307. Li, L., et al., *Argonaute proteins: potential biomarkers for human colon cancer.* BMC Cancer. **10**: p. 38.

308. Esquela-Kerscher, A. and F.J. Slack, *Oncomirs - microRNAs with a role in cancer.* Nat Rev Cancer, 2006. **6**(4): p. 259-69.

309. Wang, V. and W. Wu, *MicroRNA-based therapeutics for cancer.* BioDrugs, 2009. **23**(1): p. 15-23.

310. Krutzfeldt, J., et al., *Silencing of microRNAs in vivo with 'antagomirs'.* Nature, 2005. **438**(7068): p. 685-9.

311. Elmen, J., et al., *LNA-mediated microRNA silencing in non-human primates.* Nature, 2008. **452**(7189): p. 896-9.

312. Lanford, R.E., et al., *Therapeutic silencing of microRNA-122 in primates with chronic hepatitis C virus infection.* Science, 2010. **327**(5962): p. 198-201.

# 9. Publications

Parts of this thesis have already been published :

Burdach S, Plehm S, Unland R, Dirksen U, Borkhardt A, Staege MS, Müller-Tidow C, Richter GH. *Epigenetic maintenance of stemness and malignancy in peripheral neuroectodermal tumors by EZH2.* Cell Cycle, 2009. **8**(13): p. 1991-6.

Richter GH *, Plehm S *, Fasan A, Rössler S, Unland R, Bennani-Baiti IM, Hotfilder M, Löwel D, von Luettichau I, Mossbrugger I, Quintanilla-Martinez L, Kovar H, Staege MS, Müller-Tidow C, Burdach S. *EZH2 is a mediator of EWS/FLI1 driven tumor growth and metastasis blocking endothelial and neuro-ectodermal differentiation.* Proc Natl Acad Sci U S A, 2009. **106**(13): p. 5324-9.

* these authors contributed equally

# 10. Appendices

## 10.1. Cluster Analysis

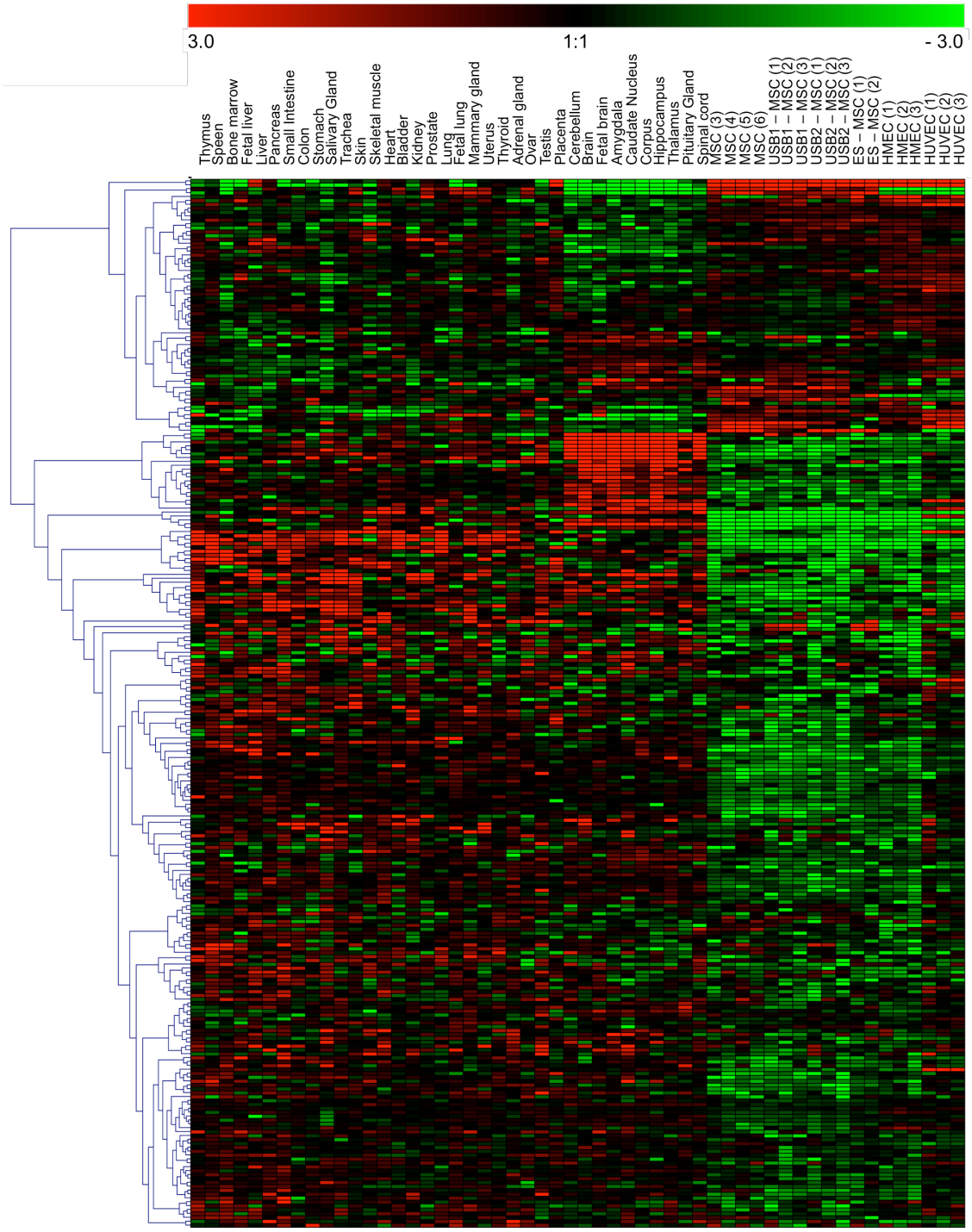


**Figure 43: Cluster analysis with significantly up-regulated genes upon EZH2 suppression in A673 ET cells.** For this cluster analysis (Manhattan distance, complete linkage clustering) a panel of datasets from normal tissues, endothelial cells as well as mesenchymal stem cells were used and compared to genes that were significantly up-regulated (identified by SAM analysis) in EZH2 siRNA treated ET cells. HMEC, human microvasculature endothelial cells ; HUVEC, human macro vasculature (umbilical cord) endothelial cells ; MSC, bone marrow derived mesenchymal stem cells ; UCB-MSC, two types of umbilical cord blood derived MSC ; ES-MSC, embryonic stem cell derived MSC.

## 10.2. Counting of the liver metastases grown upon EZH2 suppression

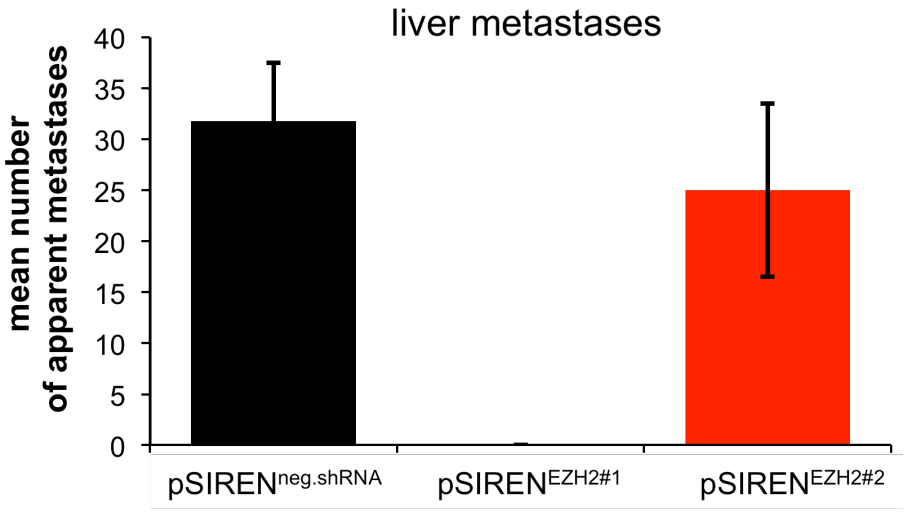


**Figure 44: Mean number of apparent liver metastases after injection of pSIREN$^{neg.shRNA}$, pSIREN$^{EZH2\#1}$ and pSIREN$^{EZH2\#2}$ infected A673 ET cells.** 4 x $10^6$ cells were injected intravenously into the tail vein of immunodeficient Rag2$^{-/-}\gamma_C^{-/-}$ mice. Treatment occurs with four mice per group. The graphic shows the average amount of counted liver metastases for each group, represented by the bars.

## 10.3. List of Figures

## 10.4. List of Tables

## 10.5. List of Abbreviations

| | |
|---|---|
| ABCD | Avidin biotin complex DNA |
| ABCG2 | ATP-binding cassette, sub-family G (WHITE), member 2 |
| ALCAM | activated leukocyte cell adhesion molecule |
| AGO1 | Argonaute 1 protein |
| AGO2 | Argonaute 2 protein |
| APC | Allophycocyanin |
| BCP | 1-bromo-3-chloropropane |
| BHA | Butylated hydroxyanisole |
| bp | Base pairs |
| BrdU | Bromodeoxyuridine |
| cALL | common acute lymphoblasic leukemia |
| cDNA | complementary DNA |

| | |
|---|---|
| CDKN1A (p21) | cyclin-dependent kinase inhibitor 1A |
| CDKN1C (p57kip) | cyclin-dependent kinase inhibitor 1C |
| ChIP | Chromatin immunoprecipitation |
| DMSO | Dimetylsulfoxide |
| DNA | Desoxyribonucleic acid |
| DNMT | DNA methyltransferase |
| dNTP | Deoxyribonucleotide triphosphate |
| ds | double stranded |
| EDTA | ethane-1,2-diyldinitrilo tetraacetic acid |
| EED | embryonic ectoderm development |
| ET | Ewing Family of Tumors |
| ELISA | Enzyme Linked Immunoabsorbent Assay |
| EMP1 | epithelial membrane protein 1 |
| EPHB2 | ephrin type-B receptor 2 |
| ES cell | Embryonic stem cell |
| ETS transcription factor | E-twenty six transcription factor (leukemia virus E26) |
| EWS | Ewing's Sarcoma oncogene |
| EZH1 | enhancer of zeste (Drosophila) homolog 1 |
| EZH2 | enhancer of zeste (Drosophila) homolog 2 |
| FACS | fluorescence activated cell sorting |
| FAM | 6-carboxy-fluorescein |
| FBS | Fetal bovine serum |
| FITC | Fluoresceinisothiocyanat |
| FLI1 | Friend leukemia integration |
| for (primer) | forward |
| FSC | Forward scatter |
| G1P2 (ISG15) | interferon, alpha-inducible protein (clone IFI-15K) |
| GAP43 | growth associated protein 43 |
| GAPDH | Glyceraldehyde 3-phosphate dehydrogenase |
| gDNA | genomic DNA |
| GFAP | glial fibrillary acidic protein |
| H3 | Histone 3 |
| H3K27me3 | Histone 3 lysine 27 trimethylation |
| HDACi | Histone deacetylase inhibitior |
| H&E | Hematoxylin & Eosin |
| HPRT | hypoxanthine-guanine phosphoribosyltransferase |
| HRP | Horse radish peroxidase |
| IFITM1 | interferon induced transmembrane protein 1 |
| IFN | Interferon |
| IgG | Immunoglobulin G |

| | |
|---|---|
| IHC | immunohistochemistry |
| kDa | Kilo Dalton |
| LTR | Long terminal repeats |
| miRNA | microRNA |
| mRNA | messenger RNA |
| MSC | Mesenchymal stem cell |
| NANOG | Nanog homeobox |
| NGFR | nerve growth factor receptor |
| NTC | Non-template control |
| OCT4 | Octamer binding transcription factor 4 |
| PBS | phosphate buffered saline |
| PCR | Polymerase chain reaction |
| PE | R-Phycoerythrin |
| PI | Propidium iodide |
| POU5F1 (OCT4) | POU class 5 homeobox 1 |
| PRC2 | Polycomb repressive complex 2 |
| PROM1 (CD133) | prominin 1 |
| PVDF | Polyvinylidene Fluoride |
| qRT-PCR | quantitative real time PCR |
| rev (primer) | reverse |
| RNU19 | RNA, U19 small nucleolar |
| RT | Reverse transcriptase or room temperature |
| SAM | Significance analysis of microarrays |
| s.c. | sub-cutaneous |
| SDS | sodium dodecyl sulfate |
| SDS-PAGE | SDS polyacrylamide gel electrophoresis |
| shRNA | Small hairpin RNA |
| siRNA | Short interfering RNA |
| ss | single stranded |
| SSC | Sideward scatter |
| SUZ12 | suppressor of zeste 12 homolog (Drosophila) |
| TBST | Tris-Buffered Saline Tween-20 |
| TEMED | N,N,N′,N′-Tetramethylethan-1,2-diamin |
| TSA | Trichostatin A |
| TSS | transcriptional start site |
| VC | Vector control |

# 11. Acknowledgements

Ich möchte mich an dieser Stelle bei allen bedanken, die zum Gelingen dieser Doktorarbeit beigetragen haben.

Mein besonderer Dank gilt :

Herrn Prof. Dr. Stefan Burdach und Herrn Dr. Günther Richter für die Möglichkeit, meine Promotion am Forschungszentrum für krebskranke Kinder der TU München durchzuführen, für die Überlassung eines so interessanten und anspruchvollen Themas sowie für ihr entgegengebrachtes Vertrauen und ihre Begleitung der Arbeit, die größtenteils von der Else-Kröner-Fresenius Stiftung (Special Grants P31/08//A123/07) finanziert wurde.

Frau Prof. Dr. Gabriele Multhoff für die Betreuung meiner Doktorarbeit und Herrn Prof. Dr. Siegfried Scherer für die Übernahme des Prüfungsvorsitzes und für die Organisation des Prüfungsverfahrens.

Frau Dr. Ilona Moßbrugger, Frau PD Dr. Leticia Quintanilla-Martinez und Frau Univ.-Prof. Dr. Irene Esposito vom Institut für Pathologie am Helmholtz Zentrum München für die zahlreichen histologischen Untersuchungen und die sorgfältigen Berichte.

Frau Rebekka Unland, Herrn Dr. Marc Hotfilder sowie Herrn Prof. Dr. Carsten Müller-Tidow vom Universitätsklinikum Münster - Klinik und Poliklinik für Kinder und Jugendmedizin - Pädiatrische Hämatologie und Onkologie – für die engagierte und zuverlässige Kooperation sowie allen anderen Kooperationspartnern, die nicht nur zur Veröffentlichung einzelner Ergebnisse, sondern auch zur Auszeichnung von Teilen der Arbeit mit dem Kind-Philipp-Preis 2009 geführt haben.

Sabine Rößler für die essentiellen Vorarbeiten, Annette Fasan für die Einarbeitung und den Beistand in jeglicher Form sowie Colette Zobywalski für die Übernahme vieler kleiner und großer experimenteller Arbeiten und die Organisation des Labors.

Thomas Grünewald, Uwe Thiel und Kristina Hauer sowie meinen allerliebsten Studienkollegen und Freunden Nathalie Zatula und Wolfgang Hiegl für die kritische und produktive Durchsicht dieser Arbeit, für den Austausch, Rückhalt und Zuspruch.

Maria-Magdalena Brandt und ihrem kleinen Theo für die effektiven und schönen „geistigen Pausen“.

Und nicht zuletzt meiner Familie, besonders meinen Eltern, die immer an mich geglaubt und mich unterstützt haben.